NTNU

Norwegian University of
Science and Technology

Synchronization and Control of Attitude for Spacecrafts:

Design, Analysis and Experiments

Ulrik Jørgensen

Master of Science in Engineering Cybernetics

Submission date: June 2010

Supervisor: Jan Tommy Gravdahl, ITK

Norwegian University of Science and Technology
Department of Engineering Cybernetics

Problem Description

Subject: Engineering Cybernetics

Background:
Based on previous results and experience from the student project [1], the candidate is to improve and design new controller structures for the attitude coordination problem. The results are to be experimentally verified on the AUVSAT-setup.

Assignment:
1) Derive dynamic models describing the dynamics and kinematics of internally actuated rigid bodies.
2) Design and analyze the stability properties of trajectory tracking controllers for attitude.
3) In the absence of angular velocity measurements, derive an observer for this quantity, and investigate the stability of the complete system.
4) Extend the synchronization design of [2] to the case of internal actuation.
5) Conduct experiments to test and verify the results of assignments 1-4.
6) Based on the results from this project, write and submit a paper to the IEEE Conference on Decision and Control.

To be handed in by: 14. June 2010

[1] U. Jørgensen, Attitude control for satellites: AUVSAT, 5th year project, Department of Engineering Cybernetics, NTNU, 2009
[2] A.K. Bondhus, K.Y. Pettersen and J.T. Gravdahl, Leader/Follower synchronization of satellite attitude without angular velocity measurements, in proc. of the 44th IEEE Conference on Decision and Control, Seville, Spain, December 2005

Assignment given: 11. January 2010
Supervisor: Jan Tommy Gravdahl, ITK

Abstract

The topic of this paper is to control and synchronize sphere-shaped spacecrafts in a leader-follower synchronization scheme. In order to achieve this objective, a nonlinear mathematical model of the vehicles has been developed. The design is based on rigid body dynamics where the vessel is actuated by means of three orthogonally mounted reaction wheels. The attitude dynamics is derived using Euler parameters.

In the pursuit of reaching the main goal of controlling and synchronizing the satellites, it is natural to first develop control algorithms for single vehicle control. A sliding mode controller and a backstepping controller have been derived for this matter, and are compared for optimality. Both controllers are based on nonlinear control theory and are designed to control the angular velocity of the satellite. The system in combination with both the controllers is proven to be asymptotically stable.

Due to cases where the spacecraft does not have angular velocity measurements, an estimator for the angular velocity is derived. Using LaSalle's theorem, asymptotic stability is proven for the observer in the time-invariant case, while Matrosov's theorem is utilized for system explicitly dependent on time.

For operational assignments where it is not sufficient with only one satellite, a synchronizing scheme for several satellites has been proposed. The scheme is based on a leader-follower synchronization design, and is derived assuming that none of the satellites are equipped with angular velocity measurements. It is therefore possible to implement and utilize the nonlinear observer for angular velocity estimation in each vehicle. The controllers are designed in a similar manner for both the leader and the follower using backstepping control. The leader is set to follow an arbitrarily smooth trajectory, while the follower's objective is to track the leader's attitude, given by measurements and estimations.

The various systems are tested in a lab setup with the AUVSAT. The AUVSAT is a sphere shaped, autonomous underwater satellite actuated by means of three reaction wheels. The experiments are performed when the AUVSAT is submerged in a water tank, making it possible to emulate a gravity free environment equal to what a satellite traveling in space is experiencing. The AUVSAT build up is presented where hardware and software components are chosen with respect to simplicity, cost and space restrictions.

Several experiments are carried out using the AUVSAT to evaluate the performance of the controllers, observer and the synchronization scheme. For all cases, the system tracks a time-varying sinusoidal reference signal in addition to a square-shaped sequence. In this way, one can truly validate transient responses, steady-state and tracking maneuvers to determine the performance of the various systems.

The experiments show that the sliding mode controller and backstepping controller works quite similar and with a satisfactorily behavior throughout the experiments. However, there are some lack of performance of the combined observer and controller system when tracking the sinusoidal time-varying reference. In the synchronization scheme, the leader follows the desired trajectory and the follower tracks the leader's attitude to some extent. Comments on the results are presented in addition to proposed strategies and thoughts on how to improve the overall performance of the various systems.

Preface

This thesis presents the research and results from the final semester of my Master of Science degree at the Department of Engineering Cybernetics at the Norwegian University of Science and Technology. The research has been carried out from January to June, 2010.

I would like to use this opportunity to acknowledge important people who deserve recognition for making it possible for me to finalize this thesis.

First of all I would like to thank my supervisor Professor Jan Tommy Gravdahl for recommending me to the subject of aerospace control. Without his optimism, encouragement and constructive feedback this work would clearly not have been constructed. I would also like to thank my external examiner for examining my specialization project and pointing out important shortcomings of the stability proofs. With these notes in mind, I am sure that the possibility of an approval of the article submitted to the "49th IEEE Conference on Decision and Control" is more likely. In this matter, I will once again thank Professor Gravdahl for his cooperation skills and encouragements in the procedure of submitting the scientific article which can be seen in Appendix E.

Special thanks are given to Doctor Thomas R. Krogstad. If it were not for his efforts of assembling and programming the AUVSAT, I would not have had the opportunity to test my theories. In addition, Dr. Krogstad has helped me getting familiar with the AUVSAT and showing me invaluable tips and tricks. He has also replied to every email sent, and is eager to know the progress of my work. For this, I am truly grateful.

Gratitude is also given to my fellow students for the invaluable help when unforeseen problems arose. We have several times been discussing various issues, and in most of these cases ended the dialog by solving the problems ourselves.

Finally, I would like to thank my family for their constant support and encouragement, and especially my partner Rina for her love and support, and for her patience during late nights at the office.

Trondheim, June 2010 — Ulrik Jørgensen

Contents

List of Figures

List of Tables

Abbreviations

ADC	Analog to Digital converter
AS	Asymptotically Stable
AUV	Autonomous Underwater Vehicle
AUVSAT	Autonomous Underwater Vehicle Satellite
CB	Center of Buoyancy
CG	Center of Gravity
DAC	Digital to Analog converter
DOF	Degrees of Freedom
ECEF	Earth-centered Earth-fixed
ECI	Earth-centered Inertial
GAS	Global Asymptotic Stable
IMU	Inertial Measurement Unit
LAN	Local Area Network
MRP	Modified Rodrigues Parameter
NED	North-East-Down frame
NTI	Nonlinear Time-Invariant
NTV	Nonlinear Time-Varying
OS	Operating System
PD	Proportional-Derivative
PID	Proportional-Integral-Derivative
RTOS	Real-time Operating System
RTW	Real-time workshop
RWA	Reaction wheel assembly
SM	Sliding mode
UAS	Uniformly Asymptotically Stable
UGAS	Uniformly Globally Asymptotically Stable
UGS	Uniformly Globally Stable
US	Uniformly Stable
e.g.	for example (Latin: exempli gratiā)
etc.	and so forth (Latin: Et cetera)
et al.	and others (Latin: et alii)
i.e.	in other words (Latin: id est)

Chapter 1

Introduction

1.1 Purpose

The purpose of this thesis is to design and test an attitude leader-follower synchronization scheme for the sphere shaped underwater satellite, AUVSAT. The AUVSAT is equipped with three reaction wheels that are mounted orthogonally inside the hull, which makes it possible to control the attitude of the satellite in all three degrees of freedom. The satellite has also a ballast system so that the sphere can behave like a naturally buoyant rigid body. When the underwater satellite is lowered into a water tank and submerged, it will emulate a weightless state, equal to the condition for a satellite in space. You thereby get a mixture of theories from both the aerospace and maritime literature.

In the pursuit of designing the leader-follower synchronization scheme it is essential to investigate different attitude control methods and therefore, two nonlinear controllers have been designed for single vehicle control and compared for optimality.

The first method proposed for controlling the angular velocity of the underwater satellite is a sliding mode controller. This is a well known nonlinear controller considered to be very robust and thereby practical for systems with external disturbances (Alfaro-Cid, McGookin, Murray-Smith, and Fossen, 2005). The second proposed controller is a backstepping controller. The backstepping control method is a systematic and recursive design methodology for nonlinear control where it is possible to utilize "good nonlinearities" (Khalil, 2002).

Both the sliding mode and the backstepping controller require knowledge about the angular velocity of the satellite, and in the first part of the experiments, this is given as a direct feedback from a filtered angular velocity measurement. However, in some cases it can be of interest to estimate the angular velocity instead, and hence a nonlinear observer for the angular velocity is developed for this purpose.

The system with both the sliding mode and the backstepping controller are proven to be asymptotically stable. This is also the case for the observer.

After the controllers and the observer have been developed, one is ready to design the leader-follower attitude synchronization scheme. The synchronization scheme assumes

that angular velocity measurements are not available, and the previously developed angular velocity observer is therefore implemented in both the leader and the follower satellite. In addition, a backstepping controller is implemented in the leader satellite to make sure that it tracks a mathematically given trajectory, while a similar backstepping controller is implemented in the follower to track the leader attitude. Finally, it is proved that the attitude of the leader will track the desired attitude, and the follower's attitude will converge towards the leader's attitude as time goes to infinity.

The thesis is completed by implementing the controllers, observers and the synchronizing scheme in the underwater satellite, AUVSAT, and experiments are carried out to evaluate the performance of the different systems.

1.2 Previous work

Attitude control of rigid bodies is a well researched field, and numerous text and monographs have been developed on this subject. A comprehensive introduction to the theory of spacecraft attitude dynamics can be seen in (Hughes, 1986) whereas a solid foundation of control, modeling and analyzes of spacecrafts is given by (Wie, 1998).

For controlling the attitude of a spacecraft, (Bryson, Jr., 1994) gives a good introduction, and presents popular strategies which are thorough researched and well tested. Some of the proposed methods include the use of reaction wheels, but also thrusters, and spin stabilization is evaluated for the purpose of attitude control. In (Hall, 1995) the derivation of the rigid body dynamics with one reaction wheel is presented where the differential equations are put into a non canonical Hamiltonian form. The article also indicates how to apply the result when more than one reaction wheel is needed. However this is done in (Hall, 2002), and (Tsiotras, Shen, and Hall, 2001) includes the aspect of using momentum wheels as an energy storage mechanism, providing power to the vehicle.

The proposed control schemes used for attitude control range from simple PD-regulator presented in (Wen and Kreutz-Delgado, 1991), to nonlinear regulator with reaction wheels and thrusters in (Hall, Tsiotras, and Shen, 2002). On the other hand (Fjellstad and Fossen, 1994) presents a unit quaternion feedback approach for underwater vehicles, which is an excellent reference for the maritime part of the assignment.

The specific sliding mode controller is presented in general settings in (Young, Utkin, and Ozguner, 1999) and proposed in combination with spacecraft dynamics in (Yongqiang, Xiangdong, Wei, and Chaozhen, 2008) and (Chen and Lo, 1993). A Lyapunov function candidate has been constructed to prove asymptotic stability.

For the case of backstepping controllers, numerous texts and papers exist. An excellent introduction to the backstepping control method and some area of application can be seen in (Krstić, Kanellakopoulos, and Kokotović, 1995). The backstepping algorithm has also been proposed in various spacecraft systems and an example can be seen in (Xiao, Hu, and Ma, 2010). Another is seen in (Li and Ma, 2007) and proposes an adaptive attitude backstepping controller where the attitude is parameterized using Modified Rodrigues Parameter (MRP), whereas (Hu, Friswell, Wagg, and Neild, 2009) utilizes the quaternion

parameters.

When angular velocity measurements are not available, it is a natural solution to use an observer and thereby estimate the needed angular velocities. However, (Costic, Dawson, De Queiroz, and Kapila, 2000) shows that it is possible to control the attitude of a spacecraft without using observers. The paper proposes a solution where the attitude controller is developed assuming that angular velocity is available, and then redesigning the controller such that the need of angular velocity measurements is eliminated. The proof of asymptotic attitude tracking is also presented. Nonetheless, it is of course possible to use observers for estimation of the angular velocity, and a proposed solution is presented in (Salcudean, 1991). The article is essential for most spacecrafts without angular velocity measurements and the principles have been used in many solutions. Another, slightly different observer scheme is presented in (Tayebi, 2006). This paper shows that the proposed observer is passive and maps the observer input to the estimated attitude error. It is therefore possible to design a simple linear feedback in terms of the vector part of the estimation error, to ensure asymptotic stability.

The topic of spacecraft formation flying has been investigated closely in the last couple of years. A comprehensive survey on formation flying guidance can be seen in (Scharf, Hadaegh, and Ploen, 2003) whereas a widespread survey on formation flying control can be seen (Scharf, Hadaegh, and Ploen, 2004). A solution of the attitude control problem is presented in (Ren, 2007) and the article proposes three different attitude control laws. One of them applies a passivity approach to remove the requirement for angular velocity measurements between the neighboring rigid bodies. (Krogstad, 2010), on the other hand, presents a mutual six degrees of freedom synchronization scheme for satellites actuated by means of thrusters and reaction wheels. In addition to the 6 DOF synchronization scheme, an attitude leader-follower synchronization scheme has also been developed. The paper also presents real experiments, using the AUVSAT presented in this thesis (see Section 8). However, the angular velocities are assumed to be known for both the cases.

There has also been a noticeable research in the area of spacecraft formation control when angular velocity is not present. In (Abdessameud and Tayebi, 2009) this subject has been investigated, and a synchronizing control-law independent of the angular velocity has been developed. Numerical simulation has also been carried out where four satellites are synchronized, to validate the results. (Bondhus, 2010) on the other hand, adapts the principles from (Salcudean, 1991) and develops a leader-follower synchronization scheme using backstepping control in combination with the observer presented in (Salcudean, 1991). In addition, asymptotic stability is proven for the complete system and a numerical simulation is carried out and confirms the findings.

1.3 Outline of the thesis

- **Chapter 2** - A short introduction to the theoretical background for reference frames, notations, definitions, attitude representations and rotational kinematic differential equations.

- **Chapter 3** - The derivation of equations of motions and modeling of both external and internal forces are presented in this chapter.
- **Chapter 4** - A sliding mode and a backstepping controller is developed based on calculated error dynamics. Asymptotical stability is proven for each combined controller and system.
- **Chapter 5** - A short introduction of some of the non-modeled aspects in the lab setup is presented in this chapter.
- **Chapter 6** - De deduction of the nonlinear observer for estimation of angular velocity is carried out in this chapter. The stability proof for the time-independent and time-varying case is carried out, using LaSalle's, and Matrosov's theorem, respectively.
- **Chapter 7** - Based on work presented in (Bondhus, 2010), a leader-follower attitude synchronization scheme is presented. The nonlinear observer developed in Chapter 6 is implemented for both the leader and the follower. In addition, a backstepping controller is implemented in the leader satellite to follow the mathematically given trajectory, while a similar backstepping controller is implemented in the follower to track the leader. Finally, it is proved that the leader attitude will converge towards the desired trajectory, while the follower will converge towards the leader attitude.
- **Chapter 8** - This chapter contains a short description of the hardware and software used in the AUVSAT. The description includes actuators, measurements, CPU, communication, hull design and software programs.
- **Chapter 9** - The results from the experiments with the underwater satellite are presented in this chapter. First, experiments of the system are performed with filtering of the angular velocity measurements as feedback. Two controllers, a sliding mode and a backstepping controller, are also implemented. Then, the sliding mode controller is tested in a combination with the nonlinear angular velocity observer. Finally, the synchronization scheme is tested with a leader and a follower satellite where both vehicles have the nonlinear observer implemented.
- **Chapter 10** - The results from the experiments are discussed to illustrate strength and weaknesses of the controllers, observer and synchronization scheme. In addition, thoughts of how to improve the behavior are presented.
- **Appendix A** - Some extensive calculations and derivations are presented, including the attitude dynamic error equation.
- **Appendix B** - Matrosov's stability theorem, as it is presented in (Hahn, 1967), is stated in this appendix.
- **Appendix C** - Some pictures of the AUVSAT and a sketch of the lab setup is shown in this appendix.

- **Appendix D** - Another sliding mode controller experiment is presented in this appendix. The only difference compared with the first experiment in Chapter 9 is that another set of gains have been chosen.

- **Appendix E** - The paper submitted to the 49th IEEE Conference on Decision and Control in Atlanta, USA, is presented in this appendix.

1.4 Contributions of the thesis

In the section the contributions of the work presented in this thesis are summarized.

- The preliminary theories presented in Chapter 2–3 are mostly based on previous published materials by other authors, e.g. (Egeland and Gravdahl, 2002) and (Fossen, 2002). However, the detailed deduction of the sphere-shaped satellite actuated by means of three orthogonal reaction wheels is, to the author's best knowledge, not published before.

- The sliding mode and the backstepping controller presented in Chapter 4 are also proposed and published in many variations before. However, the small section where it can be seen that the sliding mode controller has in fact finite-time convergence to the sliding manifold is a new contribution for sphere-shaped satellite control. One can thereby find an upper bound for the convergence time and utilize it for finding suitable tuning-gain values.

- In Chapter 5 it is especially the observation of the twisting effect from the Ethernet cable that can be seen as an important finding. The plots in this section clearly show that vessels with small drag forces should have wireless transmission if possible.

- The nonlinear angular velocity observer for an internally actuated satellite, shown in Chapter 6 is an important contribution to aerospace control. However, (Krogstad, 2010) have shown similar results, but the proposed solution presents the findings in an alternative way. In addition, the last proof in this chapter, showing asymptotic stability of the observer using Matrosov's theorem is new, and has not been published in this content before.

- The synchronization scheme in Chapter 7 is the main contribution of this thesis. To the author's best knowledge, a leader-follower synchronization scheme where the vehicles are internally actuated and none of the vessels have angular velocity measurements have not been published before. The findings in this chapter are therefore important and should be investigated even further.

- Chapter 9–10 are devoted for testing and validation of the earlier theoretical findings. The experiments carried out in Chapter 9 show that that the various systems behave quite good, and thereby validates the theoretical findings. However, the there are

always rooms for improvements and the discussion in Chapter 10 presents strategies and thoughts on how to improve the performance of the various systems.

- Finally, the work performed in the specialization project (Jørgensen, 2009) and during this thesis has cumulated in a scientific article submitted to the 49th IEEE Conference on Decision and Control in Atlanta, USA. The article can be seen in Appendix E and shows an excerpt of the results presented in this thesis where the scope has been on the proposed sliding mode controller in combination with the nonlinear angular velocity observer.

Chapter 2

Kinematics

In this chapter some important mathematical definitions and notations will be presented. The material is mainly taken from (Egeland and Gravdahl, 2002) and (Fossen, 2002), and is essentially the same as in (Jørgensen, 2009). However, some changes have been made for better consistency with the rest of the thesis.

This chapter presents the theory about describing the motion of a vessel without concerning the cause that provoked it. This theory, called kinematics, deals with the basic relationship between vessel velocity, vessel position and vessel orientation. Since the studied vessel can not move in a translational way, the focus of this section is the relationship between angular velocity and orientation.

The experiments takes place in a water tank, and one will thereby only need two different coordinate frames to represent the kinematics. However, since the thesis is used to simulate a satellite in space, also relevant coordinate frames for this purpose will be presented.

2.1 Reference frames

The main idea about kinematics is to describe the motions as relative to some reference frames and the following reference frames is convenient when describing satellite in 6 DOF. The first two are Earth-Centered reference frames whereas the last three are geographical reference frames. The NED reference frame is usually not used for describing satellite movement, but since the project takes place in a water tank, the NED frame is relevant for this purpose also.

2.1.1 ECI - Earth-Centered Inertial frame

This frame is a non-rotating reference frame and is assumed fixed in space. The Newton's laws of motion applies in this frame, and therefore this frame is used to evaluate the equations of motion. The origin of the ECI coordinate frame is located at the center of earth with axes x_i, y_i and z_i shown in Figure 2.1.

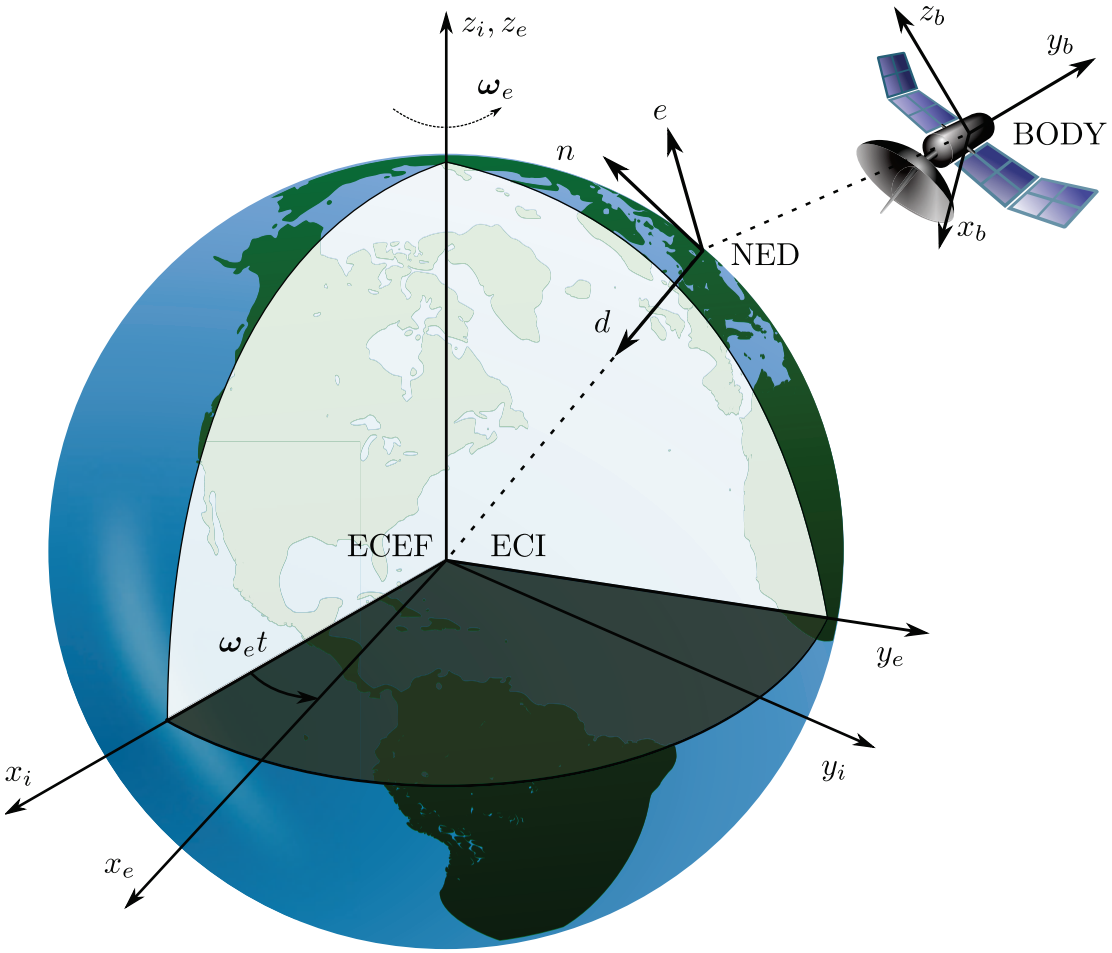

Figure 2.1: A sketch of the Earth-centered Earth-fixed (ECEF) frame, Earth-centered Inertial (ECI) frame, North-East-Down (NED) frame and the BODY reference frame.

2.1.2 ECEF - Earth-Centered Earth Fixed frame

This frame has its origin fixed to the center of earth, coinciding with the ECI-frame origin. However the axes x_e and y_e rotate relative to the ECI frame about the axis z_e with angular velocity $\omega_e = 7.2921 \cdot 10^{-5}$ rad/s as stated in (Fossen, 2002). This will make it rotate 360° about the z_e-axis for each day.

2.1.3 NED - North-East-Down frame

The North-East-Down reference frame is a geographical reference frame we refer to in our daily life. The origin is placed relative to the Earth's reference ellipsoid. The x-axis points towards true *north*, the y-axis points *East*, while the z-axis points *downwards* to the center of Earth as shown in Figure 2.1.

For vessel working in a local area, the NED reference frame can be assumed to be

inertial and thereby the Newton's laws of motion will still apply (Fossen, 2002).

2.1.4 BODY fixed frame

The body-fixed reference frame is fixed to the vessel, and the origin is usually placed in the center of gravity (CG) with the body-axis chosen to coincide with the principal axes of inertia. This is done to exploit the symmetry of the system.

2.1.5 Orbital frame

The orbital frame has the origin located at the center of gravity of the satellite. The z-axis points towards the center of Earth. The x-axis points along the orbit trajectory and is perpendicular to the vector towards the center of the orbit. If the orbit is circular, then the x-axis points in the velocity direction. The y-axis completes the right hand rule, and is thereby normal to the orbital plane.

2.2 Definitions

The following section describes some important definitions and notations used in this thesis.

2.2.1 Vectors

The vector $\vec{u}$ can be described by its magnitude $|\vec{u}|$ and its direction, and is thereby a good representation for forces, torques, velocities, acceleration etc. If the Cartesian coordinate frame a is defined by the orthogonal unit vectors $\vec{a}_1$, $\vec{a}_2$ and $\vec{a}_3$, then the vector, denoted $\mathbf{u}^a$, can be expressed in the reference frame a by a 3×1 matrix. Such a vector is called a *column vector* and must be distinguished from the *coordinate free* vector $\vec{u}$.

Definition 2.1. *The column vector* $\mathbf{u}^a$ *with respect to the reference frame a, is defined by*

$$\mathbf{u}^a \triangleq \begin{bmatrix} u_1 \\ u_2 \\ u_3 \end{bmatrix}, \tag{2.1}$$

where the components u_i *is the scalar product between* $\vec{u}$ *and the unit vectors* $\vec{a}_i$ *of the reference frame a as*

$$u_i = \vec{u} \cdot \vec{a}_i, \quad i \in \{1, 2, 3\}. \tag{2.2}$$

The *coordinate free* vector $\vec{u}$ can be expressed as a linear combination of the orthogonal vectors $\vec{a}_1$, $\vec{a}_2$ and $\vec{a}_3$ by

$$\vec{u} = u_1\vec{a}_1 + u_2\vec{a}_2 + u_3\vec{a}_3, \tag{2.3}$$

where the components u_i are the same as in Equation (2.2).

2.2.2 Vectorial notation used in the thesis

We define the three coordinate systems $\{a\}$, $\{b\}$ and $\{c\}$ with the origin o_a, o_b and o_c, respectively. Then the following notations for angular velocity, vectors, scalars and matrices will be used in this paper:

- $\boldsymbol{\omega}_{ab}^{c}$ is the angular velocity of $\{b\}$ relative to the $\{a\}$-frame decomposed in the $\{c\}$-frame. If the sub- and superscript is left out, it means that the angular velocity $\boldsymbol{\omega}$ is the angular velocity of the BODY-frame relative the NED-frame expressed in the BODY coordinate system, i.e. $\boldsymbol{\omega}_{nb}^{b}$.
- $\mathbf{v}^a$ is a three-dimensional vector decomposed in the $\{a\}$-frame. When the superscript is left out, it is assumed that the vector is decomposed in the BODY-frame.
- $k \in \mathbb{R}$ is a scalar and is in general written with non-bold letters.
- $\mathbf{A} \in \mathbb{R}^{m \times n}$ is a matrix and i expressed using bold fonts. The scalars $m, n \geq 2$.

2.2.3 Vector cross product

The cross product with reference to the Cartesian frame a can be evaluated from

$$\vec{u} \times \vec{v} = \begin{vmatrix} \vec{a}_1 & \vec{a}_2 & \vec{a}_3 \\ u_1 & u_2 & u_3 \\ v_1 & v_2 & v_3 \end{vmatrix}. \tag{2.4}$$

To evaluate the cross product between the two column vectors, the skew symmetric matrix operator $\mathbf{S}(\,\cdot\,)$ is defined.

Definition 2.2. *The Skew-symmetric cross product matrix*

$$\mathbf{S}(\vec{u}) \triangleq \begin{bmatrix} 0 & -u_3 & u_2 \\ u_3 & 0 & -u_1 \\ -u_1 & u_1 & 0 \end{bmatrix}, \tag{2.5}$$

where u_i is given by Equation (2.2)*.*

By using the skew-symmetric operator the cross product in Equation (2.4) can be evaluated by an ordinary matrix product as

$$\vec{u} \times \vec{v} = \mathbf{S}(\mathbf{u})\mathbf{v} = \begin{bmatrix} 0 & -u_3 & u_2 \\ u_3 & 0 & -u_1 \\ -u_2 & u_1 & 0 \end{bmatrix} \begin{bmatrix} v_1 \\ v_2 \\ v_3 \end{bmatrix}, \tag{2.6}$$

where u_i and v_i are the same as in previous notation.

The skew-symmetric cross product matrix has some nice properties. If $\mathbf{x}$ and $\mathbf{y}$ are vectors $\in \mathbb{R}^{3\times 1}$, α and β are scalars, then some of the properties of the skew-symmetric cross product matrix can be shown:

- $\mathbf{S}(-\mathbf{x}) = -\mathbf{S}(\mathbf{x})$.
- $\mathbf{S}(\mathbf{x}) + \mathbf{S}(\mathbf{x})^T = \mathbf{0}$.
- $\mathbf{S}(\mathbf{x})\mathbf{x} = \mathbf{0}$.
- $\mathbf{x}^T\mathbf{S}(\mathbf{y})\mathbf{x} = 0$.
- $\mathbf{S}(\mathbf{x})\mathbf{y} = -\mathbf{S}(\mathbf{y})\mathbf{x}$.
- $\mathbf{S}(\alpha\mathbf{x} + \beta\mathbf{y}) = \alpha\mathbf{S}(\mathbf{x}) + \beta\mathbf{S}(\mathbf{y})$.

2.3 Rotation matrix

To describe the attitude of a rigid body, the rotation matrix is essential, and some of the properties of the rotation matrix are stated in this section.

Since the dynamic model of a satellite can be expressed in several different coordinate frames, a way to convert between them is needed. This can be done by introducing the coordinate transformation from frame b to a, given by

$$\mathbf{v}^a = \mathbf{R}_b^a \mathbf{v}^b, \tag{2.7}$$

where

$$\mathbf{R}_b^a = \{\vec{a}_i \cdot \vec{b}_j\} \tag{2.8}$$

is called the rotation matrix from a to b. The elements $r_{ij} = \vec{a}_i \cdot \vec{b}_j$ of the rotation matrix $\mathbf{R}_b^a$ are called the direction cosines.

2.3.1 Properties of the rotation matrix

It has been shown that the rotation matrix from a to b, $\mathbf{R}_b^a$ is orthogonal and satisfies

$$\mathbf{R}_a^b = (\mathbf{R}_b^a)^{-1} = (\mathbf{R}_b^a)^T. \tag{2.9}$$

The rotation matrix $\mathbf{R}_b^a$ has two interpretations:

1. If two vectors $\mathbf{v}^b$ and $\mathbf{v}^a$ are expressed in b and a, then $\mathbf{R}_b^a$ transforms the coordinate vector in b to the coordinate vector in a according to Equation (2.7) and $\mathbf{R}_b^a$ acts as a coordinate transformation matrix.
2. If the vector $\mathbf{p}^a$ in a is rotated to the vector $\mathbf{q}^b = \mathbf{p}^a$ by Equation (2.10), then $\mathbf{R}_b^a$ acts as a pure rotation matrix.
$$\mathbf{q}^a = \mathbf{R}_b^a \mathbf{p}^a. \tag{2.10}$$

It is also proven that the determinant of the rotation matrix, $\det(\mathbf{R}) = 1$ and one can thereby introduce the set $SO(3)$ where $\mathbf{R}$ is a member, that is,

$$SO(3) = \{\mathbf{R} | \mathbf{R} \in \mathbb{R}^{3\times 3},\ \mathbf{R}^T\mathbf{R} = \mathbf{I} \ \text{ and } \ \det \mathbf{R} = 1\}, \tag{2.11}$$

where $\mathbf{I}$ is the 3×3 identity matrix.

2.3.2 Composite rotations

A rotation from frame a to frame c can be split into two rotations. The first by a rotation from frame a to b, and then followed by a rotation from frame b to c:

$$\mathbf{R}_c^a = \mathbf{R}_b^a \mathbf{R}_c^b. \tag{2.12}$$

2.4 Attitude representation

As stated before, the rotation matrix can act as a pure rotation and thereby represent the attitude of the satellite relative to the initial reference frame. Since the rotation matrix is a 3×3 matrix, it needs nine elements to be fulfilled. This is not computational effective, but luckily most of the elements in the rotational matrix are dependent and can thereby be presented with less than nine parameters.

In this section three of the most popular parameterizations of the rotation matrix are described; the Euler angles, the angle axis and the unit quaternion. The two first are briefly explained, whereas the latter is presented thoroughly. The reason for presenting the Euler angles and the angle axis is because they are very popular and/or make up fundamental principles for the quaternion representation. The section is completed with a discussion to evaluate the different parameterizations.

2.4.1 Euler angles

The Euler angles $\mathbf{\Theta} = \begin{bmatrix} \phi & \theta & \psi \end{bmatrix}^T$ is a three element representation of the rotation matrix. The three elements in $\mathbf{\Theta}$ are called the roll-, pitch- and yaw angle (Fossen, 2002). The rotation matrix can be considered as a composite rotation consisting of ϕ degree rotation about the z-axis, θ degree rotation about the current y-axis and finally ψ degree rotation about the current x-axis. This is shown in Equation (2.13)

$$\mathbf{R}(\mathbf{\Theta}) = \mathbf{R}_z(\phi)\mathbf{R}_y(\theta)\mathbf{R}_x(\psi), \tag{2.13}$$

where $\mathbf{R}_z(\phi)$, $\mathbf{R}_y(\theta)$ and $\mathbf{R}_x(\psi)$ are "simple rotations"(Egeland and Gravdahl, 2002) about the z, y and x axis, respectively.

The Euler angles is an intuitive way of describing rotations, and thereby very popular. One great drawback with the Euler angle representation is that it is singular for $\theta = \pm\frac{\pi}{2}$. This is an inconvenience for satellites, and the Euler angle representation is thereby not a useful alternative for the sphere-shaped vessel.

2.4.2 Angle axis parameter

Every rotation can be viewed as a rotation θ about an arbitrary axis $\vec{k}$. This is referred to as an angle-axis parameterization and the rotation matrix $\mathbf{R}_k(\theta)$ can be expressed as

$$\mathbf{R}_k(\theta) \triangleq \cos\theta\mathbf{I} + \mathbf{S}(\mathbf{k})\sin\theta + \mathbf{k}\mathbf{k}^T(1 - \cos\theta), \tag{2.14}$$

where $\mathbf{I}$ is the 3×3 identity matrix, $\mathbf{S}(\cdot)$ is the skew-symmetric cross product matrix and $\mathbf{k}$ is the unit column vector of $\vec{k}$.

2.4.3 Unit Quaternion

Unit quaternion is a four parameter representation for the rotation matrix, and the motivation for having this alternative method is to avoid the singularities that can occur when using Euler angles. A unit quaternion is defined with one real part η and three imaginary parts given by the vector $\boldsymbol{\epsilon} = \begin{bmatrix} \epsilon_1 & \epsilon_2 & \epsilon_3 \end{bmatrix}^T$ and expressed in one combined vector.

Definition 2.3. *The unit quaternion attitude representation with real part η and imaginary part $\boldsymbol{\epsilon}$ is defined by the angle axis parameters $\mathbf{k}$ and θ as*

$$\eta = \cos(\frac{1}{2}\theta), \tag{2.15a}$$

$$\boldsymbol{\epsilon} = \mathbf{k}\sin(\frac{1}{2}\theta), \tag{2.15b}$$

and combined in one vector $\mathbf{q}$ as

$$\mathbf{q} \triangleq \begin{bmatrix} \eta & \epsilon_1 & \epsilon_2 & \epsilon_3 \end{bmatrix}^T = \begin{bmatrix} \eta & \boldsymbol{\epsilon}^T \end{bmatrix}^T. \tag{2.16}$$

The unit quaternion must satisfy the unit condition:

$$\mathbf{q}^T\mathbf{q} = \eta^2 + \boldsymbol{\epsilon}^T\boldsymbol{\epsilon} = \eta^2 + \epsilon_1^2 + \epsilon_2^2 + \epsilon_3^2 \equiv 1. \tag{2.17}$$

The rotation matrix $\mathbf{R}_e$ parameterized by the unit quaternion can be stated as (Egeland and Gravdahl, 2002):

$$\mathbf{R}_e(\eta, \boldsymbol{\epsilon}) = \mathbf{I} + 2\eta\mathbf{S}(\boldsymbol{\epsilon}) + 2\mathbf{S}(\boldsymbol{\epsilon})\mathbf{S}(\boldsymbol{\epsilon}), \tag{2.18a}$$

$$= \begin{bmatrix} 1 - 2(\epsilon_2^2 + \epsilon_3^2) & 2(\epsilon_1\epsilon_2 - \epsilon_3\eta) & 2(\epsilon_1\epsilon_3 + \epsilon_2\eta) \\ 2(\epsilon_1\epsilon_2 + \epsilon_3\eta) & 1 - 2(\epsilon_1^2 + \epsilon_2^2) & 2(\epsilon_2\epsilon_3 + \epsilon_1\eta) \\ 2(\epsilon_1\epsilon_3 + \epsilon_2\eta) & 2(\epsilon_2\epsilon_3 + \epsilon_1\eta) & 1 - 2(\epsilon_1^2 + \epsilon_2^2) \end{bmatrix}, \tag{2.18b}$$

where $\mathbf{I}$ is the 3×3 identity matrix and $\mathbf{S}(\cdot)$ is the skew-symmetric cross product matrix.

Composite rotations with quaternions

To introduce composite rotations, expressed using quaternions, it is necessary to introduce the quaternion multiplication. Quaternion multiplication is distributive and associative, but not commutative. This means in general, that $\mathbf{q}_1 \otimes \mathbf{q}_2 \neq \mathbf{q}_2 \otimes \mathbf{q}_1$. The quaternion product is denoted $\otimes$ and defined as in Definition 2.4.

Definition 2.4. *The quaternion product between the two quaternions $\mathbf{q}_1 = \begin{bmatrix} \eta_1 & \boldsymbol{\epsilon}_1^T \end{bmatrix}^T$ and $\mathbf{q}_2 = \begin{bmatrix} \eta_2 & \boldsymbol{\epsilon}_2^T \end{bmatrix}^T$ is defined as*

$$\mathbf{q}_1 \otimes \mathbf{q}_2 = \begin{bmatrix} \eta_1\eta_2 - \boldsymbol{\epsilon}_1^T\boldsymbol{\epsilon}_2 \\ \eta_2\boldsymbol{\epsilon}_1 + \eta_1\boldsymbol{\epsilon}_2 + \mathbf{S}(\boldsymbol{\epsilon}_1)\boldsymbol{\epsilon}_2 \end{bmatrix} = \begin{bmatrix} \eta_1 & -\boldsymbol{\epsilon}_1^T \\ \boldsymbol{\epsilon}_1 & \eta_1\mathbf{I} + \mathbf{S}(\boldsymbol{\epsilon}_1) \end{bmatrix} \mathbf{q}_2, \tag{2.19}$$

where $\mathbf{S}(\cdot)$ is the skew-symmetric cross product matrix.

Let $\mathbf{R}_c^a = \mathbf{R}_b^a \mathbf{R}_c^b$ as shown in Section 2.3.2. Then, let the quaternions $\mathbf{q}_{ac}$, $\mathbf{q}_{ab}$ and $\mathbf{q}_{bc}$ correspond to the respective rotation matrices. It can then be seen that:

$$\mathbf{q}_{ac} = \mathbf{q}_{ab} \otimes \mathbf{q}_{bc}, \tag{2.20}$$

and quaternion multiplication thereby corresponds to rotation matrix multiplication.

Also inverting a quaternion works in much the same way as for rotation matrices. For a unit quaternion $\mathbf{q} = \begin{bmatrix} \eta & \boldsymbol{\epsilon}^T \end{bmatrix}^T$ the following relationship always holds:

$$\mathbf{q} \otimes \mathbf{q}^{-1} = \mathbf{q}^{-1} \otimes \mathbf{q} = \mathbf{1}_q, \tag{2.21}$$

where $\mathbf{1}_q = \begin{bmatrix} 1 & \mathbf{0}^T \end{bmatrix}^T$ and $\mathbf{q}^{-1} = \begin{bmatrix} \eta & -\boldsymbol{\epsilon}^T \end{bmatrix}^T$ is called the complex-conjugate of $\mathbf{q}$.

2.5 Rotational kinematic differential equations

In this section the differential equations for the rotation matrix and the unit quaternion are presented. Derivation from the rotational matrix forms the basis for the quaternion-differential equations.

2.5.1 Rotation matrix

The time derivative of the rotation matrix can most easily be calculated based on the relationship $(\mathbf{R}_b^a)(\mathbf{R}_b^a)^T = \mathbf{I}$ from Equation (2.11) and taking the time derivative on both sides;

$$\begin{aligned} \frac{\mathrm{d}}{\mathrm{d}t}\left[(\mathbf{R}_b^a)(\mathbf{R}_b^a)^T\right] &= \frac{\mathrm{d}}{\mathrm{d}t}\mathbf{I}, \\ (\dot{\mathbf{R}}_b^a)(\mathbf{R}_b^a)^T + (\mathbf{R}_b^a)(\dot{\mathbf{R}}_b^a)^T &= \mathbf{0}, \end{aligned}$$

and it can thereby be seen that $(\dot{\mathbf{R}}_b^a)(\mathbf{R}_b^a)^T$ is skew symmetric.

Any 3×3 skew symmetric matrix can be formed by a 3×1 vector, and this is also the case for $(\dot{\mathbf{R}}_b^a)(\mathbf{R}_b^a)^T$. It turns out that this vector actually is the *angular velocity* vector of frame b relative to frame a decomposed in frame a (Egeland and Gravdahl, 2002). This gives us the kinematic differential equation of the rotation matrix:

$$\dot{\mathbf{R}}_b^a = \mathbf{S}(\boldsymbol{\omega}_{ab}^a)\mathbf{R}_b^a, \tag{2.22}$$

or by using the coordinate transformation rule, an alternative representation is given as:

$$\dot{\mathbf{R}}_b^a = \mathbf{R}_b^a \mathbf{S}(\boldsymbol{\omega}_{ab}^b). \tag{2.23}$$

2.5.2 Unit Quaternion

The derivation of the kinematic differential equations for the unit quaternion is quite complex, as can be seen in (Egeland and Gravdahl, 2002). Therefore the calculation is left out in this paper and only the result for the kinematic differential equation in vector form is presented:

$$\dot{\mathbf{q}} = \begin{bmatrix} \dot{\eta} & \dot{\boldsymbol{\epsilon}}^T \end{bmatrix}^T, \tag{2.24a}$$

$$= \frac{1}{2} \begin{bmatrix} -\boldsymbol{\epsilon}^T \\ \eta\mathbf{I} - \mathbf{S}(\boldsymbol{\epsilon}) \end{bmatrix} \boldsymbol{\omega}^a, \tag{2.24b}$$

$$= \frac{1}{2} \begin{bmatrix} -\boldsymbol{\epsilon}^T \\ \eta\mathbf{I} + \mathbf{S}(\boldsymbol{\epsilon}) \end{bmatrix} \boldsymbol{\omega}^b, \tag{2.24c}$$

where $\mathbf{I}$ is the 3×3 identity matrix, $\mathbf{S}(\,\cdot\,)$ is the skew-symmetric cross product matrix, $\boldsymbol{\omega}^i$ is the angular velocity decomposed in frame i, for $i \in \{a, b\}$.

Another representation for the quaternion differential equations can be seen in (Bondhus, 2010). This representation utilizes the quaternion product and defines an "angular velocity-quaternion". The representation is compact in its writing and is therefore suited when expressions becomes long and complicated.

Definition 2.5. *For an angular velocity $\boldsymbol{\omega}$, the angular velocity-quaternion $[\boldsymbol{\omega}]_q$ is defined as the quaternion with real part equal to zero, and the imaginary part equal to $\boldsymbol{\omega}$, such that:*

$$[\boldsymbol{\omega}]_q \triangleq \begin{bmatrix} 0 & \boldsymbol{\omega}^T \end{bmatrix}^T. \tag{2.25}$$

In the literature $[\boldsymbol{\omega}]_q$ is also called a "pure quaternion".

The kinematic differential equations in terms of the quaternion $\mathbf{q}_{ab}$, that corresponds to the rotation matrix $\mathbf{R}_b^a$, can then be written as:

$$\dot{\mathbf{q}}_{ab} = \frac{1}{2}[\boldsymbol{\omega}_{ab}^a]_q \otimes \mathbf{q}_{ab}, \tag{2.26a}$$

$$= \frac{1}{2}\mathbf{q}_{ab} \otimes [\boldsymbol{\omega}_{ab}^b]_q, \tag{2.26b}$$

where $\boldsymbol{\omega}_{ab}^i$ is the angular velocity of frame b relative to frame a, decomposed in frame i, for $i \in \{a, b\}$.

Remark 2.1. Note that the norm $||[\boldsymbol{\omega}]_q||$ of the angular velocity-quaternion in Definition 2.5 is in general *not* equal 1.

2.6 Discussion about choice of attitude parameterization

Using quaternions as attitude representation has some advantages compared to other representations. The most important property is that the representation is not singular for

any global attitude. It is therefore a popular and frequently used attitude representation in the literature of spacecraft and satellites. Another important fact is that rotation matrix parameterized by the unit quaternion is more computational efficient, since it does not contain any trigonometric functions. This makes it attractive for applications with limited computational resources, which often are the case for small satellites.

There are also some drawbacks with this choice of orientation representation. First of all, unit quaternion needs four parameters in stead of the minimum three parameters. This implies that quaternions do have to satisfy a constraint. This constraint can be seen in Equation (2.17) and one need to make sure that this "unit constraint" is satisfied at all time. In addition, the unit quaternion also suffers from a less intuitive representation compared to Euler angles. More importantly though, unit quaternion is not uniquely defined (Owen, 2009). Even though the physical interpretation of the two attitudes $\mathbf{q}$ and $-\mathbf{q}$ is the same, they are not the same mathematically. This introduces a problem since one usually will get two equilibrium-points, and it is therefore not possible to show global stability result. This is, among others, pointed out in (Fjellstad, 1994), (Wen and Kreutz-Delgado, 1991) and (Egeland and Godhavn, 1994).

There are also other orientation parameterizations, each with advantages and disadvantages (Bauchau and Trainelli, 2009), (Diebel, 2006), but since the unit quaternion does not suffer from singularities and is widely used in the satellite literature, we choose the unit quaternion as the orientation representation for the rest of this thesis.

Chapter 3

Kinetics

In this chapter the kinetic concept will be introduced and the equations of motions for the complete system will be derived. In addition, external forces like gravity and damping, are considered.

The motion of a body consists of rigid translations and rotations, and the theory of kinetics describes the relationship between these motions and its causes. The kinetic quantities associated with translations are forces, whereas rotations are associated with torques. Since the satellite only has actuators that can rotate the vessel, only the relationship between rotations and torques is studied in detail in this paper.

The section starts by introducing some of the internal and external torques, before the chapter is ended with the deduction of the system equations.

3.1 Internal torques - Reaction wheels

The given AUVSAT is sphere shaped and equipped with three reaction wheels that are placed orthogonally inside the sphere, with one wheel along each axis. This gives the theoretical possibility of controlling the vessel's attitude in three degrees of freedom.

A reaction wheel is essentially a rotor with a motor attached, where the motor can be controlled. The motor has relatively high inertia and can thereby provide and absorb momentum to and from the surroundings. The overall angular momentum of the satellite does not change, and therefore the reaction wheel is often referred as a momentum exchange device (Krogstad, 2005). The amount of torque that is provided is dependent of the motor and the size of the rotor, and is often in the range between 0.01 Nm to 1 Nm. For this specific case, each reaction wheel assembly (RWA) can produce torques up to 0.358 Nm in loaded condition. It is also common to implement more than three RWA's for better performance and redundancy, but this is not the case for the given implementation.

3.2 External forces

A marine vessel moving through a fluid will be subject to external forces and moment. The most obvious external force is drag, but also gravity and buoyancy will affect the sphere. We start by investigating the gravity and buoyancy effect.

3.2.1 Gravity

The origin of the BODY frame is placed in the center of gravity and we can define the vector $\mathbf{r}_b^b = \begin{bmatrix} x_b & y_b & z_b \end{bmatrix}^T$ as the vector in 3 DOF, expressed in BODY coordinates, from CG to the center of buoyancy (CB).

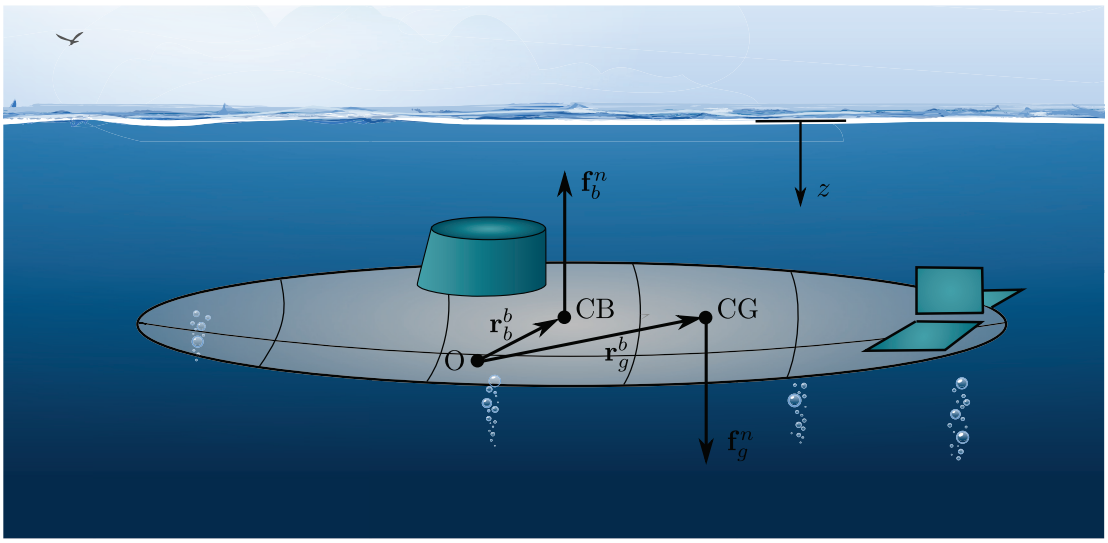

Figure 3.1: Gravity and buoyancy forces acting on a submerged submarine.

To calculate the buoyancy and gravity forces we start by defining the gravity and buoyancy forces like in Figure 3.1. $\mathbf{f}_g^b$ will act through the center of gravity and $\mathbf{f}_b^b$ will act through the center of buoyancy. According to (Society of Naval Architects and Marine Engineers, 1950) notation, the gravity force $\mathbf{f}_g^n$ and the buoyancy force $\mathbf{f}_b^n$ will be defined in the inertial NED-frame as

$$\mathbf{f}_g^n = \begin{bmatrix} 0 & 0 & mg \end{bmatrix}^T, \tag{3.1}$$

$$\mathbf{f}_b^n = -\begin{bmatrix} 0 & 0 & \rho g \nabla \end{bmatrix}^T, \tag{3.2}$$

where m is the mass of the sphere, $g = 9.81\ \mathrm{m/s^2}$ is the gravity constant, $\rho = 1000\ \mathrm{kg/m^3}$ is the mass density of water and ∇ is the submerged volume of the vessel.

The following calculations will be derived in all 6 DOF to demonstrate some results, but it will be seen that we only need 3 DOF, given some assumptions.

Translational movement

The translational movement of the vessel due to gravity and buoyancy can be stated as

$$\mathbf{M}\mathbf{a}^b = \mathbf{f}_g^b + \mathbf{f}_b^b, \tag{3.3a}$$

$$= \mathbf{R}_n^b \left(\mathbf{f}_g^n + \mathbf{f}_b^n\right), \tag{3.3b}$$

where $\mathbf{a}^b$ is the acceleration of the vessel in BODY coordinates, $\mathbf{M}$ is the mass matrix of the sphere, and $\mathbf{R}_n^b$ is the rotation matrix that rotates the n-frame to the b-frame.

The satellite sphere is equipped with a ballast tank. This ballast tank can pump the surrounding water in or out of the sphere, and thereby change the mass of the satellite. This can be exploited to balance the mass to be equal $\rho\nabla$ and thereby making the force sum $\mathbf{f}_g^n + \mathbf{f}_b^n = \mathbf{0}$. If this is the case, then the sphere is called *naturally buoyant* and as long as the initial translational movement is zero, then the satellite will stay in its starting point all the time. If we assume this is fulfilled, we can thereby ignore the translational movement of the satellite and only investigate the rotational movement.

Rotational movement

The moment $\mathbf{T}_g$ applied to the system due to gravity and buoyancy can be stated as

$$\mathbf{T}_g = \mathbf{r}_g^b \times \mathbf{f}_g^b + \mathbf{r}_b^b \times \mathbf{f}_b^b, \tag{3.4a}$$

$$= \mathbf{r}_g^b \times (\mathbf{R}_n^b \mathbf{f}_g^n) + \mathbf{r}_b^b \times (\mathbf{R}_n^b \mathbf{f}_b^n), \tag{3.4b}$$

where $\mathbf{R}_n^b$ is the rotation matrix that rotates the force vectors $\mathbf{f}_g^n$ and $\mathbf{f}_b^n$ to the BODY frame and $\mathbf{r}_g^b$ is the vector from the origin to the center of gravity expressed in BODY coordinates.

Since the origin is placed in the center of gravity, $\mathbf{r}_g^b = \mathbf{0}$, simplifying the expression for $\mathbf{T}_g$. Using one of the properties of the rotation matrix shown in Equation (2.9), it can also be seen that $\mathbf{R}_n^b = (\mathbf{R}_b^n)^T$ where $\mathbf{R}_b^n = \mathbf{I} + 2\eta\mathbf{S}(\boldsymbol{\epsilon}) + 2\mathbf{S}(\boldsymbol{\epsilon})\mathbf{S}(\boldsymbol{\epsilon})$ and (Egeland and Gravdahl, 2002) have proven that $(\mathbf{R}_b^n)^T = \mathbf{R}(\eta, -\boldsymbol{\epsilon})$ giving the simplest form of $\mathbf{T}_g$ as

$$\mathbf{T}_g = \mathbf{r}_b^b \times (\mathbf{R}^T \mathbf{f}_b^n), \tag{3.5}$$

with $\mathbf{R}^T = \mathbf{R}(\eta, -\boldsymbol{\epsilon}) = \mathbf{I} - 2\eta\mathbf{S}(\boldsymbol{\epsilon}) + 2\mathbf{S}(\boldsymbol{\epsilon})\mathbf{S}(\boldsymbol{\epsilon})$, and $\mathbf{f}_b^n = -\begin{bmatrix} 0 & 0 & \rho g \nabla \end{bmatrix}^T$.

Notice that in the design of the sphere satellite it has been attempted to place the center of gravity in the same position as the center of buoyancy. If this has been perfectly performed, then $\mathbf{T}_g = \mathbf{0}$ and the system will not be affected by torques due to gravity and buoyancy at all. Unfortunately this is not the case and even though $\mathbf{r}_b^b$ is small, $\mathbf{r}_b^b \neq \mathbf{0}$, and the system will thus be exposed to momentum due to gravity and buoyancy.

Gravity gradient for satellite in space

Our satellite is supposed to emulate real satellites in space. It is therefore of interest to investigate the similarities and differences between gravity experienced for the sphere submerged in water with the gravity field influencing satellites in space.

The gravitational force field in space is due to the gravitational forces that act between every element in the universe. The gravitational forces that act between two of the elements is a function of the element's masses and the square of the distance between them and is thereby non uniform. This means that any satellite that is not symmetrical in all three degrees of freedom will experience a torque about its center of mass. The expression for the torque $\mathbf{T}_g^*$ can, with some simplifications and assumptions (Krogstad, 2005), be expressed as

$$\mathbf{T}_g^* = 3\left(\frac{\mu}{R_c^3}\right)\vec{z} \times \vec{L}\vec{z}, \tag{3.6}$$

where μ is the gravitational constant for the primary celestial body, R_c is the distance between mass centers of the two bodies, $\vec{z}$ is the nadir pointing vector and $\vec{L}$ is the inertia matrix.

If we decompose Equation (3.6) in the BODY frame we get the following expression

$$\mathbf{T}_g^* = 3\left(\frac{\mu}{R_c^3}\right)\mathbf{z}^b \times \mathbf{L}\mathbf{z}^b, \tag{3.7}$$

where $\mathbf{z}^b = \mathbf{R}_n^b \begin{bmatrix} 0 & 0 & 1 \end{bmatrix}^T$ and $\mathbf{L}$ is the inertia matrix.

The expression for the torque due to gravity for the sphere submerged in water, shown in Equation (3.5), can be re-written as

$$\mathbf{T}_g = C\mathbf{r}_b^b \times \mathbf{z}^b, \tag{3.8}$$

where $C = \rho g \nabla$ is a constant. It can thereby be seen that the expression for the torque experienced by a sphere submerged in water is quite similar with the expression for a non-symmetrical satellite in space.

3.2.2 Drag

Drag is another external force that will affect the satellite submerged in water. This might be the biggest conceptual difference between a satellites circling in space compared to a vehicle submerged in water. A satellite operating in space will have almost no drag at all, but a vessel moving in water can potentially experience high drag forces. This makes it interesting to investigate the subject closer.

A normal way of modeling the drag forces due to vortex shedding for a marine vessel moving in a viscous fluid, is by the formula:

$$f(U) = -\frac{1}{2}\rho C_D(R_e) A |U| U, \tag{3.9}$$

where U is the speed of the vessel, A is the projected cross-sectional area under water, ρ is the density of water and $C_D(R_e)$ is the drag-coefficient as a function of the *Reynolds number*:

$$R_e = \frac{UD}{\nu}, \tag{3.10}$$

where ν is the kinematic viscosity coefficient and D is the diameter of the body (Fossen, 2002). The drag coefficient C_D is also dependent of the surface roughness, where a smooth surface has a small drag coefficient and a rough surface has a bigger drag coefficient value. It is therefore a complex task to derive an acceptable value for the drag coefficient C_D.

Nevertheless, experiments were carried out in the pursuit of finding suitable drag coefficients and an open-loop setup with a commanded constant torque-level about the z-axis were performed. The main idea was to assume that rotation about the x and y-axes were going to be insignificant and only rotation about the z-axis could be considered. Then, one could use the measurements of the angular velocity about the z-axis and curve-fit the measured result with the model seen in Equation (3.9). One could thereby find a suitable drag-coefficient for the satellite about the z-axis, and due to symmetry, it is most likely that the coefficient also would be appropriate for the x and y-axes.

Unfortunately, this turned out to be a difficult task to perform due to several reasons. The main reason was the problem experienced with the transmission wire between the computer host and the submerged target. The force from the twisting effect of the cable was clearly higher than the drag force, making it difficult to find suitable coefficient values (see Section 5.1). In addition, another unforeseen problem arisen. Due to the non-perfectly balanced satellite, it turned out that angular velocity about the x and y-axes became noticeable, and thereby influencing the experiment. A final problem arises due to the fact that it is not possible to know the actual torque provided to the reaction wheels. In the given setup, one commands a given torque value, but the actual used torque is however unknown.

All these inconveniences made it hard to find appropriate drag-coefficients. However, the experiments indicate that the actual drag-forces are small, and can probably be approximated to be neglected. This is also assumed for the remaining part of the thesis.

3.3 Angular dynamic equations

The rigid body kinetics for the satellite is now to be derived for a BODY reference frame for which the origin is placed in the center of gravity (CG). Euler's second axiom can be used to calculate the angular dynamics of the vessel and is stated in Equation (3.11a)–(3.11b):

$$\dot{\vec{h}} \triangleq \vec{m}, \tag{3.11a}$$

$$\vec{h} = L\vec{\omega}, \tag{3.11b}$$

where $\vec{h}$ is the angular momentum, L is the inertia tensor with respect to CG, and $\vec{m}$ is the external moments applied to the system.

The complete system can be considered as two combined systems; the wheel system, and the total system. The total system angular momentum $\mathbf{W}$ can be expressed as a sum of the angular momentum due to the total satellite system, and the wheel system:

$$\mathbf{W} = \mathbf{J}\boldsymbol{\omega} + \mathbf{J}_w\boldsymbol{\Omega}, \tag{3.12}$$

where $\mathbf{J}$ is the total moment of inertia, $\mathbf{J}_w$ is the inertia matrix for the wheel system and $\boldsymbol{\Omega} = \begin{bmatrix} \Omega_1 & \Omega_2 & \Omega_3 \end{bmatrix}^T$ is the vector that consist of the wheel velocities.

Remark 3.1. Notice that the total moment of inertia matrix $\mathbf{J}$ is symmetric (Fossen, 2009), meaning $\mathbf{J} = \mathbf{J}^T$, and the inertia matrix of the wheels $\mathbf{J}_w$ is diagonal.

The angular momentum $\mathbf{H}$ for the wheels can be expressed as:

$$\mathbf{H} = \mathbf{J}_w \left(\boldsymbol{\omega} + \boldsymbol{\Omega} \right), \tag{3.13}$$

By using Equation (3.11a) you get the following set of equations:

$$\frac{{}^n\mathrm{d}}{\mathrm{d}t} \left(\mathbf{W} \right) = \mathbf{T}_{ex}^n, \tag{3.14a}$$

$$\frac{\mathrm{d}}{\mathrm{d}t} \left(\mathbf{H} \right) = \mathbf{T}_u, \tag{3.14b}$$

where $\mathbf{T}_{ex}^n$ it the external moments applied to the system and $\mathbf{T}_u$ is the torque applied to the wheels form the motors and thereby our control variable. Notice that Equation (3.14a) is expressed in the NED frame, which is an inertial frame. By using Equation (3.14a) and derive (3.12) with respect to the inertial n frame, you get the following expression:

$$\begin{aligned} \frac{{}^n\mathrm{d}}{\mathrm{d}t}(\mathbf{W}) &= \frac{{}^b\mathrm{d}}{\mathrm{d}t}(\mathbf{J}\boldsymbol{\omega}_{nb}^b) + \boldsymbol{\omega}_{nb}^b \times (\mathbf{J}\boldsymbol{\omega}_{nb}^b) + \frac{{}^b\mathrm{d}}{\mathrm{d}t}(\mathbf{J}_w\boldsymbol{\Omega}) + \boldsymbol{\omega}_{nb}^b \times (\mathbf{J}_w\boldsymbol{\omega}_{nb}^b), \\ &= \mathbf{J}\dot{\boldsymbol{\omega}}_{nb}^b + \mathbf{J}_w\dot{\boldsymbol{\Omega}} + \mathbf{S}(\boldsymbol{\omega}_{nb}^b)\mathbf{W}, \end{aligned}$$

which gives the following relationship:

$$\mathbf{J}\dot{\boldsymbol{\omega}} + \mathbf{J}_w\dot{\boldsymbol{\Omega}} = -\mathbf{S}(\boldsymbol{\omega})\mathbf{W} + \mathbf{T}_{ex}. \tag{3.15}$$

If we now concentrate about Equation (3.14b), we get that

$$\begin{aligned} \mathbf{J}_w(\dot{\boldsymbol{\omega}} + \dot{\boldsymbol{\Omega}}) &= \mathbf{T}_u, \\ \Rightarrow \mathbf{J}_w\dot{\boldsymbol{\Omega}} &= \mathbf{T}_u - \mathbf{J}_w\dot{\boldsymbol{\omega}}. \end{aligned} \tag{3.16}$$

This can be substituted into Equation (3.15) and we get the final expression which is used throughout the paper:

$$\mathbf{J}_s\dot{\boldsymbol{\omega}} = -\mathbf{S}(\boldsymbol{\omega}) \left\{ \mathbf{J}_s\boldsymbol{\omega} + \mathbf{J}_\omega \left(\boldsymbol{\omega} + \boldsymbol{\Omega} \right) \right\} - \mathbf{T}_u + \mathbf{T}_{ex}, \tag{3.17}$$

where $\mathbf{J}_s = \mathbf{J} - \mathbf{J}_w$ is the moment of inertia for the system without the wheels.

We can then set up the complete equation set for the combined kinetics and kinematics for the satellite.

$$\dot{\mathbf{q}} = \frac{1}{2} \begin{bmatrix} -\boldsymbol{\epsilon}^T \\ \mathbf{T}(\mathbf{q}) \end{bmatrix} \boldsymbol{\omega}, \tag{3.18a}$$

$$\mathbf{J}_s\dot{\boldsymbol{\omega}} = -\mathbf{S}(\boldsymbol{\omega}) \left\{ \mathbf{J}_s\boldsymbol{\omega} + \mathbf{J}_\omega \left(\boldsymbol{\omega} + \boldsymbol{\Omega} \right) \right\} - \mathbf{T}_u + \mathbf{T}_{ex}, \tag{3.18b}$$

$$\mathbf{J}_\omega\dot{\boldsymbol{\Omega}} = -\mathbf{J}_\omega\dot{\boldsymbol{\omega}} + \mathbf{T}_u, \tag{3.18c}$$

where $\mathbf{T}(\mathbf{q}) = \eta\mathbf{I} + \mathbf{S}(\boldsymbol{\epsilon})$, $\mathbf{S}(\,\cdot\,)$ is the skew-symmetric cross product matrix, $\mathbf{T}_{ex}$ is the external moments applied to the system, $\mathbf{T}_u$ is the moments applied to the system from the motors, $\mathbf{J}_w$ and $\mathbf{J}_s$ is the moments of inertia for the wheels and the rest of the system, respectively.

These calculations have also been carried out and used by others in satellite literature (Jin et al. (2008), Wang et al. (2003), Won (1999), Ismail and Varatharajoo (2009)) and is thereby a well proven model for a satellite actuated by means of reaction wheels.

3.4 Inertial coordinate model

The system derived in the previous section can also be expressed in inertial coordinates. The advantage of expressing the system in this form is that the system equations turns out to be equal to those of a robot manipulator system (Spong et al., 2006), seen in Equation (3.19). The robot manipulator is a highly researched area, and it exists several control schemes for controlling robot manipulators. Therefore it is motivating to present the system in this manner and it is reasonable to expect that some of those control methods also can be used for the sphere shaped vehicle.

$$\mathbf{M}(\mathbf{q})\ddot{\mathbf{q}} + \mathbf{C}(\mathbf{q},\dot{\mathbf{q}})\dot{\mathbf{q}} + \mathbf{g}(\mathbf{q}) = \mathbf{u} \tag{3.19}$$

Using the kinematic relationship in Equation (2.24) and the fact that $\mathbf{E}(\mathbf{q})^T\mathbf{E}(\mathbf{q}) = \mathbf{I}_{3\times 3}$ it can easily be seen that

$$\boldsymbol{\omega} = 2\mathbf{E}^T(\mathbf{q})\dot{\mathbf{q}} \tag{3.20a}$$

$$\dot{\boldsymbol{\omega}} = 2\mathbf{E}^T(\mathbf{q})\ddot{\mathbf{q}} + \cancel{2\mathbf{E}^T(\dot{\mathbf{q}})\dot{\mathbf{q}}} = 2\mathbf{E}^T(\mathbf{q})\ddot{\mathbf{q}}. \tag{3.20b}$$

Inserting the equation for $\boldsymbol{\omega}$ and $\dot{\boldsymbol{\omega}}$ into Equation (3.18b) and pre-multiply with $\mathbf{E}(\mathbf{q})$ we obtain:

$$\mathbf{M}^*(\mathbf{q})\ddot{\mathbf{q}} + \mathbf{C}^*(\mathbf{q},\dot{\mathbf{q}})\dot{\mathbf{q}} + \mathbf{g}^*(\mathbf{q}) = \mathbf{u}^* \tag{3.21}$$

where

$$\mathbf{M}^*(\mathbf{q}) = 2\mathbf{E}(\mathbf{q})\mathbf{J}_s\mathbf{E}^T(\mathbf{q}) \tag{3.22a}$$

$$\mathbf{C}^*(\mathbf{q},\dot{\mathbf{q}}) = -2\mathbf{E}(\mathbf{q})\mathbf{S}\left(2\mathbf{J}\mathbf{E}^T(\mathbf{q})\dot{\mathbf{q}} + \mathbf{J}_w\boldsymbol{\Omega}\right)\mathbf{E}^T(\mathbf{q}) \tag{3.22b}$$

$$\mathbf{g}^*(\mathbf{q}) = -\mathbf{E}(\mathbf{q})\mathbf{T}_{ex} \tag{3.22c}$$

$$\mathbf{u}^* = -\mathbf{E}(\mathbf{q})\mathbf{T}_u. \tag{3.22d}$$

It can also be seen that the matrices have the following important properties:

$$\mathbf{M}^*(\mathbf{q}) = \mathbf{M}^*(\mathbf{q})^T \geq 0 \tag{3.23a}$$

$$\mathbf{x}^T\left(\dot{\mathbf{M}}^* - 2\mathbf{C}^*(\mathbf{q},\dot{\mathbf{q}})\right)\mathbf{x} = \mathbf{0},\ \forall\ \mathbf{x} \in \mathbb{R}^3. \tag{3.23b}$$

Remark 3.2. An important drawback with this representation is that $\mathbf{M}^*$ becomes singular when $\eta = \pm 1$. This contradicts the reason for choosing unit quaternion as attitude representation and therefore; the inertial coordinate model will *not* be used in this thesis.

Chapter 4

Controller Design

This section starts by making an expression of the error-dynamic based on the system equations described earlier in Chapter 3. The error-dynamic will be used to develop two different control algorithms; a sliding mode controller and a backstepping controller. It will also be proven that the system combined with each controller is asymptotically stable.

4.1 Error dynamic

The complete system with kinetics and kinematics combined developed in Chapter 3 is repeated for the sake of easier reading:

$$\dot{\mathbf{q}} = \frac{1}{2}\begin{bmatrix} -\boldsymbol{\epsilon}^T \\ \mathbf{T}(\mathbf{q}) \end{bmatrix}\boldsymbol{\omega}, \tag{4.1a}$$

$$\mathbf{J}_s\dot{\boldsymbol{\omega}} = -\mathbf{S}(\boldsymbol{\omega})\left\{\mathbf{J}_s\boldsymbol{\omega} + \mathbf{J}_\omega\left(\boldsymbol{\omega} + \boldsymbol{\Omega}\right)\right\} - \mathbf{T}_u + \mathbf{T}_{ex}, \tag{4.1b}$$

where $\mathbf{T}(\mathbf{q}) = \eta\mathbf{I} + \mathbf{S}(\boldsymbol{\epsilon})$ and $\mathbf{I}$ is the 3×3 identity matrix and $\mathbf{S}$ is the skew-symmetric cross product matrix.

Remark 4.1. Notice that the last equation in Equation-set (3.18) has been removed, since the scope of this thesis does not include controlling the dynamics of the reaction wheels.

The angular error velocity $\boldsymbol{\omega}_e$ is then defined as the difference between the satellite's angular velocity $\boldsymbol{\omega}$ and the desired angular velocity $\boldsymbol{\omega}_d$ in BODY coordinates:

Definition 4.1. *The angular velocity error $\boldsymbol{\omega}_e$ is defined as the difference between the satellite's angular velocity $\boldsymbol{\omega}$ and the desired angular velocity $\boldsymbol{\omega}_d$ in the BODY-frame:*

$$\boldsymbol{\omega}_e \triangleq \boldsymbol{\omega} - \boldsymbol{\omega}_d, \tag{4.2a}$$

$$\boldsymbol{\omega}_e = \boldsymbol{\omega} - \mathbf{R}^T(\eta, \boldsymbol{\epsilon})\boldsymbol{\omega}_d^n, \tag{4.2b}$$

where $\boldsymbol{\omega}_d^n$ is the desired angular velocity expressed in the NED-frame and $\mathbf{R}^T(\eta, \boldsymbol{\epsilon})$ is the rotation matrix that rotates the NED-vector $\boldsymbol{\omega}_d^n$ to the BODY-frame.

The attitude error is somewhat more difficult to define since the difference between two quaternions does not make any physically sense. However, if the desired attitude is given by $\mathbf{q}_d$, the quaternion product, defined in Definition 2.4, can be exploited to give a better representation of the attitude error. This can then be used to define the relative attitude error $\mathbf{q}_e$ which is used throughout this thesis.

Definition 4.2. *The relative attitude error quaternion* $\mathbf{e}$ *is given by the quaternion product (Kristiansen et al., 2009):*

$$\mathbf{e} \triangleq \mathbf{q}_d^{-1} \otimes \mathbf{q}, \tag{4.3}$$

where $\mathbf{q}_d$ *is the desired attitude and* $\mathbf{q}$ *is the rigid body's present attitude.*

In (Egeland and Gravdahl, 2002) it can be seen that the expression $\mathbf{q}_d^{-1} = \begin{bmatrix} \eta_d & -\boldsymbol{\epsilon}_d^T \end{bmatrix}^T$, which gives the relative attitude quaternion $\mathbf{e}$:

$$\mathbf{e} = \begin{bmatrix} \eta_d\eta + \boldsymbol{\epsilon}_d^T\boldsymbol{\epsilon} \\ \eta_d\boldsymbol{\epsilon} - \eta\boldsymbol{\epsilon}_d - \mathbf{S}(\boldsymbol{\epsilon}_d)\boldsymbol{\epsilon} \end{bmatrix} \triangleq \begin{bmatrix} \eta_e \\ \boldsymbol{\epsilon}_e \end{bmatrix}, \tag{4.4}$$

where $\mathbf{S}$ is the skew-symmetric cross product matrix.

The control objective is to get the attitude $\mathbf{q}$ to be aligned with the desired attitude $\mathbf{q}_d$, meaning $\mathbf{q} = \mathbf{q}_d$. This expression is substituted into the definition of relative attitude error:

$$\mathbf{e} = \mathbf{q}_d^{-1} \otimes \mathbf{q}_d, \tag{4.5a}$$

$$= \begin{bmatrix} \eta_d^2 + \boldsymbol{\epsilon}_d^T\boldsymbol{\epsilon}_d \\ \eta_d\boldsymbol{\epsilon}_d - \eta_d\boldsymbol{\epsilon}_d - \mathbf{S}(-\boldsymbol{\epsilon}_d)\boldsymbol{\epsilon}_d \end{bmatrix}, \tag{4.5b}$$

Since $\mathbf{q}$ is a unit quaternion, the expression $\eta_d^2 + \boldsymbol{\epsilon}_d^T\boldsymbol{\epsilon}_d = 1$. It can also be seen that $\mathbf{S}(-\boldsymbol{\epsilon}_d)\boldsymbol{\epsilon}_d = \mathbf{0}_{3\times 1}$ by using some of the properties of the skew-symmetric cross product matrix stated in Section 2.2.3. In addition, as discussed in Section 2.6, it is known that the quaternion attitude $\mathbf{q}$, and $-\mathbf{q}$ correspond to the same physical attitude. This gives the result stated in Definition 4.3.

Definition 4.3. *The satellite's attitude* $\mathbf{q}$ *is aligned with the desired attitude* $\mathbf{q}_d$ *when the relative attitude error becomes:*

$$\mathbf{e} = \begin{bmatrix} \pm 1 \\ \mathbf{0} \end{bmatrix} \triangleq \mathbf{q}_{id}, \tag{4.6}$$

where $\mathbf{0}$ *is the* 3×1 *zero vector.*

Dynamic Error Equation

The attitude dynamic error equation can be derived by time differentiation of $\mathbf{e}$ in Equation (4.4). The complete derivation is shown in Appendix A.1, but the result is shown here;

$$\dot{\mathbf{e}} = \frac{1}{2}\begin{bmatrix} -\boldsymbol{\epsilon}_e^T \\ \mathbf{T}(\mathbf{e}) \end{bmatrix}\boldsymbol{\omega}_e, \tag{4.7}$$

and $\mathbf{T}(\mathbf{e}) = \eta_e \mathbf{I} + \mathbf{S}(\boldsymbol{\epsilon}_e)$.

The next step is to derive the angular velocity error $\boldsymbol{\omega}_e$, stated in Equation (4.2b), with respect to time:

$$\dot{\boldsymbol{\omega}}_e = \dot{\boldsymbol{\omega}} - \left(\dot{\mathbf{R}}^T(\eta, \boldsymbol{\epsilon}) \boldsymbol{\omega}_d^n + \mathbf{R}^T(\eta, \boldsymbol{\epsilon}) \dot{\boldsymbol{\omega}}_d^n \right). \tag{4.8}$$

The calculation of $\dot{\mathbf{R}}^T(\eta, \epsilon)$ have been carried out in Appendix A.2, where it can be seen that $\dot{\mathbf{R}}^T(\eta, \boldsymbol{\epsilon}) = -\mathbf{S}(\boldsymbol{\omega}_e)\mathbf{R}^T(\eta, \boldsymbol{\epsilon})$.

By pre-multiplying Equation (4.8) by the system inertia matrix $\mathbf{J}_s$ and substitute part of (4.1) into the equation, one get the error dynamics:

$$\mathbf{J}_s \dot{\boldsymbol{\omega}}_e = -\mathbf{S}(\boldsymbol{\omega}) \left\{ \mathbf{J}_s \boldsymbol{\omega} + \mathbf{J}_\omega \left(\boldsymbol{\omega} + \boldsymbol{\Omega} \right) \right\} - \mathbf{T}_u + \mathbf{T}_{ex} + \mathbf{J}_s \mathbf{S}(\boldsymbol{\omega}_e) \mathbf{R}^T \boldsymbol{\omega}_d^n - \mathbf{R}^T \dot{\boldsymbol{\omega}}_d^n. \tag{4.9}$$

This gives the total dynamic error system:

$$\dot{\mathbf{e}} = \frac{1}{2} \begin{bmatrix} -\boldsymbol{\epsilon}_e^T \\ \mathbf{T}(\mathbf{e}) \end{bmatrix} \boldsymbol{\omega}_e, \tag{4.10a}$$

$$\mathbf{J}_s \dot{\boldsymbol{\omega}}_e = -\mathbf{S}(\boldsymbol{\omega}) \mathbf{W} - \mathbf{T}_u + \mathbf{T}_{ex} + \mathbf{J}_s \mathbf{S}(\boldsymbol{\omega}_e) \mathbf{R}^T \boldsymbol{\omega}_d^n - \mathbf{R}^T \dot{\boldsymbol{\omega}}_d^n. \tag{4.10b}$$

where $\mathbf{W} = \mathbf{J}_s \boldsymbol{\omega} + \mathbf{J}_\omega \left(\boldsymbol{\omega} + \boldsymbol{\Omega} \right)$ actually is the total momentum of the system. This is explained in detail in Chapter 6.

4.2 Sliding mode control

In this section a sliding mode (SM) controller will be proposed to control the angular velocity of the satellite. The sliding mode controller is inspired by (Fossen, 2002) and (Wang et al., 2003), where some modifications are carried out to adapt it to the sphere satellite. A stability proof for the system and the controller will also be given.

The sliding mode controller is a well known controller that has been applied to many practically systems such as power systems, robot manipulators and air crafts (Ma and Boukas, 2009). The controller is nonlinear, and alters the dynamics of the system by using a switching control. The sliding mode control structure is designed to ensure that all trajectories move towards the sliding mode with the switching condition. Trajectories from this sub-space then slides along the surface to a desired equilibrium. The SM controller is considered to be a robust control method, and thereby practical for systems with external disturbances (Alfaro-Cid et al., 2005).

Definition 4.4. *The sliding control variable* $\mathbf{s} \in \mathbb{R}^{3\times 1}$ *is defined as:*

$$\mathbf{s} \triangleq \boldsymbol{\omega}_e + \mathbf{K} \boldsymbol{\epsilon}_e, \tag{4.11}$$

where $\mathbf{K} \in \mathbb{R}^{3\times 3}$, $\mathbf{K} = \mathbf{K}^T > 0$.

By differentiating the sliding mode variable $\mathbf{s}$ with respect to time and pre-multiply the equation with $\mathbf{J}_s$ you get the following expression:

$$\mathbf{J}_s\dot{\mathbf{s}} = \mathbf{J}_s\dot{\boldsymbol{\omega}}_e + \mathbf{J}_s\mathbf{K}\dot{\boldsymbol{\epsilon}}_e, \tag{4.12a}$$

$$= -\mathbf{S}(\boldsymbol{\omega})\mathbf{W} + \mathbf{J}_s\mathbf{S}(\boldsymbol{\omega}_e)\mathbf{R}^T\boldsymbol{\omega}_d^n - \mathbf{J}_s\mathbf{R}^T\dot{\boldsymbol{\omega}}_d^n - \mathbf{T}_u + \mathbf{T}_{ex} + \mathbf{J}_s\mathbf{K}\dot{\boldsymbol{\epsilon}}_e, \tag{4.12b}$$

where $\mathbf{W} = \mathbf{J}_s\boldsymbol{\omega} + \mathbf{J}_\omega(\boldsymbol{\omega} + \boldsymbol{\Omega})$.

The control input $\mathbf{T}_u$ is then chosen to cancel the nonlinearities $\mathbf{S}(\boldsymbol{\omega})\mathbf{W}$, $\mathbf{T}_{ex}$ and $\mathbf{J}_s\mathbf{K}\dot{\boldsymbol{\epsilon}}_e$ together with the terms from the reference: $\mathbf{J}_s\mathbf{S}(\boldsymbol{\omega}_e)\mathbf{R}^T\boldsymbol{\omega}_d^T$ and $\mathbf{J}_s\mathbf{R}^T\dot{\boldsymbol{\omega}}_d^n$. In addition to canceling all the terms, one also needs dampening, which is implemented by adding $-\mathbf{J}_s\left(\mathbf{D}sgn(\mathbf{s}) + \mathbf{P}\mathbf{s}\right)$ to $\mathbf{T}_u$ giving the complete controller in Equation (4.13).

Proposition 4.1. *The error dynamics in Equation* (4.10)*, with the sliding mode controller* $\mathbf{T}_u$ *given by*

$$\begin{aligned}\mathbf{T}_u = &-\mathbf{S}(\boldsymbol{\omega})\mathbf{W} + \mathbf{J}_s\mathbf{S}(\boldsymbol{\omega}_e)\mathbf{R}^T\boldsymbol{\omega}_d^n - \mathbf{J}_s\mathbf{R}^T\dot{\boldsymbol{\omega}}_d^n + \mathbf{J}_s\mathbf{K}\dot{\boldsymbol{\epsilon}}_e \\ &+ \mathbf{T}_{ex} + \mathbf{J}_s\mathbf{D}sgn(\mathbf{s}) + \mathbf{J}_s\mathbf{P}\mathbf{s},\end{aligned} \tag{4.13}$$

has an asymptotically stable equilibrium in $(\boldsymbol{\omega}_e, \mathbf{e}) = (\mathbf{0}, \mathbf{q}_{id})$ *where* $\mathbf{q}_{id} = \begin{bmatrix}\pm 1 & \mathbf{0}^T\end{bmatrix}^T$.

The gain-matrices $\mathbf{K}$, $\mathbf{P}$ and $\mathbf{D}$ are all $\in \mathbb{R}^{3\times 3}$ and positive definite. The sign function $sgn(\mathbf{s}) = \begin{bmatrix}s_1 & s_2 & s_3\end{bmatrix}^T \in \mathbb{R}^{3\times 1}$ is calculated using the scalar sign function, defined in Equation (4.14), for each element in $\mathbf{s}$.

$$sgn(x) = \begin{cases}+1 & \text{if} \quad x \geq 0 \\ -1 & \text{if} \quad x < 0\end{cases} \tag{4.14}$$

The final term to comment is $\dot{\boldsymbol{\epsilon}}_e$. This term can easily be calculated by utilizing the fact that $\dot{\boldsymbol{\epsilon}}_e = \frac{1}{2}\mathbf{T}(\mathbf{e})\boldsymbol{\omega}_e$, avoiding time differentiation of $\boldsymbol{\epsilon}_e$.

Remark 4.2. Note that $sgn(0) = 1$, which is not always the case for the sign-function. This is done to prevent an unwanted equilibrium for later calculations in the thesis.

Proof. To prove Proposition 4.1, we utilize (Shevitz and Paden, 1994). This article states that systems with discontinuous "right-hand side", can be evaluated with ordinary Lyapunov stability theory.

Given the controller in Equation (4.13), the expression for $\dot{\mathbf{s}}$ can be written as:

$$\dot{\mathbf{s}} = -\left(\mathbf{D}sgn(\mathbf{s}) + \mathbf{P}\mathbf{s}\right). \tag{4.15}$$

Consider the radially unbounded Lyapunov function candidate (Khalil, 2002):

$$V_1 = \frac{1}{2}\mathbf{s}^T\mathbf{s} > 0, \quad \forall \quad \mathbf{s} \neq \mathbf{0}, \tag{4.16}$$

and differentiating it with respect to time along the trajectory we get

$$\dot{V}_1 = \mathbf{s}^T\dot{\mathbf{s}}, \tag{4.17a}$$
$$= -\mathbf{s}^T\mathbf{D}sgn(\mathbf{s}) - \mathbf{s}^T\mathbf{P}\mathbf{s}, \tag{4.17b}$$
$$< 0 \quad \forall \quad \mathbf{s} \neq \mathbf{0}, \tag{4.17c}$$

where the fact that $\mathbf{s}^T\mathbf{P}\mathbf{s} \geq \lambda_{\min}(\mathbf{P})||\mathbf{s}||^2 > 0, \forall \mathbf{s} \neq \mathbf{0}$ where $\lambda_{\min}(\mathbf{P})$ is the smallest eigenvalue of $\mathbf{P}$, and $\mathbf{P}$ is positive definite is used. The first term $\mathbf{s}^T\mathbf{D}sgn(\mathbf{s})$ will also be grater than 0 since $\mathbf{D}$ is positive definite.

Since the Lyapunov function candidate V_1 is positive definite and $\dot{V}_1$ is negative definite, thus according to (Shevitz and Paden, 1994), this proves that the non-smooth $\mathbf{s}$-system is AS and each trajectory will thereby converge to the sliding manifold.

In fact, one can guaranty finite time convergence (Perruquetti and Barbot, 2002), since

$$\frac{\partial V_1}{\partial t} \leq -\vartheta\sqrt{V_1}, \tag{4.18}$$

where $\vartheta = \sqrt{2}\lambda_{\min}(\mathbf{D}) > 0$ and $\lambda_{\min}(\mathbf{D})$ is the smallest eigenvalue of $\mathbf{D}$. From Equation (4.18) it can easily be seen that

$$2\sqrt{V_1} \leq V_1(\mathbf{s}(0)) - \vartheta t. \tag{4.19}$$

This shows that the system will converge to the sliding manifold with the finite converge-time T_c, upper bounded by

$$T_c \leq \frac{V_1(\mathbf{s}(0))}{\vartheta}. \tag{4.20}$$

It is now proven that the controller will bring the system into the sliding mode in finite time. However, we still have not reached the control objective of getting the angular velocity error $\boldsymbol{\omega}_e$ to zero, and the attitude error $\mathbf{e}$ to $\mathbf{q}_{id}$ as stated in Proposition 4.1.

From the definition of the sliding mode variable $\mathbf{s}$ in Equation (4.11) and knowing that we are in the sliding mode $\mathbf{s} = \mathbf{0}$, we get:

$$\mathbf{s} = \mathbf{0}, \quad \Rightarrow \quad \boldsymbol{\omega}_e = -\mathbf{K}\boldsymbol{\epsilon}_e.$$

We then introduce the second Lyapunov function candidate:

$$V_2 = 1 - \eta_e \tag{4.21}$$

which is a positive definite function since $-1 \leq \eta_e \leq 1$. The time derivative along the solution then becomes:

$$\dot{V}_2 = -\dot{\eta_e} = \frac{1}{2}\boldsymbol{\epsilon}_e^T\boldsymbol{\omega}_e = -\frac{1}{2}\boldsymbol{\epsilon}_e^T\mathbf{K}\boldsymbol{\epsilon}_e \tag{4.22a}$$
$$\leq -\frac{1}{2}\lambda_{\min}(\mathbf{K})\boldsymbol{\epsilon}_e^T\boldsymbol{\epsilon}_e = -\frac{1}{2}\lambda_{\min}(\mathbf{K})(1-\eta_e^2) \tag{4.22b}$$
$$< 0, \tag{4.22c}$$

where the quaternion unit-length property has been used, in addition to the fact that $\mathbf{x}^T\mathbf{K}\mathbf{x} \geq \lambda_{\min}(\mathbf{K})||\mathbf{x}||^2 > 0$ where $\lambda_{\min}(\mathbf{K})$ is the smallest eigenvalue of $\mathbf{K}$.

Since V_2 is positive definite, and $\dot{V}_2$ is negative definite, thus, $(1-\eta_e^2) \to 0$ as time goes to infinity, and $\eta_e \to \pm 1$. Because $\eta_e^2 + \boldsymbol{\epsilon}_e^T\boldsymbol{\epsilon}_e = 1$, also $\boldsymbol{\epsilon}_e \to \mathbf{0}$ and the attitude error $\mathbf{e} \to \mathbf{q}_{id}$. It can also be noticed that $\boldsymbol{\omega}_e$ will converge to $\mathbf{0}$ since $\boldsymbol{\omega}_e = -\mathbf{K}\boldsymbol{\epsilon}_e$ in sliding mode, and when $\boldsymbol{\epsilon}_e \to \mathbf{0}$ so will $\boldsymbol{\omega}_e$. We can then conclude that the complete system, with the given controller, is asymptotically stable. □

4.3 Backstepping control

In this section a backstepping controller will be proposed to control the angular velocity of the satellite. The backstepping controller is inspired by (Jiang et al., 2010), where some modifications are carried out to adapt it to the sphere satellite. A stability proof for the system and the controller will also be given.

The backstepping control method is a systematic and recursive design methodology for nonlinear control. The control method has many similarities with *feedback linearization* (Khalil (2002),Johansen and Hunt (2000), Groves and Serrani (2004)), however some differences exist. The most important difference is that the backstepping method may utilize "good nonlinearities" as oppose to the feedback linearization method that cancels all nonlinear terms. Moreover, while the feedback linearization requires precise knowledge of the system, backstepping offers a choice of design tools for different kinds of uncertainties. For instance, in mechanical motion systems, it is often hard to model the damping term as it can be highly non-linear. However, this is not a major problem for the backstepping method. Since the damping term is dissipative, it does not need to be canceled at all.

The idea of the backstepping method is to select recursively appropriate functions of state variables as virtual-control inputs for lower dimension subsystems of the overall system. Each step of the method results in a new virtual control law, expressed as a functions of the virtual control law in the previous steps. One thereby "backs" its way from the inner subsystem, until the algorithm terminates when the overall system is reached. The resulting feedback controller is then supposed to achieve the original control objective. This is proved by a final number of Lyapunov functions formed by summing up the Lyapunov functions corresponding to each individual step in the procedure. In this way, the backstepping algorithm will thereby consist of equal number of steps as the dimension of the overall system.

We are then ready to start the recursive backstepping algorithm.

Step 1: The first step involves defining the first backstepping variable $\mathbf{z}_1$ that represent the attitude error. It is therefore of no big surprise that

$$\mathbf{z}_1 \triangleq \boldsymbol{\epsilon}_e. \tag{4.23}$$

Differentiating the definition of $\mathbf{z}_1$ with respect to time, shows that

$$\dot{\mathbf{z}}_1 = \frac{1}{2}\mathbf{T}(\mathbf{e})\boldsymbol{\omega}_e = \frac{1}{2}\left[\eta_e\mathbf{I} + \mathbf{S}(\mathbf{z}_1)\right]\boldsymbol{\omega}_e. \tag{4.24}$$

where Equation (4.7) has been used.

By considering $\boldsymbol{\omega}_e$ as the virtual control variable, defined in Definition 4.5, a Lyapunov function V_1 is constructed to prove that the dynamics of $\mathbf{z}_1$ is stable.

Definition 4.5. *The virtual control variable $\boldsymbol{\omega}_e$ in step 1 of the recursive backstepping algorithm is defined such that*

$$\boldsymbol{\omega}_e \triangleq \boldsymbol{\alpha}_1(\mathbf{z}_1) + \mathbf{z}_2, \tag{4.25}$$

where $\boldsymbol{\alpha}_1(\mathbf{z}_1)$ stabilizes the $\mathbf{z}_1$ dynamics, and $\mathbf{z}_2$ is the second backstepping variable that links the $\mathbf{z}_1$ dynamics with the outer dynamics.

Consider the positive definite Lyapunov function

$$V_1 = \frac{1}{2}k\mathbf{z}_1^T\mathbf{z}_1 + \frac{1}{2}k\left(1-\eta_e\right)^2, \quad k > 0 \quad k \in \mathbb{R}, \tag{4.26}$$

where k is a tuning parameter and the time derivative along the trajectory is given by

$$\begin{aligned}
\dot{V}_1 &= k\mathbf{z}_1^T\dot{\mathbf{z}}_1 - k\left(1-\eta_e\right)\dot{\eta}_e \\
&= \cancel{\frac{1}{2}k\eta_e\mathbf{z}_1^T\boldsymbol{\omega}_e} + \frac{1}{2}k\underbrace{\mathbf{z}_1^T\mathbf{S}(\mathbf{z}_1)}_{=\mathbf{0}}\boldsymbol{\omega}_e + \frac{1}{2}k\mathbf{z}_1^T\boldsymbol{\omega}_e - \cancel{\frac{1}{2}k\eta_e\mathbf{z}_1^T\boldsymbol{\omega}_e} \\
&= \frac{1}{2}k\mathbf{z}_1\left[\boldsymbol{\alpha}_1(\mathbf{z}_1) + \mathbf{z}_2\right]
\end{aligned}$$

Choose the stabilizing expression

$$\boldsymbol{\alpha}_1(\mathbf{z}_1) \triangleq -\mathbf{K}_1\mathbf{z}_1, \quad \mathbf{K}_1 \in \mathbb{R}^{3\times 3} > 0, \tag{4.27}$$

where $\mathbf{K}_1$ is a tuning parameter. Then

$$\dot{V}_1 = -\frac{1}{2}k\mathbf{z}_1^T\mathbf{K}_1\mathbf{z} + \frac{1}{2}k\mathbf{z}_1^T\mathbf{z}_2, \tag{4.28}$$

which is negative definite if $\mathbf{z}_2 = \mathbf{0}$ and thereby proves that the $\mathbf{z}_1$-dynamics is AS if $\mathbf{z}_2 = \mathbf{0}$.

Step 2: The second step in the recursive backstepping algorithm is going to link the $\mathbf{z}_1$-dynamics with the $\mathbf{z}_2$-dynamics and specify the final backstepping controller $\mathbf{T}_{u,s}$. We start the procedure by investigating the $\mathbf{z}_2$-dynamics by differentiating Equation (4.25) with respect to time, which shows that

$$\begin{aligned}
\mathbf{J}_s\dot{\mathbf{z}}_2 &= \mathbf{J}_s\dot{\boldsymbol{\omega}}_e - \mathbf{J}_s\dot{\boldsymbol{\alpha}}_1(\mathbf{z}_1) \\
&= -\mathbf{S}(\boldsymbol{\omega})\mathbf{W} - \mathbf{T}_{u,s} + \mathbf{T}_{ex} + \mathbf{J}_s\mathbf{S}(\boldsymbol{\omega})_e\mathbf{R}^T\boldsymbol{\omega}_d^n - \mathbf{J}_s\mathbf{R}^T\dot{\boldsymbol{\omega}}_d^n - \mathbf{J}_s\dot{\boldsymbol{\alpha}}_1(\mathbf{z}_1).
\end{aligned}$$

Consider the radially unbounded Lyapunov function,

$$V_2 = V_1 + \frac{1}{2}\mathbf{z}_2^T\mathbf{J}_s\mathbf{z}_2, \tag{4.29}$$

and its time-derivative along the solution:

$$\begin{aligned}\dot{V}_2 &= \dot{V}_1 + \mathbf{z}_2^T \mathbf{J}_s \dot{\mathbf{z}}_2 \\ &= -\frac{1}{2} k \mathbf{z}_1 \mathbf{K}_1 \mathbf{z}_1 + \mathbf{z}_2^T \Big\{ \frac{1}{2} k \mathbf{z}_1 - \mathbf{S}(\boldsymbol{\omega}) \mathbf{W} - \mathbf{T}_{u,s} + \mathbf{T}_{ex} \\ &\quad + \mathbf{J}_s \mathbf{S}(\boldsymbol{\omega}_e) \mathbf{R}^T \boldsymbol{\omega}_d^n - \mathbf{J}_s \mathbf{R}^T \dot{\boldsymbol{\omega}}_d^n - \mathbf{J}_s \dot{\boldsymbol{\alpha}}_1 \Big\}.\end{aligned}$$

We continue by designing the backstepping controller $\mathbf{T}_{u,s}$ such that it cancels all the terms inside the bracket, and add a damping-term $\mathbf{K}_2 \mathbf{z}_2$. The backstepping controller $\mathbf{T}_{u,s}$ can then be written as

$$\mathbf{T}_{u,s} = \frac{1}{2} k \mathbf{z}_1 - \mathbf{S}(\boldsymbol{\omega}) \mathbf{W} + \mathbf{T}_{ex} + \mathbf{J}_s \mathbf{S}(\boldsymbol{\omega}_e) \mathbf{R}^T \boldsymbol{\omega}_d^n - \mathbf{J}_s \mathbf{R}^T \dot{\boldsymbol{\omega}}_d^n - \mathbf{J}_s \dot{\boldsymbol{\alpha}}_1 + \mathbf{K}_2 \mathbf{z}_2. \tag{4.30}$$

which results in the negative definite Lyapunov function

$$\dot{V}_2 = -\frac{1}{2} k \mathbf{z}_1^T \mathbf{K}_1 \mathbf{z}_1 - \mathbf{z}_2^T \mathbf{K}_2 \mathbf{z}_2. \tag{4.31}$$

Remark 4.3. Time-differentiation of $\boldsymbol{\alpha}_1(\mathbf{z}_1)$ in the controller $\mathbf{T}_{u,s}$ can be avoided since $\dot{\boldsymbol{\alpha}}_1(\mathbf{z}_1) = -\mathbf{K}_1 \dot{\boldsymbol{\epsilon}}_e = -\frac{1}{2} \mathbf{K}_1 \mathbf{T}(\mathbf{e}) \boldsymbol{\omega}_e$.

Proposition 4.2. *The closed-loop error dynamics*

$$\dot{\mathbf{z}}_1 = -\frac{1}{2} \mathbf{T}(\mathbf{e}) \mathbf{K}_1 \mathbf{z}_1 + \frac{1}{2} \mathbf{T}(\mathbf{e}) \mathbf{z}_2 \tag{4.32a}$$

$$\mathbf{J}_s \dot{\mathbf{z}}_2 = -\frac{1}{2} k \mathbf{z}_1 - \mathbf{K}_2 \mathbf{z}_2, \tag{4.32b}$$

obtained through the backstepping procedure, has an asymptotically stable equilibrium $(\mathbf{z}_1, \mathbf{z}_2) = (\mathbf{0}, \mathbf{0})$*, which corresponds to asymptotically stability of the closed-loop equilibrium* $(\boldsymbol{\omega}_e, \mathbf{e}) = (\mathbf{0}, \mathbf{q}_{id})$.

Proof. The proof of Proposition 4.2 is straightforward when (Khalil, 2002, Theorem 4.9) is used. Choose the Lyapunov function candidate V_2, as shown in Equation (4.29), with its derivative, seen in Equation (4.31). Then choose

$$\mathbf{z} \triangleq \begin{bmatrix} \mathbf{z}_1^T & \mathbf{z}_2^T \end{bmatrix}^T \tag{4.33a}$$

$$W_1(\mathbf{z}) \triangleq \frac{1}{2} k \mathbf{z}_1^T \mathbf{z}_1 + \frac{1}{2} \mathbf{z}_2^T \mathbf{J}_s \mathbf{z}_2 > 0 \tag{4.33b}$$

$$W_2(\mathbf{z}) \triangleq W_1(\mathbf{z}) + \frac{1}{2} k (1 - \eta_e)^2 > 0 \tag{4.33c}$$

$$W_3(\mathbf{z}) \triangleq \frac{1}{2} k \mathbf{z}_1^T \mathbf{K}_1 \mathbf{z}_1 + \mathbf{z}_2^T \mathbf{K}_2 \mathbf{z}_2 > 0, \tag{4.33d}$$

such that

$$W_1(\mathbf{z}) \leq V_2(\mathbf{z}, t) \leq W_2(\mathbf{z}) \tag{4.34a}$$

$$\frac{\partial V_2}{\partial t} + \frac{\partial V_2}{\partial \mathbf{z}}\dot{\mathbf{z}} \leq -W_3(\mathbf{z}) < 0. \tag{4.34b}$$

All assumptions of Theorem 4.9 are then satisfied and thus, $\mathbf{z} = \mathbf{0}$ is an asymptotically stable equilibrium. Moreover, we have that $\mathbf{z} \equiv \mathbf{0} \Rightarrow \boldsymbol{\omega}_e \equiv \mathbf{0}$ and $\mathbf{z}_1 \equiv \mathbf{0} \Rightarrow \boldsymbol{\epsilon}_e \equiv \mathbf{0}$ and $\eta_e = \pm 1$. Therefore also $(\boldsymbol{\omega}_e, \mathbf{e}) = (\mathbf{0}, \mathbf{q}_{id})$ is an asymptotically stable equilibrium. □

Remark 4.4. In (Krogstad, 2010) a similar result has been shown, where the author also includes integral action. In addition he proves exponential stability (ES) by switching to modified Rodriguez parameters. This trick allows inversion of the attitude-matrix that corresponds to the attitude matrix for the unit quaternion; $\mathbf{T}(\mathbf{q})$.

Chapter 5

Non-ideal situations

A model will never be perfectly equal to the physics, even if one uses a nonlinear model, and this is of course also the situation for the underwater satellite. In this chapter one will try to point out some of the elements that the model does not take into account, and if it is possible, try to implement correction action to improve the overall performance.

5.1 Lab environment

In the given lab setup (see Appendix C.1) a water tank with dimensions $(55 \times 53 \times 67)$ cm is used. This is a relatively small tank, compared to the satellite, since the diameter of the satellite is about 43 cm, leaving a maximum of 6 cm free space on each side in the horizontal plane. Idealistic this should be enough space since the sphere should not move in the translational direction at all, but this is not the case. Since the sphere has almost no damping, even small irregularities will cause the sphere to start moving, and only walls will dampen the movement. However, this will not be the case for a satellite in space or for our sphere if it was placed in the ocean. The problem with this irregularity is that it is almost impossible to model, and the only solution is to construct a good controller that corrects the angular velocity when a crash arises.

The data communication cable between the satellite and the server represents another problem. This cable has different buoyancy depending on its orientation, but more importantly, the cable works as a spring when it is twisted. It is quite remarkable that a 42.1 kg heavy sphere should be affected by this effect, but as can be seen from Figure 5.1 it is quite noticeable. The plot shows the system affected by a commanded constant torque about the z-axis, and one should expect that the sphere in steady state had a constant angular velocity in the positive direction. However this is not the case, and it can be seen that the satellite has a negative angular acceleration (from about 9 s in the plot) which imply that the angular velocity of the satellite will go towards zero. Even more surprisingly: it can be seen that the angular velocity crosses the zero-line and thereby spins in the negative direction. The reason for this is mostly due to the fact that the sphere experiences very little friction and thus, only small forces from the cable can influence the movement.

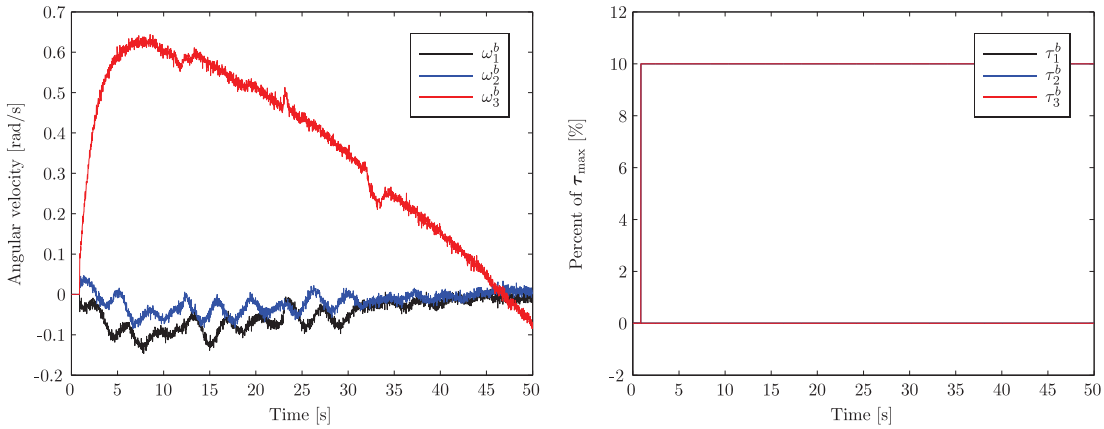

(a) Angular velocity $\boldsymbol{\omega}$. (b) Commanded torque $\mathbf{T}_u$.

Figure 5.1: The spring effect of the cable can be seen when a commanded, constant torque T_z is pushed on the system about the z-axis.

The best way to fix this problem is by removing the cable between the satellite and the server completely and use wireless transmission instead. However, this requires a lot of research, where different solutions for transmitting signals through water must be evaluated. Smart solutions for placement of sender and receiver equipments are also essential and analyzes have to be carried out.

5.2 Filtering of angular velocity measurements

The AUVSAT has restricted space and limited budget, and therefore it is equipped with small and low-cost sensors for attitude and angular velocity (see Section 8.3). This implies that the measurements are not perfect, and especially the angular velocity is quite noisy with high frequent oscillations, as can be seen in Figure 5.2. If these high-frequency measurements were to be used by the controller, the actuators would respond to the high-frequency signal and cause wear and tear of the actuators. This is not efficient, and should be avoided.

The best way to avoid this problem is to filter the noisy measurements in each direction. A simple first order filter is maybe the best choice of filter, since use of higher order filter will produce greater phase shifts, which is important to avoid in rapid moving systems. The filter $H_i(s)$ from input ω_i to the filtered output $\omega_{i,filt}$ with time constant T then becomes:

$$H_i(s) = \frac{\omega_{i,filt}}{\omega_i}(s) = \frac{1}{Ts+1}, \ \forall\, i \in \{x, y, z\}. \tag{5.1}$$

The next part is to find a suitable value for the time constant T. A great value will give a smooth filtered signal, but with a significant phase shift. A small time constant will have

the opposite effect, and one should therefore choose something in between. The result for the chosen filter can be seen in Figure 5.2 with time constant $T = 0.5$ s.

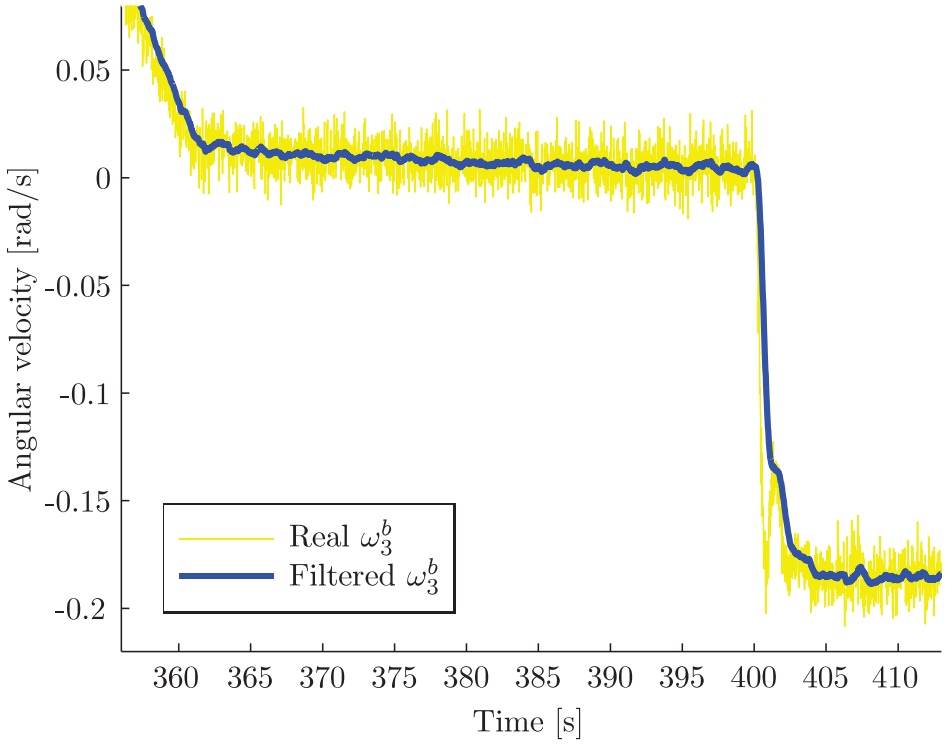

Figure 5.2: Filtering the angular velocity about the z-axis with time constant $T = 0.5$ s.

5.3 Estimation

In low cost satellites, measurements of different parameters are often left out. Therefore it has been done a lot of research of estimation of different parameters that are essential for rigid bodies. This includes among others, unknown inertia matrices in (Ahmed and Bernstein, 1999) and (Li and Ma, 2007) and estimation of position in (Gawronski and Craparo, 2002). Especially estimation of angular velocity has received a lot of attention in the latest couple of years. The reason for this is that systems for measuring angular velocity are often expensive, failure-prone, heavy and require a significant amount of power (Köprübasi and Thein, 2003). Therefore, it is of interest to avoid having angular velocity measurements at all. Another aspect is for synchronization between more than one satellite. Information sent between the spacecrafts is often limited and it can therefore be of interest to synchronize only the orientation instead of both orientation and angular velocity. Each satellite can estimate its angular velocity locally and one can thereby save precious bandwidth between the satellites.

On the other hand, if the system actually has angular velocity measurements, it is still useful to estimate the generalized velocity. One can thereby use it as backup or in case of equipment failure. This motivates the following chapter, where an observer for the angular velocity of the sphere-shaped satellite is presented.

Chapter 6

Observer Design

The problem of controlling motion of rigid bodies has been studied in great detail in the literature of aerospace, marine and robotics. Many different control algorithms have been attempted and tested out, ranging from simple linear control schemes to non-linear control based on backstepping, feedback linearization, adaptive control etc. Most of these control techniques require knowledge of the actual angular velocity (Salcudean, 1991).

If it is assumed that measurement of angular velocity is not present, then the required angular velocity must be estimated in some way. One solution is to evaluated the angular velocity by making use of the derivative and filtering of some orientation parameters. However, this usually leads to noisy and inaccurate estimates. Another solution is to use different kinds of observers. This idea will be investigated further in this chapter and a nonlinear observer will be presented.

The observer is inspired by (Bondhus et al., 2005) and (Krogstad et al., 2005) where a leader-follower output feedback synchronization scheme for two satellites is developed. It is assumed that the two satellites do not have measurements of the angular velocity and it is therefore developed two nonlinear observers for the rigid body angular velocity estimate. The observer is based on a simple copy of the system with correction terms which are steered in such a way that the error between the actual and the estimated angular velocity goes to zero as time goes to infinity. The implementation of the observer will also act as a filter for the angular velocity, removing the high frequent oscillation mentioned in Section 5.2.

6.1 Angular velocity observer

In this section a nonlinear observer will be presented, and the stability proof will be carried out, where it can be seen that the proposed observer is locally asymptotically stable.

Assuming that only attitude and rotation speed of the wheels are available for measurements, an observer is needed to estimate the angular velocity of the satellite. This can be done in different ways, including an extended Kalman filter and a nonlinear observer. In this paper the latter alternative is designed and implemented.

We start by repeating the expressions for the total angular momentum $\mathbf{W}$ and the total axial angular momentum $\mathbf{H}$ for the wheels given in the BODY-coordinate frame, respectively:

$$\mathbf{W}^b = \mathbf{J}\boldsymbol{\omega}^b_{nb} + \mathbf{J}_w\boldsymbol{\Omega}, \tag{6.1a}$$

$$\mathbf{H}^b = \mathbf{J}_w\boldsymbol{\omega}^b_{nb} + \mathbf{J}_w\boldsymbol{\Omega}. \tag{6.1b}$$

Since the calculations are easier expressed by the momentum dynamics in the inertial frame, the system is stated as:

$$\mathbf{W}^n = \mathbf{R}^n_b\mathbf{W}^b = \mathbf{R}^n_b\left[\mathbf{J}\boldsymbol{\omega}^b_{nb} + \mathbf{J}_w\boldsymbol{\Omega}\right], \tag{6.2a}$$

$$\mathbf{H}^n = \mathbf{R}^n_b\mathbf{H}^b = \mathbf{R}^n_b\left[\mathbf{J}_w\boldsymbol{\omega}^b_{nb} + \mathbf{J}_w\boldsymbol{\Omega}\right]. \tag{6.2b}$$

The time derivative of $\mathbf{W}^n$ is equal to the external torques applied to the system $\mathbf{T}^n_{ex}$ in NED-coordinates as:

$$\dot{\mathbf{W}}^n = \mathbf{T}^n_{ex} = \mathbf{R}^n_b\mathbf{T}^b_{ex}. \tag{6.3}$$

Rearranging Equation (6.2a), using the kinematic relations shown in Equation (2.24) and collecting the other terms gives the equation set for the system Σ as:

$$\Sigma : \begin{cases} \dot{\mathbf{W}}^n &= \mathbf{R}^n_b\mathbf{T}^b_{ex}, \\ \dot{\mathbf{q}} &= \frac{1}{2}\mathbf{E}(\mathbf{q})\left[\underbrace{\left(\mathbf{R}^n_b\mathbf{J}\right)^{-1}\mathbf{W}^n - \mathbf{J}^{-1}\mathbf{J}_w\boldsymbol{\Omega}}_{\boldsymbol{\omega}}\right], \end{cases} \tag{6.4}$$

where $\mathbf{E}(\mathbf{q}) = \begin{bmatrix} -\boldsymbol{\epsilon}^T \\ \mathbf{T}(\mathbf{q}) \end{bmatrix}$ and $\mathbf{T}(\mathbf{q}) = \eta\mathbf{I} + \mathbf{S}(\boldsymbol{\epsilon})$. We then define the observer system $\hat{\Sigma}$ as the copy of the dynamics with correction terms $\mathbf{g}_1(\tilde{\mathbf{q}})$ and $\mathbf{g}_2(\tilde{\mathbf{q}})$ as:

$$\hat{\Sigma} : \begin{cases} \dot{\hat{\mathbf{W}}}^n &= \mathbf{R}^n_b\left[\mathbf{T}^b_{ex} + \mathbf{g}_1(\tilde{\mathbf{q}})\right], \\ \dot{\hat{\mathbf{q}}} &= \frac{1}{2}\mathbf{E}(\hat{\mathbf{q}})\left[\underbrace{\left(\mathbf{R}^n_b\mathbf{J}\right)^{-1}\hat{\mathbf{W}}^n - \mathbf{J}^{-1}\mathbf{J}_w\boldsymbol{\Omega}}_{\hat{\boldsymbol{\omega}}} + \mathbf{g}_2(\tilde{\mathbf{q}})\right], \end{cases} \tag{6.5}$$

where $\mathbf{g}_1$ and $\mathbf{g}_2$ are to be determined later.

Definition 6.1. *The error variables between the real and estimated values for attitude, momentum and angular velocity, respectively, are defined as:*

$$\tilde{\mathbf{q}} \triangleq \mathbf{q}^{-1} \otimes \hat{\mathbf{q}}, \tag{6.6a}$$

$$\tilde{\mathbf{W}}^n \triangleq \hat{\mathbf{W}}^n - \mathbf{W}^n, \tag{6.6b}$$

$$\tilde{\boldsymbol{\omega}}^b_{nb} \triangleq \hat{\boldsymbol{\omega}}^b_{nb} - \boldsymbol{\omega}^b_{nb}, \tag{6.6c}$$

where $\otimes$ is the quaternion product, defined in Equation (2.19), and $\mathbf{q}^{-1} = \begin{bmatrix} \eta & -\boldsymbol{\epsilon}^T \end{bmatrix}^T$ is the complex conjugate of $\mathbf{q}$.

From the definition of the momentum and angular velocity estimation error you get that:

$$\begin{aligned}\tilde{\mathbf{W}}^n &= \hat{\mathbf{W}}^n - \mathbf{W}^n, \\ &= \left(\mathbf{R}_b^n \mathbf{J}\hat{\boldsymbol{\omega}}_{nb}^b + \mathbf{R}_b^n \mathbf{J}_w \boldsymbol{\Omega}\right) - \left(\mathbf{R}_b^n \mathbf{J}\boldsymbol{\omega}_{nb}^b + \mathbf{R}_b^n \mathbf{J}_w \boldsymbol{\Omega}\right), \\ &= \mathbf{R}_b^n \mathbf{J}\tilde{\boldsymbol{\omega}}_{nb}^b. \end{aligned} \tag{6.7}$$

If Equation (6.6b) is differentiated with respect to time, it can be seen that $\dot{\tilde{\mathbf{W}}}^n = \mathbf{R}_b^n \mathbf{g}_1(\tilde{\mathbf{q}})$. Furthermore, it can also be seen by using similar calculations as in Appendix A.1, that:

$$\dot{\tilde{\mathbf{q}}} = \begin{bmatrix} \dot{\tilde{\eta}} \\ \dot{\tilde{\boldsymbol{\epsilon}}} \end{bmatrix} = \frac{1}{2}\mathbf{E}(\tilde{\mathbf{q}}) \left[\tilde{\boldsymbol{\omega}}_{nb}^b + \mathbf{g}_2(\tilde{\mathbf{q}})\right]. \tag{6.8}$$

Therefore, the complete error dynamics $\tilde{\Sigma}$ between the estimated system $\hat{\Sigma}$ and the actual system Σ can be written as:

$$\tilde{\Sigma} : \begin{cases} \dot{\tilde{\mathbf{W}}}^n & = \mathbf{R}_b^n \mathbf{g}_1(\tilde{\mathbf{q}}), \\ \dot{\tilde{\mathbf{q}}} & = \frac{1}{2}\mathbf{E}(\tilde{\mathbf{q}}) \left[\underbrace{\left(\mathbf{R}_b^n \mathbf{J}\right)^{-1} \tilde{\mathbf{W}}^n}_{\tilde{\boldsymbol{\omega}}} + \mathbf{g}_2(\tilde{\mathbf{q}}) \right], \end{cases} \tag{6.9}$$

which leads to the following proposition:

Proposition 6.1. *The observer $\hat{\Sigma}$, defined in Equation (6.5), with*

$$\mathbf{g}_1(\tilde{\mathbf{q}}) = -k_p sgn(\tilde{\eta})\mathbf{J}^{-1}\tilde{\boldsymbol{\epsilon}}, \tag{6.10a}$$

$$\mathbf{g}_2(\tilde{\mathbf{q}}) = -k_v sgn(\tilde{\eta})\tilde{\boldsymbol{\epsilon}}, \tag{6.10b}$$

will converge asymptotically towards the actual system Σ, seen in Equation (6.4), if the tuning parameters $k_p, k_v > 0$. This results in an asymptotic stable equilibrium $(\tilde{\boldsymbol{\omega}}, \tilde{\mathbf{q}}) = (\mathbf{0}, \mathbf{q}_{id})$ for the closed-loop observer.

6.2 Proof of AS observer without trajectory tracking

Nonlinear systems can be divided into two classes based on whether they are dependent on time t or not. A system that is nonlinear, but not directly dependent on t can be expressed with the equation $\dot{\mathbf{x}} = \mathbf{f}(\mathbf{x})$ and is called a nonlinear time-invariant system (NTI). If a system on the other hand, is dependent on t, it can be expressed with the equation $\dot{\mathbf{x}} = \mathbf{f}(\mathbf{x}, t)$ and is called a nonlinear time-varying system (NTV).

Whether the system is NTI or NTV is quite important for the upcoming proof of Proposition 6.1. If the system is NTI, it means that LaSalle's Invariance Principle (Khalil, 2002, Corollary 4.1) can be utilized when the Lyapunov function candidate only is negative semidefinite.

For this specific system, it is dependent on the angular velocity reference $\boldsymbol{\omega}_d^n$ whether the system is time-invariant or time-varying. If $\boldsymbol{\omega}_d^n$ is constant, it means that the system is NTI, whereas if $\boldsymbol{\omega}_d^n(t)$ is dependent on t, it is a NTV-system.

In the proof of Proposition 6.1 for a NTI system, one utilize Theorem 3.1 and Theorem 3.2 in (Shevitz and Paden, 1994). Theorem 3.1 states that a system with discontinuous "right-hand side" can be shown asymptotically stable with a non-smooth Lyapunov function. However, the Lyapunov function candidate has to belong to the "regular" function class, stated in Appendix A.3. Moreover, Theorem 3.2 proves that LaSalle's Invariance Principle also can be used for systems even when the system has "discontinuous right-hand side".

Proof. Assume that the angular velocity reference $\boldsymbol{\omega}_d^n$ is constant, which gives a nonlinear time-invariant system. Consider the "regular" Lyapunov function candidate:

$$V_o = \frac{1}{2}\left(\tilde{\mathbf{W}}^n\right)^T \tilde{\mathbf{W}}^n + k_p(1-|\tilde{\eta}|)^2 + k_p\tilde{\boldsymbol{\epsilon}}^T\tilde{\boldsymbol{\epsilon}}, \tag{6.11}$$

where $k_p > 0$ is a scalar. The time derivative of V_o along the trajectories then becomes:

$$\begin{aligned}
\dot{V}_o &= \left(\tilde{\mathbf{W}}^n\right)^T \dot{\tilde{\mathbf{W}}}^n - 2k_p sgn(\tilde{\eta})\dot{\tilde{\eta}} + 2k_p\tilde{\eta}\dot{\tilde{\eta}} + 2k_p\tilde{\boldsymbol{\epsilon}}^T\dot{\tilde{\boldsymbol{\epsilon}}}, \\
&= \left(\tilde{\mathbf{W}}^n\right)^T \mathbf{R}_b^n\mathbf{g}_1(\tilde{\mathbf{q}}) + k_p sgn(\tilde{\eta})\tilde{\boldsymbol{\epsilon}}^T\left[\tilde{\boldsymbol{\omega}} + \mathbf{g}_2(\tilde{\mathbf{q}})\right] \\
&\quad \cancel{- k_p sgn(\tilde{\eta})\tilde{\boldsymbol{\epsilon}}^T\left[\tilde{\boldsymbol{\omega}} + \mathbf{g}_2(\tilde{\mathbf{q}})\right]} + \cancel{k_p\tilde{\boldsymbol{\epsilon}}^T\left(\tilde{\eta}\mathbf{I} + \mathbf{S}(\tilde{\boldsymbol{\epsilon}})\right)\left[\tilde{\boldsymbol{\omega}} + \mathbf{g}_2(\tilde{\mathbf{q}})\right]}. \\
&= -k_p sgn(\tilde{\eta})\underbrace{\left[\left(\tilde{\mathbf{W}}^n\right)^T \mathbf{R}_b^n\mathbf{J}^{-1} - \left(\tilde{\boldsymbol{\omega}}_{nb}^b\right)^T\right]}_{\boldsymbol{\Upsilon}}\tilde{\boldsymbol{\epsilon}} - k_p k_v\left(sgn(\tilde{\eta})\right)^2\tilde{\boldsymbol{\epsilon}}^T\tilde{\boldsymbol{\epsilon}}
\end{aligned}$$

where Equation (6.9)–(6.10) have been used in addition to the fact that $\mathbf{x}^T\mathbf{S}(\mathbf{x}) = \mathbf{0},\ \forall\ \mathbf{x} \in \mathbb{R}^3$.

Let us concentrate about the expression for $\boldsymbol{\Upsilon}$. Notice from Equation (6.7) that $\tilde{\mathbf{W}}^n = \mathbf{R}_b^n\mathbf{J}\tilde{\boldsymbol{\omega}}_{nb}^b$. This means that $\boldsymbol{\Upsilon}$ becomes:

$$\begin{aligned}
\boldsymbol{\Upsilon} &= \left(\tilde{\mathbf{W}}^n\right)^T \mathbf{R}_b^n\mathbf{J}^{-1} - \left(\tilde{\boldsymbol{\omega}}_{nb}^b\right)^T, \\
&= \left(\tilde{\boldsymbol{\omega}}_{nb}^b\right)^T\left[\mathbf{J}^T(\mathbf{R}_b^n)^T\mathbf{R}_b^n\mathbf{J}^{-1}\right] - \left(\tilde{\boldsymbol{\omega}}_{nb}^b\right)^T.
\end{aligned}$$

Since $(\mathbf{R}_b^n)^T\mathbf{R}_b^n = \mathbf{I}$ and the inertia matrix $\mathbf{J}$ is symmetric, meaning $\mathbf{J}^T = \mathbf{J}$, you get that $\boldsymbol{\Upsilon} = \mathbf{0}$, and the derivative of V_o then becomes:

$$\dot{V}_o = -k_v k_p\left(sgn(\tilde{\eta})\right)^2\tilde{\boldsymbol{\epsilon}}^T\tilde{\boldsymbol{\epsilon}} \leq 0. \tag{6.12}$$

Clearly, $\dot{V}_o$ is negative semidefinite, and one can thereby conclude that the observer is stable. Unfortunately $\dot{V}_o$ is only negative semidefinite, and therefore one can not conclude with

asymptotically stability. However, by using LaSalle's theorem (Khalil, 2002) asymptotic stability can be proven as it is done in the following section:

We define the set $\mathbb{S}$ according to LaSalle's theorem as:

$$\mathbb{S} \triangleq \left\{ (\tilde{\boldsymbol{\epsilon}}, \tilde{\mathbf{W}}^n) \in \mathbb{R}^6 | \dot{V}_o = 0 \right\} = \left\{ (\tilde{\boldsymbol{\epsilon}}, \tilde{\mathbf{W}}^n) \in \mathbb{R}^6 | \tilde{\boldsymbol{\epsilon}} = \mathbf{0} \right\}. \tag{6.13}$$

This leads to the following calculations:

$$\begin{aligned}
\tilde{\boldsymbol{\epsilon}} \equiv 0, \Rightarrow \dot{\tilde{\boldsymbol{\epsilon}}} \equiv 0 &= \frac{1}{2} \left(\tilde{\eta} \mathbf{I} + \mathbf{S}(\tilde{\boldsymbol{\epsilon}}) \right) \left[\tilde{\boldsymbol{\omega}}_{nb}^b + \mathbf{g}_2(\tilde{\mathbf{q}}) \right], \\
&= \frac{1}{2} \tilde{\eta} \left[\tilde{\boldsymbol{\omega}}_{nb}^b - k_v sgn(\tilde{\eta}) \tilde{\boldsymbol{\epsilon}} \right], \\
&= \frac{1}{2} \tilde{\eta} \tilde{\boldsymbol{\omega}}_{nb}^b, \\
&= \pm \frac{1}{2} \sqrt{(1 - \tilde{\boldsymbol{\epsilon}}^T \tilde{\boldsymbol{\epsilon}})} \, \tilde{\boldsymbol{\omega}}_{nb}^b, \\
&= \pm \frac{1}{2} \left(\mathbf{R}_b^n \mathbf{J} \right)^{-1} \tilde{\mathbf{W}}^n,
\end{aligned}$$

where Equation (6.8), (6.10b), (2.17) and (6.7), have been used respectively.

Since the expression $(\mathbf{R}_b^n \mathbf{J})^{-1}$ never is equal the zero-matrix, it means that $\tilde{\mathbf{W}}^n = \mathbf{0}$. Therefore, the only solution that can stay identically in the set $\mathbb{S}$ is the trivial solution $(\tilde{\boldsymbol{\epsilon}}, \tilde{\mathbf{W}}^n) = \mathbf{0}$. Thus, according to LaSalle's theorem, the equilibrium $(\tilde{\boldsymbol{\epsilon}}, \tilde{\mathbf{W}}^n) = \mathbf{0}$ is asymptotically stable and the observer $\hat{\Sigma}$ will converge to the actual system Σ as time goes to infinity. □

Remark 6.1. Notice that we still require $sgn(x) \neq 0 \; \forall \; x \in \mathbb{R}$ to avoid getting an extra equilibrium point for $\tilde{\eta} = 0$.

6.3 Proof of AS observer with trajectory tracking

Assume now that the desired angular velocity $\boldsymbol{\omega}_d^n(t)$ is explicit dependent on time. We will therefore have to deal with a nonlinear time-varying system. This adds some difficulties to the stability analysis, since the invariance principle due to LaSalle is no longer valid. A common solution for this problem is to use Barbalat's lemma (Khalil, 2002) and prove convergence, but this does not allow to conclude with asymptotic stability. Instead we use the stability results due to Matrosov's theorem (Matrosov, 1962) which can be used to analyzing nonlinear time-varying systems where the Lyapunov function candidate derivative is only negative semi-definite. The theorem propose to use an auxiliary function W, where the time derivative of this auxiliary function must be "definitely non-zero" on the set where the Lyapunov function derivative is identically zero. The Matrosov's theorem is stated in Appendix B with its four requirements.

We are now ready to state the proof of Proposition 6.1 when the system is tracking a trajectory that is an explicit function of time:

Proof. First of all, define the state-vector $\mathbf{x} \in \mathbb{R}^7$ as the combined vector consisting of the two vectors $\tilde{\mathbf{W}}^n$ and $\tilde{\boldsymbol{\epsilon}}$, and one scalar such that

$$\mathbf{x}^T \triangleq \left[\left(\tilde{\mathbf{W}}^n \right)^T \quad \tilde{\boldsymbol{\epsilon}}^T \quad 1 - |\tilde{\eta}| \right]. \tag{6.14}$$

Satisfying Assumption B.1: Choose the same Lyapunov function candidate as seen in Equation (6.11) such that $V(\mathbf{x}, t) = V_o$, with its time derivative

$$\dot{V} = -k_p k_v \tilde{\boldsymbol{\epsilon}}^T \tilde{\boldsymbol{\epsilon}}. \tag{6.15}$$

This proves that the system is uniformly stable (US) and the system is therefore bounded. In addition, V is positive definite and decrescent and thereby satisfying Assumption B.1.

Satisfying Assumption B.2: Choose the non-positive continuous time-independent function

$$\begin{aligned} U(\mathbf{x}) &\triangleq -k_p k_v \tilde{\boldsymbol{\epsilon}}^T \tilde{\boldsymbol{\epsilon}} \\ \Rightarrow \dot{V}(\mathbf{x}, t) &\leq U(\mathbf{x}) \leq 0 \end{aligned}$$

which satisfies Assumption B.2.

Satisfying Assumption B.3: Since the origin is US, then $\tilde{\mathbf{W}}^n$, $\tilde{\boldsymbol{\epsilon}}$ and $\tilde{\eta}$ are bounded functions of time. We can therefore construct the auxiliary function $W(\mathbf{x}, t)$ as shown in Equation (6.16). We choose

$$W(\mathbf{x}, t) \triangleq -\tilde{\eta} \left(\mathbf{W}^n \right)^T \mathbf{J} \tilde{\boldsymbol{\epsilon}}, \tag{6.16}$$

and thereby satisfying Assumption B.3 of the Matrosov's theorem.

Remark 6.2. Notice that W does not need to be positive definite, but may be chosen freely as long as it is bounded.

Satisfying Assumption B.4: The derivative $\dot{W}$ then becomes

$$\dot{W}(\mathbf{x}, t) = -\dot{\tilde{\eta}} \left(\mathbf{W}^n \right)^T \mathbf{J} \tilde{\boldsymbol{\epsilon}} - \tilde{\eta} \left(\dot{\mathbf{W}}^n \right)^T \mathbf{J} \tilde{\boldsymbol{\epsilon}} - \tilde{\eta} \left(\mathbf{W}^n \right)^T \mathbf{J} \dot{\tilde{\boldsymbol{\epsilon}}}, \tag{6.17}$$

and on the set $\mathbb{N} = \{ \mathbf{x} \mid U(\mathbf{x}) = \mathbf{0} \} = \{ \mathbf{x} \mid \tilde{\boldsymbol{\epsilon}} = \mathbf{0} \}$ it can easily be seen that

$$\dot{W}(\mathbf{x}, t) = -\tilde{\eta} \left(\mathbf{W}^n \right)^T \mathbf{J} \dot{\tilde{\boldsymbol{\epsilon}}}. \tag{6.18}$$

Inserting for $\dot{\tilde{\boldsymbol{\epsilon}}}$, and using Equation (2.17), (6.7) and (6.10b), you get the following calculations:

$$\begin{aligned} \dot{W}(\mathbf{x}, t) &= -\frac{1}{2} \tilde{\eta} \left(\mathbf{W}^n \right)^T \mathbf{J} \left(\tilde{\eta} \mathbf{I} + \mathbf{S}(\tilde{\boldsymbol{\epsilon}}) \right) \left[\tilde{\boldsymbol{\omega}} + \mathbf{g}_2(\tilde{\mathbf{q}}) \right] \\ &= -\frac{1}{2} \tilde{\eta}^2 \left(\mathbf{W}^n \right)^T \mathbf{J} \tilde{\boldsymbol{\omega}} \\ &= -\frac{1}{2} \left(1 - \tilde{\boldsymbol{\epsilon}}^T \tilde{\boldsymbol{\epsilon}} \right) \left(\mathbf{W}^n \right)^T \mathbf{J} \left(\mathbf{R}_b^n \mathbf{J} \right)^{-1} \mathbf{W}^n \\ &= -\frac{1}{2} \left(\mathbf{W}^n \right)^T \mathbf{R}_n^b \mathbf{W}^n \\ &< 0 \end{aligned}$$

Therefore, the derivative $\dot{W}$ is definitely non-zero on the set $\mathbb{N}$, and Assumption B.4 is also satisfied.

Remark 6.3. This holds as long as $\tilde{\eta}$ differ from zero. However, (Krogstad, 2010) states that if the US property of Assumption B.1 is used in addition to the fact that $\tilde{\eta} = 0$ is an unstable equilibrium point, it can be seen that the conditions are meat by requiring $\tilde{\eta} \neq 0$ initially.

Finally, all the Assumptions of Matrosov's theorem are satisfied, and we may conclude that the error-dynamics in Equation (6.9) has an asymptotic stable equilibrium in $(\tilde{\boldsymbol{\omega}}, \tilde{\mathbf{q}}) = (\mathbf{0}, \mathbf{q}_{id})$ for the closed-loop observer. □

6.4 Stability for the complete system

In Section 4.2–4.3 it was proven that the system with the given controller was asymptotically stable, assuming that the system is modeled exactly and that the system is not effected by noise. In Chapter 6 it was also proven that the observer would converge to the real angular velocity, and asymptotic stability was proven. The idea is then to hope that the combined observer and controller system, seen in Figure 9.5, also is asymptotically stable. If the system was linear this would clearly be the case due to the *separation property* (Chen, 1999). However this is not necessarily the case for a nonlinear system.

To prove the stability for the system with the nonlinear observer and controller, there are essentially two methods. The first is to look at the system as one big and complex system and try to find a Lyapunov function candidate that can prove asymptotic stability. The other method is to use the theory of cascaded systems (Khalil, 2002). Both methods can be quite complex and hard to solve, and is therefore not performed in this paper. In future studies this should however be investigated more closely. Nevertheless, the asymptotically stable observer and controller give a good stability-guess about the complete stability for the combined observer and controller system.

Chapter 7

Synchronization Design

A scheme for synchronization of the attitude of two (or more) rigid bodies will be presented in this chapter. The work is based on (Bondhus, 2010), where changes have been carried out to adapt it to satellites actuated by means of reaction wheels.

7.1 Motivation

Synchronization has been seen in biological system as long as man has lived. It is therefore no big surprise that phenomenons like synchronized herring motions and bird flocks have inspired several directions within control theory. And all the theories have the same aim of utilizing the advantages that synchronization brings.

Since the subject of this thesis is the autonomous underwater satellite, it is natural to present submerged synchronization schemes in addition to systems where satellites are synchronized. There are of coarse other areas where synchronization has been utilized, including robotic manipulators (Bouteraa and Ghommam, 2009), unmanned air vehicles (Casbeer et al., 2005) and formation control of floating marine crafts (Kyrkjebø et al., 2007).

Use of autonomous underwater vehicles (AUV) can be used to perform difficult tasks which are too complicated or time consuming for a single autonomous vehicle. In particular, the mapping of the seabed (see Figure 7.1) and monitoring of large objects are excellent examples where synchronization is desirable. Using synchronized AUVs for mine sweeping is also advantageous, since it is vital to avoid risking human lives. Another area of research that suddenly became extremely relevant after the agreement of the Norwegian continental shelf, is surveillance of ice behavior. It is now possible to produce oil in the northern regions where ice exists, but if this should render possible, it is essential to know how ice behaves and how it affects different types of vessels. One can thus use the synchronized AUVs to monitor the ice from below, and thereby use the information to perform the optimal action.

Spacecraft formation flying missions is an area that has gained more interest in recent years. The reason for this is that synchronization brings essential advantages compared to having only one complex spacecraft. The main benefit is that having multiple space-

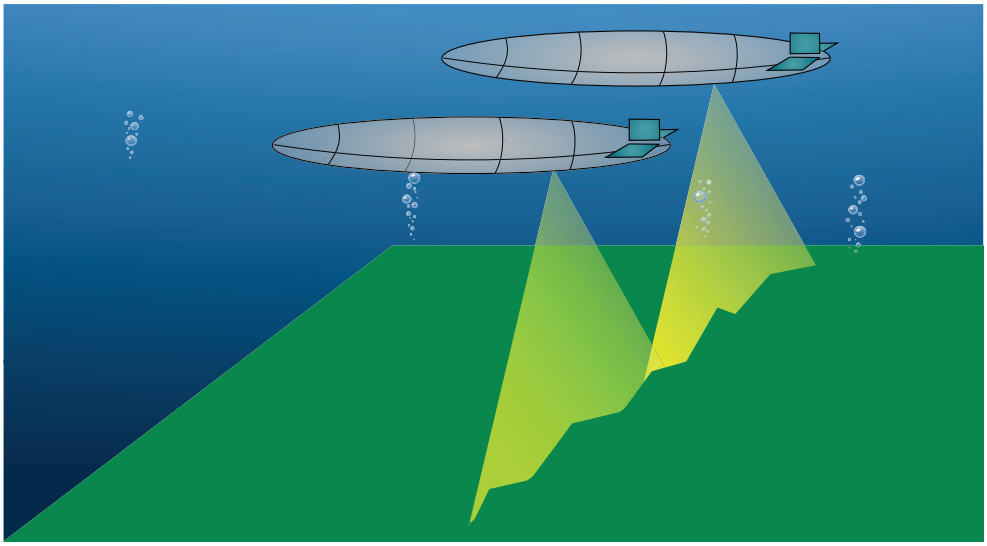

Figure 7.1: Two AUVs mapping the seabed.

craft avoids the risk of total mission failure, and one thereby gains crucial redundancy. Several cooperating spacecraft can in addition perform assignments that are more difficult and expensive, or even impossible to do for a single spacecraft. Launching of several distributed vehicles will also be less expensive since the payload can be split onto several vehicles, making it is possible to use smaller and cheaper launching systems. However, the major disadvantage of formation flying is that it requires feedback control to be able to function as specified. This results in strengthen requirements on the control algorithm and measurement accuracy.

Figure 7.2: Satellites scanning the Earth-surface is a possible area of application for synchronized space vehicles.

7.2 Different synchronization schemes

Synchronization control means in general that the difference between state trajectories of two or more systems are controlled in a more direct way than by controlling each system on its own. This implies that there are some interactions between the systems. However, there are several different main structures used in synchronization schemes. Among others, this includes "speed-synchronization along geometric paths", "leader-follower synchronization" and "tight synchronization" (Bondhus, 2010).

A formation of vehicles may be achieved by designing a geometric path for each vessel given by a supervisor. Each vessel can then synchronize its speed along this given trajectory to achieve a desired formation. This specific scheme is called *speed-synchronization along geometric paths* and an illustration of the structure can be seen in Figure 7.3(a). However, it is also possible to define one of the vessels as supervisor.

The leader-follower synchronization scheme is illustrated in Figure 7.3(b) and is the scheme used for this thesis. A vehicle is defined leader, while the others are followers. The head vehicle sends its position and velocity to its followers, and they are going to follow the leader. It is however possible to add an offset. The leader can either be controlled manually by an operator or a supervisory unit can generate a desired mathematical trajectory. Using this scheme implies that the followers are more complex to design since they have to take care of both the leader information in addition to its own. A disadvantage with this configuration is that the leader is a single point of failure for the formation. However, it is possible to design redundancy algorithms such that another vessel takes leadership in case of leader failure.

A variation of the leader-follower configuration is achieved by rearranging the information flow seen in Figure 7.3(b). This is done by letting the follower follow each closest neighbor in stead of following the master vehicle. This is called *leader-follower synchronization with nearest neighbor as leader*.

A tighter form of synchronization is seen in Figure 7.3(c). As seen from the figure, information is sent between all, or at leas many of the vehicles. This implies that the communication load is significantly higher, and each vehicle will have a complicated control structure. The advantage is that it is now possible to make each vessel behave such that the overall system looks like one rigid/virtual structure.

7.3 Modeling and definition of parameters

The notation from (Bondhus, 2010) is borrowed in this chapter, and an example can be seen in Section 2.5.2. Nevertheless, some of the fundamental notations will be presented again, to facilitate the readability.

From Equation (2.22) and (2.23) it can be seen that

$$\dot{\mathbf{R}}_b^a = \mathbf{S}(\boldsymbol{\omega}_{ab}^a)\mathbf{R}_b^a = \mathbf{R}_b^a\mathbf{S}(\boldsymbol{\omega}_{ab}^b) \tag{7.1}$$

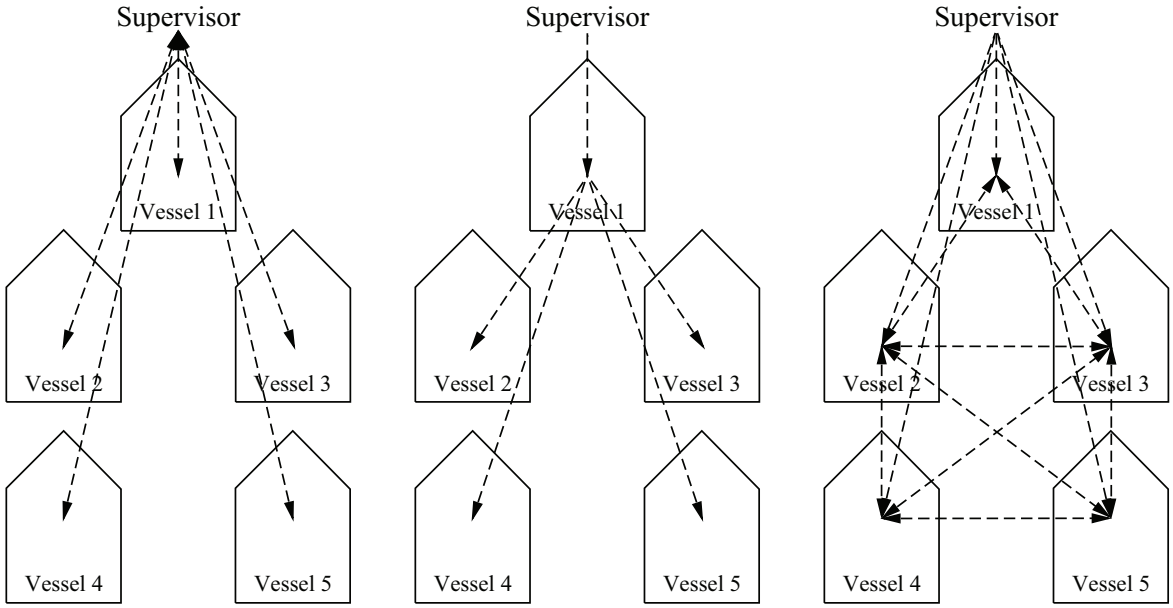

(a) Formation keeping by speed-synchronization along geometric path.

(b) Formation keeping by leader-follower synchronization.

(c) Formation keeping by tight synchronization.

Figure 7.3: Schemes for synchronization control.

and written in terms of the corresponding unit quaternion $\mathbf{q}_{ab}$ such that

$$\dot{\mathbf{q}}_{ab} = \frac{1}{2}[\boldsymbol{\omega}^a_{ab}]_q \otimes \mathbf{q}_{ab} = \frac{1}{2}\mathbf{q}_{ab} \otimes [\boldsymbol{\omega}^b_{ab}]_q \tag{7.2}$$

where $\otimes$ is the quaternion product operator defined in Definition 2.4, and $[\boldsymbol{\omega}^i_{ab}]_q$ is the angular-velocity quaternion defined in Definition 2.5 with $i \in \{a, b\}$. Further, it can be shown that

$$\boldsymbol{\omega}^c_{ab} = \boldsymbol{\omega}^c_{nb} - \boldsymbol{\omega}^c_{na} \tag{7.3}$$

for any frame a, b, c and n. This is quite an important relationship and will be used in the upcoming calculations.

To carry on, it is essential to define different variables and error variables used in the calculations. This includes five different attitudes variables and all the attitude errors between them. The angular velocity errors between the estimated and actual generalized velocities for the leader and the follower come in addition.

Definition 7.1. *Define the following quaternions for the tracking and synchronization scheme, such that all the different frames can be compared against each other and the inertial frame* $\{n\}$*:*

$$\begin{aligned}
\mathbf{q}_d &= \mathbf{q}_{nd} &&= \begin{bmatrix}\eta_d & \boldsymbol{\epsilon}_d^T\end{bmatrix}^T && : \textit{Desired attitude of the leader}\\
\mathbf{q}_l &= \mathbf{q}_{nl} &&= \begin{bmatrix}\eta_l & \boldsymbol{\epsilon}_l^T\end{bmatrix}^T && : \textit{Attitude of the leader}\\
\mathbf{q}_f &= \mathbf{q}_{nf} &&= \begin{bmatrix}\eta_f & \boldsymbol{\epsilon}_f^T\end{bmatrix}^T && : \textit{Attitude of the follower}\\
\hat{\mathbf{q}}_l &= \mathbf{q}_{n\hat{l}} &&= \begin{bmatrix}\hat{\eta}_l & \hat{\boldsymbol{\epsilon}}_l^T\end{bmatrix}^T && : \textit{Estimated attitude of the leader}\\
\hat{\mathbf{q}}_f &= \mathbf{q}_{n\hat{f}} &&= \begin{bmatrix}\hat{\eta}_f & \hat{\boldsymbol{\epsilon}}_f^T\end{bmatrix}^T && : \textit{Estimated attitude of the follower}
\end{aligned}$$

Table 7.1: *Quaternions for the desired attitude, the leader and the follower attitude, and the estimated attitude for the leader and the follower.*

Definition 7.2. *Define the following error quaternions for the tracking and synchronization scheme where* $\otimes$ *is the quaternion product and* $\mathbf{q}_i^{-1}$ *is the complex-conjugate quaternion for* $i \in \{d, l, f\}$*:*

$$\begin{aligned}
\mathbf{e}_l &= \mathbf{e}_{dl} &&\triangleq && \mathbf{q}_d^{-1} \otimes \mathbf{q}_l &&= \begin{bmatrix}\eta_{\mathbf{e}_l} & \boldsymbol{\epsilon}_{\mathbf{e}_l}^T\end{bmatrix}^T\\
\mathbf{e}_f &= \mathbf{e}_{lf} &&\triangleq && \mathbf{q}_l^{-1} \otimes \mathbf{q}_f &&= \begin{bmatrix}\eta_{\mathbf{e}_f} & \boldsymbol{\epsilon}_{\mathbf{e}_f}^T\end{bmatrix}^T\\
\hat{\mathbf{e}}_l &= \mathbf{e}_{d\hat{l}} &&\triangleq && \mathbf{q}_d^{-1} \otimes \hat{\mathbf{q}}_l &&= \begin{bmatrix}\hat{\eta}_{\mathbf{e}_l} & \hat{\boldsymbol{\epsilon}}_{\mathbf{e}_l}^T\end{bmatrix}^T\\
\hat{\mathbf{e}}_f &= \mathbf{e}_{\hat{l}\hat{f}} &&\triangleq && \hat{\mathbf{q}}_l^{-1} \otimes \hat{\mathbf{q}}_f &&= \begin{bmatrix}\hat{\eta}_{\mathbf{e}_f} & \hat{\boldsymbol{\epsilon}}_{\mathbf{e}_f}^T\end{bmatrix}^T\\
\tilde{\mathbf{q}}_l &= \mathbf{q}_{l\hat{l}} &&\triangleq && \mathbf{q}_l^{-1} \otimes \hat{\mathbf{q}}_l &&= \begin{bmatrix}\tilde{\eta}_l & \tilde{\boldsymbol{\epsilon}}_l^T\end{bmatrix}^T\\
\tilde{\mathbf{q}}_f &= \mathbf{q}_{f\hat{f}} &&\triangleq && \mathbf{q}_f^{-1} \otimes \hat{\mathbf{q}}_f &&= \begin{bmatrix}\tilde{\eta}_f & \tilde{\boldsymbol{\epsilon}}_f^T\end{bmatrix}^T
\end{aligned}$$

Table 7.2: *Error quaternions between all quaternions shown in Definition 7.1. An illustration can be seen in Figure 7.4*

Definition 7.3. *The angular velocity error is defined as the difference between the estimated and the actual angular velocity, similar as in Equation* (6.6c)*, such that*

$$\tilde{\boldsymbol{\omega}}_{nk}^n \triangleq \hat{\boldsymbol{\omega}}_{nk}^n - \boldsymbol{\omega}_{nk}^n \tag{7.4}$$

where $k = l$ *for the leader and* $k = f$ *for the follower.*

7.4 System equations

The calculations in (Bondhus, 2010) is done in the inertial frame, as will be the case for this section also. Calculations expressed in the BODY-coordinate has been investigated,

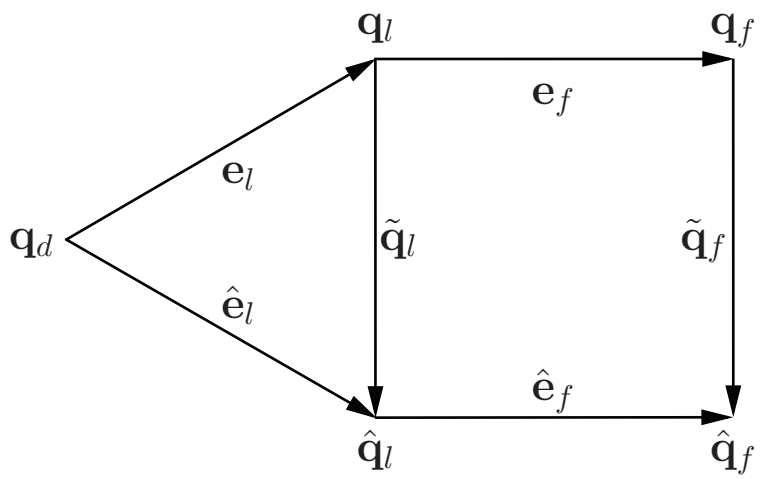

Figure 7.4: Illustration of quaternion errors and variables used in the synchronization scheme.

but it turned out that some of the needed variables for the controller where unknown when the system was stated in the BODY-frame.

The kinematic equations for the leader and the follower in the inertial frame can be expressed as one equation as

$$\dot{\mathbf{q}}_k = \frac{1}{2}[\boldsymbol{\omega}^n_{nk}]_q \otimes \mathbf{q}_k \tag{7.5}$$

where $k = l$ for the leader, and $k = f$ for the follower.

To define the kinetic system equation in the inertial frame, one need to state the inertia matrix for the wheels and for the complete satellite in the inertial frame.

Definition 7.4. *The inertia matrix for the complete system, the wheels and the system without the wheels, expressed in the inertial NED frame, is given by*

$$\mathbf{J}^n_k = \mathbf{R}^n_k \mathbf{J}_k \mathbf{R}^k_n \tag{7.6a}$$

$$\mathbf{J}^n_{\omega,k} = \mathbf{R}^n_k \mathbf{J}_{\omega,k} \mathbf{R}^k_n \tag{7.6b}$$

$$\mathbf{J}^n_{s,k} = \mathbf{J}^n_k - \mathbf{J}^n_{\omega,k} = \mathbf{R}^n_k \mathbf{J}_{s,k} \mathbf{R}^k_n \tag{7.6c}$$

where $k = l$ for the leader and $k = f$ for the follower.

One can thereby state the kinetic differential equation for the complete system, as

$$\underbrace{\frac{\mathrm{d}}{\mathrm{d}t}\left(\mathbf{J}^n_k \boldsymbol{\omega}^n_{nk}\right)}_{\mathbf{A}} + \underbrace{\frac{\mathrm{d}}{\mathrm{d}t}\left(\mathbf{J}^n_{\omega,k} \boldsymbol{\Omega}^n_k\right)}_{\mathbf{B}} = \mathbf{T}^n_{ex,k} \tag{7.7}$$

where $\mathbf{T}^n_{ex,k}$ is the external torque applied to system k. Notice that the control variable $\mathbf{T}^n_{u,k}$ is "hidden" inside the $\mathbf{B}$-dynamics, as will be seen.

First, focus on the expression for $\mathbf{A}$. From (Spong et al., 2006) it can be seen that $\boldsymbol{\omega}_{ab}^{a} = -\boldsymbol{\omega}_{ba}^{a}$ for all frames a and b, which gives the following calculations:

$$\begin{aligned}
\mathbf{A} &= \mathbf{J}_k^n \dot{\boldsymbol{\omega}}_{nk}^n + \dot{\mathbf{R}}_k^n \mathbf{J}_k \mathbf{R}_n^k \boldsymbol{\omega}_{nk}^n + \mathbf{R}_k^n \mathbf{J}_k \dot{\mathbf{R}}_n^k \boldsymbol{\omega}_{nk}^n \\
&= \mathbf{J}_k^n \dot{\boldsymbol{\omega}}_{nk}^n + \mathbf{S}(\boldsymbol{\omega}_{nk}^n) \mathbf{R}_k^n \mathbf{J}_k \mathbf{R}_n^k \boldsymbol{\omega}_{nk}^n - \mathbf{R}_k^n \mathbf{J}_k \mathbf{R}_n^k \mathbf{S}(\boldsymbol{\omega}_{nk}^n) \boldsymbol{\omega}_{nk}^n \\
&= \mathbf{J}_k^n \dot{\boldsymbol{\omega}}_{nk}^n + \mathbf{S}(\boldsymbol{\omega}_{nk}^n) \mathbf{J}_k^n \boldsymbol{\omega}_{nk}^n - \mathbf{J}_k^n \mathbf{S}(\boldsymbol{\omega}_{nk}^n) \boldsymbol{\omega}_{nk}^n \\
&= \mathbf{J}_k^n \dot{\boldsymbol{\omega}}_{nk}^n + \mathbf{L}_J \left(\boldsymbol{\omega}_{nk}^n, \mathbf{J}_k^n \right) \boldsymbol{\omega}_{nk}^n
\end{aligned}$$

where $\mathbf{L}_J(\,\cdot\,,\,\cdot\,)$ is a matrix-operator defined such that

$$\mathbf{L}_J(\boldsymbol{\omega}, \mathbf{J}) \triangleq \mathbf{S}(\boldsymbol{\omega})\mathbf{J} - \mathbf{J}\mathbf{S}(\boldsymbol{\omega}) \in \mathbb{R}^{3\times 3}. \tag{7.8}$$

In the same way as for $\mathbf{A}$, it can be seen that the following calculations holds for $\mathbf{B}$:

$$\begin{aligned}
\mathbf{B} &= \mathbf{J}_{\omega,k}^n \dot{\boldsymbol{\Omega}}_k^n + \mathbf{L}_J \left(\boldsymbol{\omega}_{nk}^n, \mathbf{J}_{\omega,k}^n \right) \boldsymbol{\Omega}_k^n \\
&= \mathbf{R}_k^n \mathbf{J}_{\omega,k} \dot{\boldsymbol{\Omega}}_k^k + \mathbf{L}_J \left(\boldsymbol{\omega}_{nk}^n, \mathbf{J}_{\omega,k}^n \right) \boldsymbol{\Omega}_k^n \\
&= \mathbf{R}_k^n \left[\mathbf{T}_{u,k}^k - \mathbf{J}_{\omega,k} \dot{\boldsymbol{\omega}}_{nk}^k \right] + \mathbf{L}_J \left(\boldsymbol{\omega}_{nk}^n, \mathbf{J}_{\omega,k}^n \right) \boldsymbol{\Omega}_k^n \\
&= -\mathbf{J}_{\omega,k}^n \dot{\boldsymbol{\omega}}_{nk}^n + \mathbf{L}_J \left(\boldsymbol{\omega}_{nk}^n, \mathbf{J}_{\omega,k}^n \right) \boldsymbol{\Omega}_k^n + \mathbf{T}_{u,k}^n
\end{aligned}$$

where Equation (3.16) have been used. Therefore, Equation (7.7) may be written as

$$\mathbf{J}_{s,k}^n \dot{\omega}_{nk}^n + \mathbf{L}_J \left(\boldsymbol{\omega}_{nk}^n, \mathbf{J}_k^n \right) \boldsymbol{\omega}_{nk}^n + \mathbf{L}_J \left(\boldsymbol{\omega}_{nk}^n, \mathbf{J}_{\omega,k}^n \right) \boldsymbol{\Omega}_k^n = \mathbf{T}_{ex,k}^n - \mathbf{T}_{u,k}^n. \tag{7.9}$$

Remark 7.1. It can be seen that the kinetic system equation above is the same as the kinetic equation, shown in Equation (3.17). The only difference is that the latter is expressed in the BODY-frame.

7.5 Control objective

The control objective for the tracking and synchronization scheme is to design $\mathbf{T}_{u,l}$ and $\mathbf{T}_{u,f}$ such that one will get asymptotic converges of $\mathbf{q}_l \to \mathbf{q}_d$ and $\mathbf{q}_f \to \mathbf{q}_l$. In addition to this, an observer will be presented for both the leader and the follower, as it is assumed that angular velocity measurements is not present.

It is important to distinguish the tracking problem from the synchronization problem. All though they are similar in many ways, there are some essential differences which will be clear through the rest of this section. Therefore, we define the tracking and synchronization problem according to Definition 7.5–7.6:

Definition 7.5. *The problem of getting the attitude of the leader $\mathbf{q}_l$ to track the desired attitude $\mathbf{q}_d$ will be called "the tracking problem".*

Definition 7.6. *The problem of getting the attitude of the follower $\mathbf{q}_f$ to track the leader attitude $\mathbf{q}_l$ will be called "the synchronization problem".*

These problems are different since for the tracking problem, the desired trajectory $\mathbf{q}_d$ is given mathematically, while the desired trajectory for the synchronization problem, $\mathbf{q}_l$, is only a measured trajectory. The advantage of having a mathematically expression for the desired trajectory, is that it is possible to design the reference $\mathbf{q}_d$ such that all higher derivatives is known at all time. Therefore, it is also possible to find the desired angular velocity $\boldsymbol{\omega}_{nd}^n$ and all higher derivatives of the desired angular velocity. This is however not the case for the synchronization problem. Since $\mathbf{q}_l$ is only measured, and since the satellites are assumed not to have angular velocity measurements, the desired angular velocity for the synchronization problem $\boldsymbol{\omega}_{nl}^n$ is unknown. This clearly adds an extra difficulty to the synchronization problem, which has to be handled. The proposed solution for this matter is to use the observer in the leader satellite to estimate its own angular velocity in addition to $\dot{\boldsymbol{\omega}}_{nl}^n$ and send this information to the follower. In addition comes the problem of that the angular velocity of itself is not known, which means that one need an observer for that as well.

Despite the differences between the tracking and synchronization problem, both problems will be designed in a similar manner, using the backstepping control method (Khalil, 2002). The structure of the system can be seen in Figure 9.7.

7.6 Observer equation

It is assumed that measurement of angular velocity is not present for the satellites, and one will therefore use the nonlinear observer presented in Chapter 6 to estimate the generalized velocity. In Chapter 6 the observer was presented using BODY-coordinates, and in order to fit the calculations with this chapter, it is necessary to state the observer equations in the inertial frame. However, the observer is essentially the same, and the proofs in Section 6.2–6.3 will also hold when the system is stated using NED-coordinates.

The observer, expressed in the inertial frame $\{n\}$, have the following structure:

$$\dot{\hat{\mathbf{q}}}_k = \frac{1}{2}[\boldsymbol{\omega}_{nk}^n + \mathbf{g}_{2,k}^n(\tilde{\mathbf{q}}_k)]_q \otimes \hat{\mathbf{q}}_k \tag{7.10a}$$

$$\underbrace{\frac{\mathrm{d}}{\mathrm{d}t}\left(\mathbf{J}_k^n \hat{\boldsymbol{\omega}}_{nk}^n\right)}_{\hat{\mathbf{A}}} + \underbrace{\frac{\mathrm{d}}{\mathrm{d}t}\left(\mathbf{J}_{\omega,k}^n \boldsymbol{\Omega}_k^n\right)}_{\hat{\mathbf{B}}} = \mathbf{T}_{ex,k}^n + \mathbf{g}_{1,k}^n(\tilde{\mathbf{q}}_k) \tag{7.10b}$$

where $k = l$ for the leader and $k = f$ for the follower.

The tuning parameters $\mathbf{g}_{1,k}^n(\tilde{\mathbf{q}}_k)$ and $\mathbf{g}_{2,k}^n(\tilde{\mathbf{q}}_k)$ are chosen to have the same expression as in Equation (6.10), only rotated such that it is aligned with the inertial frame. Therefore:

$$\mathbf{g}_{1,k}^n(\tilde{\mathbf{q}}_k) \triangleq \mathbf{R}_k^n \mathbf{g}_{1,k} = -k_{p,k} sgn(\tilde{\eta}_k) \mathbf{R}_k^n \left(\mathbf{J}_k\right)^{-1} \tilde{\boldsymbol{\epsilon}}_k \tag{7.11a}$$

$$\mathbf{g}_{2,k}^n(\tilde{\mathbf{q}}_k) \triangleq \mathbf{R}_k^n \mathbf{g}_{2,k} = -k_{v,k} sgn(\tilde{\eta}_k) \mathbf{R}_k^n \tilde{\boldsymbol{\epsilon}}_k \tag{7.11b}$$

where $k_{p,k}$ and $k_{v,k}$ are positive scalars and the observer error $\tilde{\mathbf{q}}_k^T = \begin{bmatrix} \tilde{\eta}_k & \tilde{\boldsymbol{\epsilon}}_k^T \end{bmatrix}$.

7.7 Error dynamics for the tracking and synchronization scheme

As explained in Section 7.5 the tracking and synchronization problem will be designed in a similar manner and one will therefore try to express the error dynamics for the tracking and synchronization problem equally. The kinematic and kinetic error dynamics will be presented in the following two sections.

7.7.1 Kinematic error dynamics

The error variables for the kinematics are chosen to be $\hat{\mathbf{e}}_l$ and $\hat{\mathbf{e}}_f$, and one will design $\mathbf{T}^n_{u,l}$ and $\mathbf{T}^n_{u,f}$ such that $\hat{\mathbf{e}}_l \to \mathbf{q}_{id}$ and $\hat{\mathbf{e}}_f \to \mathbf{q}_{id}$. It is also possible to use $\mathbf{e}_l$ and $\mathbf{e}_f$ as error coordinates, but (Bondhus, 2010) found out that this choice lead to a more complicated controller design. In any case, it can be seen from Figure 7.4 that if $\hat{\mathbf{e}}_l$, $\hat{\mathbf{e}}_f$, $\tilde{\mathbf{q}}_l$ and $\tilde{\mathbf{q}}_f$ converge to $\mathbf{q}_{id}$ also $\mathbf{e}_l$ and $\mathbf{e}_f$ will converge to $\mathbf{q}_{id}$. This implies that $\mathbf{q}_l \to \mathbf{q}_d$ and $\mathbf{q}_f \to \mathbf{q}_l$, which are the control objectives.

Using Equation (7.2)–(7.3) and the fact that the angular velocity of the estimated system is given by

$$\boldsymbol{\omega}^n_{n\hat{k}} = \hat{\boldsymbol{\omega}}^n_{nk} + \mathbf{g}^n_{2,k}(\tilde{\mathbf{q}}_k) \tag{7.12}$$

it can be seen that the differential equation for $\hat{\mathbf{e}}_l$ may be written as

$$\begin{aligned}
\dot{\hat{\mathbf{e}}}_l &= \frac{1}{2}\left[\boldsymbol{\omega}^d_{d\hat{l}}\right]_q \otimes \hat{\mathbf{e}}_l \\
&= \frac{1}{2}\left[\mathbf{R}^d_n \boldsymbol{\omega}^n_{d\hat{l}}\right]_q \otimes \hat{\mathbf{e}}_l \\
&= \frac{1}{2}\left[\mathbf{R}^d_n \left(\boldsymbol{\omega}^n_{n\hat{l}} - \boldsymbol{\omega}^n_{nd}\right)\right]_q \otimes \hat{\mathbf{e}}_l \\
&= \frac{1}{2}\left[\mathbf{R}^d_n \left(\hat{\boldsymbol{\omega}}^n_{nl} - \boldsymbol{\omega}^n_{nd} + \mathbf{g}^n_{2,l}\right)\right]_q \otimes \hat{\mathbf{e}}_l.
\end{aligned} \tag{7.13}$$

Similarly the differential equation for $\hat{\mathbf{e}}_f$ is given by

$$\begin{aligned}
\dot{\hat{\mathbf{e}}}_f &= \frac{1}{2}\left[\boldsymbol{\omega}^{\hat{l}}_{\hat{l}\hat{f}}\right]_q \otimes \hat{\mathbf{e}}_f \\
&= \frac{1}{2}\left[\mathbf{R}^{\hat{l}}_n \left(\boldsymbol{\omega}^n_{n\hat{f}} - \boldsymbol{\omega}^n_{n\hat{l}}\right)\right]_q \otimes \hat{\mathbf{e}}_f \\
&= \frac{1}{2}\left[\mathbf{R}^{\hat{l}}_n \left(\hat{\boldsymbol{\omega}}^n_{nf} - \hat{\boldsymbol{\omega}}^n_{nl} + \mathbf{g}^n_{2,l} - \mathbf{g}^n_{2,f}\right)\right]_q \otimes \hat{\mathbf{e}}_f.
\end{aligned} \tag{7.14}$$

Both $\dot{\hat{\mathbf{e}}}_l$ and $\dot{\hat{\mathbf{e}}}_f$ are in the form

$$\dot{\hat{\mathbf{e}}} = \frac{1}{2}\left[\mathbf{R}^T_1 \left(\hat{\boldsymbol{\omega}} - \boldsymbol{\omega}_D + \mathbf{v}_o\right)\right]_q \otimes \hat{\mathbf{e}} \tag{7.15}$$

and this equation will be used in the upcoming backstepping design. It should also be noted that $\mathbf{v}_o$ is a disturbance term caused by the observer errors. For both problem there

is a bound on $|\mathbf{v}_o|$, as can be seen from the analysis of the observer, and therefore, $\mathbf{v}_o$ will converge to zero when the observer converge to the actual value.

For the tracking problem it can easily be seen that Equation (7.15) represents Equation (7.13) if $\hat{\mathbf{e}} = \hat{\mathbf{e}}_l$, $\mathbf{R}_1 = \mathbf{R}_d^n$, $\hat{\boldsymbol{\omega}} = \hat{\boldsymbol{\omega}}_{nl}^n$, $\boldsymbol{\omega}_D = \boldsymbol{\omega}_{nd}^n$ and $\mathbf{v}_o = \mathbf{g}_{2,l}^n$. For the synchronization scheme, $\hat{\mathbf{e}} = \hat{\mathbf{e}}_f$, $\mathbf{R}_1 = \mathbf{R}_{\hat{l}}^n$, $\hat{\boldsymbol{\omega}} = \hat{\boldsymbol{\omega}}_{nf}^n$, $\boldsymbol{\omega}_D = \hat{\boldsymbol{\omega}}_{nl}^n$ and $\mathbf{v}_o = \mathbf{g}_{2,f}^n - \mathbf{g}_{2,l}^n$.

7.7.2 Kinetic error dynamics

The calculations of the kinetic error dynamics uses the definition of the kinetic observer, seen in Equation (7.10b), as basis. Then, Definition 7.3 can be used to get the following calculations for $\hat{\mathbf{A}}$ and $\hat{\mathbf{B}}$:

$$\begin{aligned}
\hat{\mathbf{A}} &= \mathbf{J}_k^n \dot{\hat{\boldsymbol{\omega}}}_{nk}^n + \mathbf{L}_J(\boldsymbol{\omega}_{nk}^n, \mathbf{J}_k^n)\hat{\boldsymbol{\omega}}_{nk}^n \\
&= \mathbf{J}_k^n \dot{\hat{\boldsymbol{\omega}}}_{nk}^n + \mathbf{L}_J(\hat{\boldsymbol{\omega}}_{nk}^n, \mathbf{J}_k^n)\hat{\boldsymbol{\omega}}_{nk}^n - \mathbf{L}_J(\tilde{\boldsymbol{\omega}}_{nk}^n, \mathbf{J}_k^n)\hat{\boldsymbol{\omega}}_{nk}^n \\
\hat{\mathbf{B}} &= -\mathbf{J}_{\omega,k}^n \boldsymbol{\omega}_{nk}^n + \mathbf{L}_J(\boldsymbol{\omega}_{nk}^n, \mathbf{J}_{\omega,k}^n)\boldsymbol{\Omega}_k^n + \mathbf{T}_{u,k}^n \\
&= -\mathbf{J}_{\omega,k}^n \dot{\hat{\boldsymbol{\omega}}}_{nk}^n + \mathbf{J}_{\omega,k}^n \dot{\tilde{\boldsymbol{\omega}}}_{nk}^n + \mathbf{L}_J(\hat{\boldsymbol{\omega}}_{nk}^n, \mathbf{J}_{\omega,k}^n)\hat{\boldsymbol{\omega}}_{nk}^n - \mathbf{L}_J(\tilde{\boldsymbol{\omega}}_{nk}^n, \mathbf{J}_{\omega,k}^n)\hat{\boldsymbol{\omega}}_{nk}^n + \mathbf{T}_{u,k}^n.
\end{aligned}$$

Then Equation (7.10b) may be written as

$$\begin{aligned}
\mathbf{J}_{s,k}^n \dot{\hat{\boldsymbol{\omega}}}_{nk}^n = \mathbf{L}_J\left(\tilde{\boldsymbol{\omega}}_{nk}^n, \mathbf{J}_k^n\right)\hat{\boldsymbol{\omega}}_k^n + \mathbf{L}_J\left(\tilde{\boldsymbol{\omega}}_{nk}^n, \mathbf{J}_{\omega,k}^n\right)\boldsymbol{\Omega}_k^n - \mathbf{L}_J\left(\hat{\boldsymbol{\omega}}_{nk}^n, \mathbf{J}_k^n\right)\hat{\boldsymbol{\omega}}_{nk}^n \\
- \mathbf{L}_J\left(\hat{\boldsymbol{\omega}}_{nk}^n, \mathbf{J}_{\omega,k}^n\right)\boldsymbol{\Omega}_k^n - \mathbf{J}_{\omega,k}^n \dot{\tilde{\boldsymbol{\omega}}}_{nk}^n + \mathbf{T}_{ex,k}^n - \mathbf{T}_{u,k}^n + \mathbf{g}_{1,k}^n(\tilde{\mathbf{q}}_k).
\end{aligned} \tag{7.16}$$

This can then be written in a more compact expression

$$\mathbf{J}_s^* \dot{\hat{\boldsymbol{\omega}}} = -\mathbf{J}_\omega^* \dot{\tilde{\boldsymbol{\omega}}} + \tilde{\Gamma}(\tilde{\boldsymbol{\omega}}, \hat{\boldsymbol{\omega}}, \boldsymbol{\Omega}) - \hat{\Gamma}(\hat{\boldsymbol{\omega}}, \boldsymbol{\Omega}) + \mathbf{T}_{ex}^* - \mathbf{T}_u^* + \mathbf{g}_1^*, \tag{7.17}$$

where

$$\tilde{\Gamma}(\tilde{\boldsymbol{\omega}}, \hat{\boldsymbol{\omega}}, \boldsymbol{\Omega}) = \mathbf{L}_J\left(\tilde{\boldsymbol{\omega}}, \mathbf{J}^*\right)\hat{\boldsymbol{\omega}} + \mathbf{L}_J\left(\tilde{\boldsymbol{\omega}}, \mathbf{J}_\omega^*\right)\boldsymbol{\Omega}, \tag{7.18a}$$

$$\hat{\Gamma}(\hat{\boldsymbol{\omega}}, \boldsymbol{\Omega}) = \mathbf{L}_J\left(\hat{\boldsymbol{\omega}}, \mathbf{J}^*\right)\hat{\boldsymbol{\omega}} + \mathbf{L}_J\left(\hat{\boldsymbol{\omega}}, \mathbf{J}_\omega^*\right)\boldsymbol{\Omega}, \tag{7.18b}$$

and $\mathbf{L}_J(\boldsymbol{\omega}, \mathbf{J})$ is the matrix operator defined in Equation (7.8).

Equation (7.17) is then going to represents Equation (7.10b) for both the leader and the follower. This implies that $\mathbf{J}^* = \mathbf{J}_k^n$, $\mathbf{J}_s^* = \mathbf{J}_{s,k}^n$, $\mathbf{J}_\omega^* = \mathbf{J}_{\omega,k}^n$, $\tilde{\boldsymbol{\omega}} = \tilde{\boldsymbol{\omega}}_{nk}^n$, $\boldsymbol{\Omega} = \boldsymbol{\Omega}_k^n$, $\mathbf{T}_{ex}^* = \mathbf{T}_{ex,k}^n$, $\mathbf{T}_u^* = \mathbf{T}_{u,k}^n$ and $\mathbf{g}_1^* = \mathbf{g}_{1,k}^n$ where $k = l$ for the leader and $k = f$ for the follower.

We are then ready to start the vectorial backstepping method for the control design.

7.8 Backstepping control

In this section a vectorial backstepping controller will be derived for the tracking and synchronization scheme. An introduction to this recursive control method is presented in Section 4.3.

Step 1: We start the recursive backstepping method by choosing $\hat{\boldsymbol{\omega}}$ as virtual control for Equation (7.17).

Definition 7.7. *The virtual control variable $\hat{\boldsymbol{\omega}}$ in step one of the recursive backstepping algorithm is defined such that*

$$\hat{\boldsymbol{\omega}} \triangleq \hat{\boldsymbol{\omega}}_r + \mathbf{u}, \tag{7.19}$$

where $\hat{\boldsymbol{\omega}}_r$ is a chosen desired reference trajectory for $\hat{\boldsymbol{\omega}}$, and $\mathbf{u}$ is a variable that connects the kinematic dynamics with the kinetics.

The stabilizing term $\hat{\boldsymbol{\omega}}_r$ may be chosen such that

$$\hat{\boldsymbol{\omega}}_r \triangleq \mathbf{R}_1 \boldsymbol{\alpha}(\hat{\mathbf{e}}) + \boldsymbol{\omega}_D \tag{7.20}$$

where $\boldsymbol{\alpha}(\hat{\mathbf{e}})$ is chosen such that it stabilizes the kinematic dynamics, given that the observer error converge to zero. In (Bondhus, 2010) several choices for $\boldsymbol{\alpha}(\mathbf{e})$ have been presented, but in this thesis, $\boldsymbol{\alpha}(\hat{\mathbf{e}})$ is chosen such that

$$\boldsymbol{\alpha}(\hat{\mathbf{e}}) \triangleq -sgn(\eta_{\hat{\mathbf{e}}})\boldsymbol{\Lambda}\boldsymbol{\epsilon}_{\hat{\mathbf{e}}}. \tag{7.21}$$

where $\boldsymbol{\Lambda}$ is a positive definite tuning parameter and $\boldsymbol{\Lambda} = \boldsymbol{\Lambda}^T \in \mathbb{R}^{3\times 3}$. One can thereby state the following proposition:

Proposition 7.1. *Chose $\boldsymbol{\alpha}(\hat{\mathbf{e}})$ according to Equation (7.21). Further, assume that $|\mathbf{u}|$ and $|\mathbf{v}_o|$ are bounded, in addition to $\mathbf{u} \to \mathbf{0}$ and $\mathbf{v}_o \to \mathbf{0}$ as $t \to \infty$, then*

$$\hat{\mathbf{e}} \to \mathbf{q}_{id} \text{ as } t \to \infty, \tag{7.22}$$

for both the leader and the follower. This means that the actual attitude will be aligned with the desired attitude when time goes to infinity.

Proof. In the proof of Proposition 7.1, one will use some of the same ideas as in previous proof of kinematic error convergence. However this time one also has to deal with the error terms from the observer. This adds an extra difficulty to the proof, but as long as $|\mathbf{u}|$ and $|\mathbf{v}_o|$ are bounded, one can utilize the proof of Theorem 9.5 in (Bondhus, 2010) and (Khalil, 2002, Theorem 4.18).

If $\boldsymbol{\alpha}(\hat{\mathbf{e}})$ is chosen as in Equation (7.21), the estimated kinematic error dynamics for the leader and the follower, may be written as

$$\dot{\hat{\mathbf{e}}} = \frac{1}{2}\left[\boldsymbol{\alpha}(\hat{\mathbf{e}}) + \boldsymbol{\Delta}\right]_q \otimes \hat{\mathbf{e}} \text{ , with } \boldsymbol{\Delta} = \mathbf{R}_1^T\left(\mathbf{u} + \mathbf{v}_o\right) \tag{7.23}$$

Consider the positive definite Lyapunov function

$$V = 1 - \sqrt{1 - \boldsymbol{\epsilon}_{\hat{\mathbf{e}}}^T \boldsymbol{\epsilon}_{\hat{\mathbf{e}}}} = 1 - |\eta_{\hat{\mathbf{e}}}| \tag{7.24a}$$

$$\Rightarrow\ 0 \leq V \leq 1, \quad \forall t. \tag{7.24b}$$

We may again think of V as either a function of $\boldsymbol{\epsilon}_{\hat{\mathbf{e}}}$ or as a function of $\eta_{\hat{\mathbf{e}}}$, and since $\eta_{\hat{\mathbf{e}}}^2 + \boldsymbol{\epsilon}_{\hat{\mathbf{e}}}^T \boldsymbol{\epsilon}_{\hat{\mathbf{e}}} = 1$ for all time, we may only use $|\eta_{\hat{\mathbf{e}}}|$ or $\boldsymbol{\epsilon}_{\hat{\mathbf{e}}}$ in the analysis.

Using Equation (7.23), (7.21) and (2.19), the time-derivative of V along solution is given by

$$\begin{aligned}\dot{V} &= -sgn(\eta_{\hat{\mathbf{e}}})\dot{\eta}_{\hat{\mathbf{e}}} \\ &= \frac{1}{2}sgn(\eta_{\hat{\mathbf{e}}})\boldsymbol{\epsilon}_{\hat{\mathbf{e}}}^T\left(\boldsymbol{\alpha}(\hat{\mathbf{e}}) + \boldsymbol{\Delta}\right) \\ &= -\frac{1}{2}\boldsymbol{\epsilon}_{\hat{\mathbf{e}}}^T\boldsymbol{\Lambda}\boldsymbol{\epsilon}_{\hat{\mathbf{e}}} + \frac{1}{2}sgn(\eta_{\hat{\mathbf{e}}})\boldsymbol{\epsilon}_{\hat{\mathbf{e}}}^T\boldsymbol{\Delta}.\end{aligned}$$

Define

$$||\boldsymbol{\Delta}||_{[t_1,\infty\rangle} = \sup_{t\in[t_1,\infty\rangle}|\boldsymbol{\Delta}| \tag{7.25}$$

From the assumption that $|\mathbf{u}| \to \mathbf{0}$ and $\mathbf{s} \to \mathbf{0}$ as $t \to \infty$, we have that $||\boldsymbol{\Delta}||_{[t_1,\infty\rangle} \to 0$ as $t_1 \to \infty$. Therefore, for $t \geq t_1$ where t_1 is any t larger than the initial time t_0, we get that

$$\begin{aligned}\dot{V} &\leq -\frac{1}{2}\boldsymbol{\epsilon}_{\hat{\mathbf{e}}}^T\boldsymbol{\Lambda}\boldsymbol{\epsilon}_{\hat{\mathbf{e}}} + \frac{1}{2}||\boldsymbol{\Delta}||_{[t_1,\infty\rangle}|\boldsymbol{\epsilon}_{\hat{\mathbf{e}}}| \\ &\leq -\frac{1}{2}\lambda_{\min}(\boldsymbol{\Lambda})|\boldsymbol{\epsilon}_{\hat{\mathbf{e}}}|^2 + \frac{1}{2}||\boldsymbol{\Delta}||_{[t_1,\infty\rangle}|\boldsymbol{\epsilon}_{\hat{\mathbf{e}}}|\end{aligned}$$

where $\lambda_{\min}(\boldsymbol{\Lambda}) > 0$ is the smallest eigenvalue of $\boldsymbol{\Lambda}$. Now we want to use parts of $-|\boldsymbol{\epsilon}_{\hat{\mathbf{e}}}|^2$ to dominate $||\boldsymbol{\Delta}||_{[t_1,\infty\rangle}|\boldsymbol{\epsilon}_{\hat{\mathbf{e}}}|$ for large $|\boldsymbol{\epsilon}_{\hat{\mathbf{e}}}|$. We thereby introduce the scalar $\theta \in \langle 0,1\rangle$ and rewrite the forgoing inequality as

$$\begin{aligned}\dot{V} &\leq -\frac{1}{2}(1-\theta)\lambda_{\min}(\boldsymbol{\Lambda})|\boldsymbol{\epsilon}_{\hat{\mathbf{e}}}|^2 - \frac{1}{2}\theta\lambda_{\min}(\boldsymbol{\Lambda})|\boldsymbol{\epsilon}_{\hat{\mathbf{e}}}|^2 + \frac{1}{2}||\boldsymbol{\Delta}||_{[t_1,\infty\rangle}|\boldsymbol{\epsilon}_{\hat{\mathbf{e}}}| \\ &\leq -\frac{1}{2}(1-\theta)\lambda_{\min}(\boldsymbol{\Lambda})|\boldsymbol{\epsilon}_{\hat{\mathbf{e}}}|^2 \triangleq -W_V(|\boldsymbol{\epsilon}_{\hat{\mathbf{e}}}|) \quad \forall \quad |\boldsymbol{\epsilon}_{\hat{\mathbf{e}}}| \geq \mu_{t_1},\end{aligned}$$

where

$$\mu_{t_1} \triangleq \frac{||\boldsymbol{\Delta}||_{[t_1,\infty\rangle}}{\theta\lambda_{\min}(\boldsymbol{\Lambda})}. \tag{7.26}$$

Therefore, Theorem 4.18 in (Khalil, 2002) is satisfied, and the solution is *uniformly ultimately bounded* for all $t_1 \geq t_0$.

Then choose t_1 so large that $\mu_{t_1} < 1$. This is possible because of the assumption that $||\boldsymbol{\Delta}||_{[t_1,\infty\rangle} \to 0$ as $t_1 \to \infty$.

We know that $V \leq 1 \; \forall \; t$, which means that V is bounded for $t = t_1$. We can therefore start the analysis at time t_1 instead of t_0. Since

$$V(|\boldsymbol{\epsilon}_{\hat{\mathbf{e}}}|) > V(\mu_{t_1}) \Rightarrow |\boldsymbol{\epsilon}_{\hat{\mathbf{e}}}| > \mu_{t_1}$$

we have that $\dot{V} \leq -W_V(|\boldsymbol{\epsilon}_{\hat{\mathbf{e}}}|)$ for $V(|\boldsymbol{\epsilon}_{\hat{\mathbf{e}}}|) > V(\mu_{t_1})$, and therefore V decreases until ultimately

$$V(|\boldsymbol{\epsilon}_{\hat{\mathbf{e}}}|) \leq V(\mu_{t_1}) \Rightarrow |\boldsymbol{\epsilon}_{\hat{\mathbf{e}}}| \leq \mu_{t_1}.$$

By letting $t_1 \to \infty$ in the above analysis we get $\mu_{t_1} \to 0$. Finally, this means that $|\boldsymbol{\epsilon}_{\hat{\mathbf{e}}}| \to 0$, $\eta_{\hat{\mathbf{e}}} \to \pm 1$ and $\hat{\mathbf{e}} \to \mathbf{q}_{id}$ which proves Proposition 7.1. □

Remark 7.2. By assuming that the initial value for $\mathbf{u}$, $\mathbf{v}_o$ and $\hat{\boldsymbol{\epsilon}}$ are small, it is possible to find a smaller bound than 1 for $|\boldsymbol{\epsilon}_{\hat{\mathbf{e}}}|$ during the transient response. This is carried out in (Bondhus, 2010).

Step 2: The aim of the second, and last step of the backstepping algorithm is to find a controller $\mathbf{T}_u^*$ such that the $\mathbf{u}$-dynamics are asymptotically stable. Remember that the the dynamics of $\mathbf{v}_o$ are already proven to be AS by the observer analysis, so we do not need to worry about that.

From the definition of $\hat{\boldsymbol{\omega}}$ in Equation (7.20) it can be seen that

$$\mathbf{J}_s^*\dot{\mathbf{u}} = \mathbf{J}_s^*\dot{\hat{\boldsymbol{\omega}}} - \mathbf{J}_u^*\dot{\hat{\boldsymbol{\omega}}}_r. \tag{7.27}$$

If the right-hand side of the above equation was exactly known, one could use Equation (7.17) and choose the ideal control as

$$\mathbf{T}_{u,ideal}^* = \tilde{\Gamma}(\tilde{\boldsymbol{\omega}}, \hat{\boldsymbol{\omega}}, \boldsymbol{\Omega}) - \hat{\Gamma}(\hat{\boldsymbol{\omega}}, \boldsymbol{\Omega}) - \mathbf{J}_\omega^*\dot{\hat{\boldsymbol{\omega}}} + \mathbf{T}_{ex}^* + \mathbf{g}_1^* - \mathbf{J}_s^*\dot{\hat{\boldsymbol{\omega}}}_r + \mathbf{J}_s^*\mathbf{A}_u\mathbf{u} \tag{7.28}$$

which will give the following closed loop system

$$\mathbf{J}_s^*\dot{\mathbf{u}} = -\mathbf{J}_s^*\mathbf{A}_u\mathbf{u}. \tag{7.29}$$

The $\mathbf{u}$-dynamics above is clearly linear, and as long as $\mathbf{A}_u = \mathbf{A}_u^T > 0$, the dynamics of $\mathbf{u}$ will converge to zero.

Unfortunately, several of the terms in the ideal controller $\mathbf{T}_{u,ideal}^*$ are not known exactly. For instance, the terms $\tilde{\Gamma}(\tilde{\boldsymbol{\omega}}, \hat{\boldsymbol{\omega}}, \boldsymbol{\Omega})$ and $\dot{\hat{\boldsymbol{\omega}}}$ are unknown for both the tracking and the synchronization problem. In addition, the time derivative of the desired reference, $\dot{\hat{\boldsymbol{\omega}}}_r$, is not known for the synchronization problem. It is therefore quite difficult to design a controller such that the system is AS independent of the observer errors. Therefore (Bondhus, 2010) presents a control design such that the $\mathbf{u}$-dynamics depend on the observer errors, but still manages to make $\mathbf{u} \to \mathbf{0}$ as $t \to \infty$. This is achieved by using an approximation to the ideal controller where the approximation error goes to zero as the observer error converges.

Firstly, let us focus on the time-derivative of the desired reference, $\dot{\hat{\boldsymbol{\omega}}}_r$ for the synchronization problem. From Equation (7.20) it can be seen that

$$\dot{\hat{\boldsymbol{\omega}}}_r = \frac{\mathrm{d}}{\mathrm{d}t}\left[\mathbf{R}_1\boldsymbol{\alpha}(\hat{\mathbf{e}})\right] + \dot{\boldsymbol{\omega}}_D. \tag{7.30}$$

In Equation (7.30), $\dot{\boldsymbol{\omega}}_D$ is unknown for the synchronization scheme and we therefore propose the approximation

$$\dot{\boldsymbol{\omega}}_D \approx \mathbf{a}_D + \boldsymbol{\delta}_D, \tag{7.31}$$

where the approximation error $\boldsymbol{\delta}_D$ goes to zero as $\tilde{\boldsymbol{\omega}}_{nl}^n$ goes to zero. To use the same equation for both the leader and the follower, we define $\boldsymbol{\delta}_D = \mathbf{0}$ and $\mathbf{a}_D = \dot{\boldsymbol{\omega}}_{nd}^n$ for the tracking problem. On the other hand, the expression for $\mathbf{a}_D$ and $\boldsymbol{\delta}_D$ for the synchronization problem, is given by

$$\mathbf{a}_D = \dot{\hat{\boldsymbol{\omega}}}_{nl}^n = \left(\mathbf{J}_{s,l}^n\right)^{-1}\left\{\mathbf{T}_{ex,l}^n - \mathbf{T}_{u,l}^n + \mathbf{g}_{1,l}^n(\tilde{\mathbf{q}}_l) - \mathbf{L}_J(\hat{\boldsymbol{\omega}}_{nl}^n, \mathbf{J}_l^n)\hat{\boldsymbol{\omega}}_{nl}^n - \mathbf{L}_J(\hat{\boldsymbol{\omega}}_{nl}^n, \mathbf{J}_{\omega,l}^n)\boldsymbol{\Omega}_l^n\right\} \tag{7.32a}$$

$$\boldsymbol{\delta}_D = \left(\mathbf{J}_{s,l}^n\right)^{-1}\left\{\mathbf{L}_J(\tilde{\boldsymbol{\omega}}_{nl}^n, \mathbf{J}_l^n)\hat{\boldsymbol{\omega}}_{nl}^n + \mathbf{L}_J(\tilde{\boldsymbol{\omega}}_{nl}^n, \mathbf{J}_{\omega,l}^n)\boldsymbol{\Omega}_l^n - \mathbf{J}_{\omega,l}^n\dot{\hat{\omega}}_{nl}^n\right\}. \tag{7.32b}$$

where Equation (7.16) has been divided into terms that are known and unknown for the controller. In addition it can be seen that $\boldsymbol{\delta}_D \to \mathbf{0}$ as $\tilde{\boldsymbol{\omega}}_{nl}^n$ goes to zero.

Further, define

$$\mathbf{a}_r = \frac{\mathrm{d}}{\mathrm{d}t}\left[\mathbf{R}_1 \boldsymbol{\alpha}(\hat{\mathbf{e}})\right] + \mathbf{a}_D \tag{7.33}$$

such that Equation (7.30) may be written as

$$\dot{\hat{\boldsymbol{\omega}}}_r = \mathbf{a}_r + \boldsymbol{\delta}_D. \tag{7.34}$$

In the above equation, $\mathbf{a}_r$ is known for both the tracking and synchronization since $\mathbf{a}_D$ and the angular velocity of $\mathbf{R}_1$, $\dot{\hat{\mathbf{e}}}$ are known.

We are now ready to state the proposed approximation for the ideal controller in the following proposition:

Proposition 7.2. *The approximation to the ideal controller, see in Equation* (7.28)*, is given by*

$$\mathbf{T}_u^* = -\hat{\Gamma}(\hat{\boldsymbol{\omega}}, \boldsymbol{\Omega}) + \mathbf{T}_{ex}^* + \mathbf{g}_1^* - \mathbf{J}_s^* \mathbf{a}_r + \mathbf{J}_s^* \mathbf{A}_u \mathbf{u} \tag{7.35}$$

where $\hat{\Gamma}(\boldsymbol{\omega}, \boldsymbol{\Omega})$ *is defined in Equation* (7.18b)*. If this controller is applied to the system, with* $\boldsymbol{\alpha}(\hat{\mathbf{e}})$ *chosen as in Equation* (7.21) *and the states of the leader and the follower are estimated with the observer seen in Equation* (7.10b)*, then*

$$\mathbf{u} \to \mathbf{0} \text{ as } t \to \infty, \tag{7.36}$$

for both the leader and the follower. This implies asymptotic stability of the closed-loop system and therefore, $\mathbf{q}_l \to \mathbf{q}_d$ *and* $\mathbf{q}_f \to \mathbf{q}_l$ *as* t *goes to infinity.*

Proof. In the proof of Proposition 7.2 we will rewrite the controller in Equation (7.35) such that

$$\mathbf{T}_u^* = \mathbf{T}_{u,ideal}^* - \tilde{\Gamma}(\tilde{\boldsymbol{\omega}}, \hat{\boldsymbol{\omega}}, \boldsymbol{\Omega}) + \mathbf{J}_\omega^* \dot{\hat{\boldsymbol{\omega}}} + \mathbf{J}_s^* \boldsymbol{\delta}_D \tag{7.37}$$

where $\tilde{\Gamma}(\tilde{\boldsymbol{\omega}}, \hat{\boldsymbol{\omega}}, \boldsymbol{\Omega})$ can be seen in Equation (7.18a). From the analysis of the observer, it is seen that the angular velocity of the observer error will converge to zero as the observer errors converge. Therefore, also the terms $\tilde{\Gamma}(\tilde{\boldsymbol{\omega}}, \hat{\boldsymbol{\omega}}, \boldsymbol{\Omega})$, $\mathbf{J}_\omega^* \dot{\hat{\boldsymbol{\omega}}}$ and $\mathbf{J}_s^* \boldsymbol{\delta}_D$ will go to zero, and the approximated controller will be equal the ideal controller.

By defining $\mathbf{w} = -\tilde{\Gamma}(\tilde{\boldsymbol{\omega}}, \hat{\boldsymbol{\omega}}, \boldsymbol{\Omega}) + \mathbf{J}_\omega^* \dot{\hat{\boldsymbol{\omega}}} + \mathbf{J}_s^* \boldsymbol{\delta}_D$ the closed-loop dynamics become

$$\mathbf{J}_s^* \dot{\mathbf{u}} = -\mathbf{J}_s^* \mathbf{A}_u \mathbf{u} + \mathbf{w} \tag{7.38}$$

and the system can thereby be seen as a perturbed system (Khalil, 2002) where $\mathbf{w}$ represents modeling errors. Note that it is also possible to remove $\mathbf{g}_1^*$ from the controller in Equation (7.35) and instead add it to $\mathbf{w}$ as also $\mathbf{g}_1^*$ goes to 0 as the observer converge.

Before we proceed in the proof of Proposition 7.2 we define two norms which is going to be used in the upcoming calculations.

For any function $\mathbf{v} : [0, \infty\rangle \to \mathbb{R}^n$ we define

$$||\mathbf{v}||_\infty \triangleq \sup_{t \in [0,\infty\rangle} |\mathbf{v}(t)| \qquad ||\mathbf{v}||_a \triangleq \limsup_{t \to \infty} |\mathbf{v}(t)|, \tag{7.39}$$

where each supremum is understood to be an essential supremum. The initial value of a function or variable x will be denoted x_0.

Consider the radially unbounded Lyapunov function

$$V_u = \frac{1}{2}\mathbf{u}^T\mathbf{u} \tag{7.40}$$

with its time-derivative along the solution

$$\begin{aligned}\dot{V}_u &= -\mathbf{u}^T\mathbf{A}_u\mathbf{u} + \mathbf{u}^T\mathbf{w} \\ &\leq -\lambda_{\min}(\mathbf{A}_u)|\mathbf{u}|^2 \quad \forall \quad |\mathbf{u}| \geq \frac{|\mathbf{w}|}{\lambda_{\min}(\mathbf{A}_u)} > 0,\end{aligned}$$

where $\lambda_{\min}(\mathbf{A}_u) > 0$ is the smallest eigenvalue of $\mathbf{A}_u$. Using the theorem of uniform ultimated boundedness (Khalil, 2002, Theorem 4.18) one get that the solution can be bounded by

$$||\mathbf{u}||_\infty \leq \max\left\{\beta_u(|\mathbf{u}_0|, t - t_0), \frac{||\mathbf{w}||_\infty}{\lambda_{\min}(\mathbf{A}_u)}\right\}, \tag{7.41}$$

where β_u is a class-$\mathcal{KL}$ function. According to (Bondhus, 2010) it is possible to choose $\beta_u(|\mathbf{u}_0|, 0) \leq |\mathbf{u}_0|$ since, if $|\mathbf{u}_0| \geq \frac{||\mathbf{w}||_\infty}{\lambda_{\min}(\mathbf{A}_u)}$ it can be seen that V_u decreases, which implies $|\mathbf{u}| \leq |\mathbf{u}_0|$. Using time invariance and taking the limit when $t \to \infty$ on each side of the bound in Equation (7.41), gives that

$$\lim_{t\to\infty} ||\mathbf{u}||_\infty \leq \max\left\{\lim_{t\to\infty}\beta_u(|\mathbf{u}_0|, t - t_0), \lim_{t\to\infty}\frac{||\mathbf{w}||_\infty}{\lambda_{\min}(\mathbf{A}_u)}\right\}. \tag{7.42}$$

The left-hand side of the above bound is equal $||\mathbf{u}||_a$. In addition, due to the definition of $\mathcal{KL}$-class functions,

$$\lim_{t\to\infty}\beta_u(|\mathbf{u}_0|, t - t_0) = 0$$

Therefore, using Equation (7.39), it can be seen that

$$||\mathbf{u}||_a \leq \lim_{t\to\infty}\frac{||\mathbf{w}||_\infty}{\lambda_{\min}(\mathbf{A}_u)} = \frac{||\mathbf{w}||_a}{\lambda_{\min}(\mathbf{A}_u)}.$$

We know from the analysis of the observer that $||\mathbf{w}||_a = 0$ and therefore $||\mathbf{u}||_a = 0$. This implies that $\mathbf{u} \to \mathbf{0}$ as $t \to \infty$. Further, it can be seen from Figure 7.4 that

$$\mathbf{e}_l = \hat{\mathbf{e}}_l \otimes \tilde{\mathbf{q}}_l^{-1} \tag{7.43a}$$

$$\mathbf{e}_f = \tilde{\mathbf{q}}_l \otimes \hat{\mathbf{e}}_f \otimes \tilde{\mathbf{q}}_f^{-1}. \tag{7.43b}$$

Then Proposition 7.1 and Proposition 6.1 shows that $\hat{\mathbf{e}}_l$, $\hat{\mathbf{e}}_f$, $\tilde{\mathbf{q}}_l$ and $\tilde{\mathbf{q}}_f$ converge to $\mathbf{q}_{id}$, which implies the convergence of $\mathbf{e}_l$ and $\mathbf{e}_f$. Finally, this means that the main object of the controller of getting $\mathbf{q}_l \to \mathbf{q}_d$ and $\mathbf{q}_f \to \mathbf{q}_l$ are satisfied. □

Chapter 8

Lab setup: Hardware and software

In this chapter a short summary of hardware and software used in the underwater satellite are presented. The section is based on (Krogstad et al., 2008) and describes the designing and planning of the underwater satellite. It must be noted that the article was written *before* the assembly of the satellite and therefore, small modifications have been made after the article was written. The AUVSAT is shown in Figure 8.1.

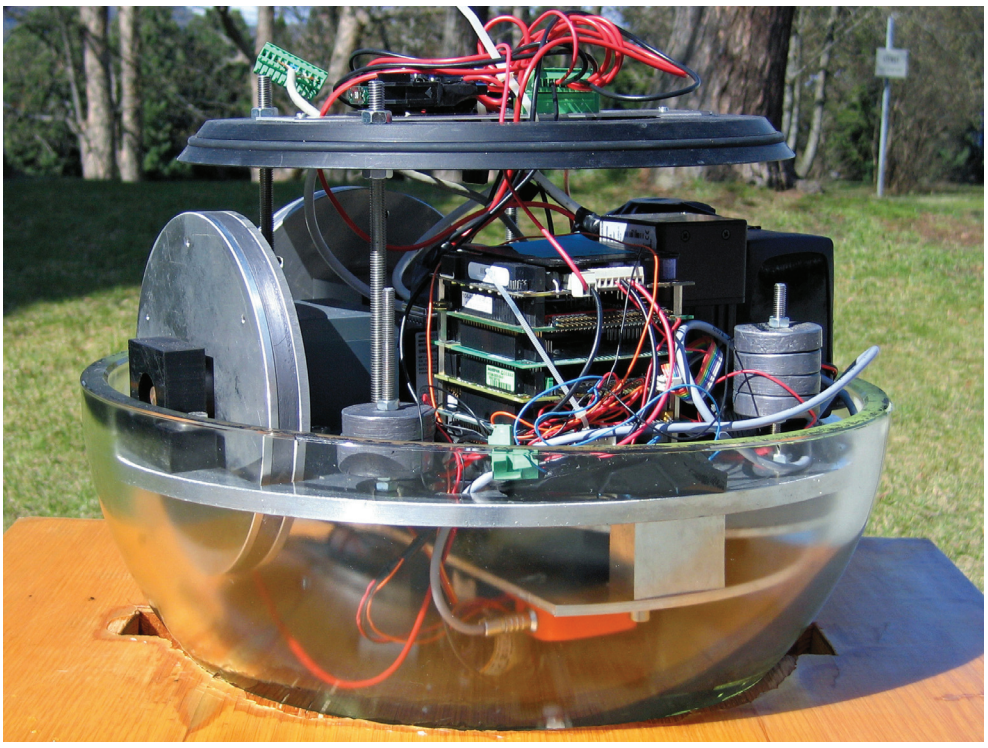

Figure 8.1: The AUVSAT opened to revel the inner constructions of the satellite.

Device	Name	Description
Actuators:		
Motor	SmartMotor SM2330D	Compact servo motor with integrated motor control hardware.
Ballast System	XP250-12 Piston Tank	Ballast system capable of adjusting the mass of the vessel by 250 g.
Computer:		
PC/104 CPU card	Kontron MOP-SlcdLX	Main board with 0.5 GHz Pentium processor and 1 GB RAM.
PC/104 Serial communication extension card	Xtreme-4/104	Four extra 16C654 UARTS, RS232/RS484 connections.
PC/104 IO card	Access 104-AIO12-8	Analog and digital inputs and outputs.
Power supply	HESC104 Vehicle power supply	Powers the PC/104 stack together with the sensors and piston ballast motor.
Solid state storage	Flash-Drive/104	4 GB of flash storage.

Table 8.1: Hardware overview (Krogstad et al., 2008).

Background

The underwater satellite is a part of the AUVSAT project at NTNU, with a goal of creating an experimental laboratory for formation control of underwater vessels:

> The motivation for building an experimental platform is to provide a setup for experimental verification of theoretical results on spacecraft formation flying demonstrating the strength and shortcomings of the theory, and in this way contribute to bridge the gap between theory and practice. (Krogstad et al., 2008).

8.1 Hull design

The main consideration when the hull was designed was to minimize the drag and other hydrodynamic forces. It was also important to have a hull that made the center of mass coincide with the center of buoyancy. It is therefore an obvious choice to use a spherical hull. Due to the space requirements for actuators, batteries, CPU and other necessary equipments a 17" spherical housing was chosen. The spherical shape has a lot of buoyancy force, and therefore it was important that the housing was dense, and glass housing seemed

to be a sensible solution. Another practical effect by this choice is that it always is handy to see what is going on inside of the vessel. Both for fault detection, but perhaps more importantly, to "show off" the rotating and flashing parts of the assembly to a potential audience. The housing is manufactured by Nautilus Marine Service GmbH, and is typically used in deep sea research, and can be used in depth down to 3000 m below sea level.

8.2 Internal lineup

The hardware components are mounted on a solid aluminum framework, to avoid vibration and free floating objects. In addition to the required hardware, also lead weights are placed to make the center of gravity coincide with the center of buoyancy and thereby making the vessel naturally buoyant.

8.3 Sensor

The available space and budget for the underwater satellite is limited. That is why the low-cost and small-size Xsens MTi inertial measurement unit (IMU) is chosen. The IMU is easy to use and it has earlier been used in underwater vehicles. The Xsens MTi consists of a three-axis gyro combined with a magnetometer and can thereby obtain the attitude and the angular velocity for all three dimensions.

The sensor can be programmed to send the attitude data as quaternions, Euler Angles or as a direction cosine matrix. This is practical and one can thereby use the representations that suit oneself or experience with different representations to compare them. The sensor is connected to the CPU with a serial connection and can be programmed to send data at different rates with a maximum rate of 100 Hz. This is sufficient for our use, since the controller runs at 50 Hz.

In addition to the IMU, a pressure sensor is also implemented. The pressure sensor is used to control the vertical position of the vessel and thereby keeping the satellite natural buoyant at all time.

The accuracy of the IMU and the pressure sensor can be seen in Table 8.2.

8.4 Actuators

8.4.1 Reaction wheels

The main actuators for the underwater satellite are the reaction wheels. They are mounted orthogonally along the x, y and z-BODY-axis inside the hull. This solution has the advantage of reduced drag force compared to actuators placed outside of the hull. Each reaction wheel assembly consists of an aluminum and lead momentum wheel, mounted to a servo motor. By controlling the servos you also control the momentum delivered and absorbed by the reaction wheels.

Sensor	Property	Accuracy
XSens MTi	Angular resolution	0.05°
	Static accuracy (Roll/Pitch)	$< 0.05°$
	Static accuracy (Yaw)	$< 1°$
	Dynamic accuracy	2° RMS
Pressure sensor	Range	$0 - 1$ bar
	Accuracy	0.01 m

Table 8.2: Sensor properties and accuracy (Krogstad et al., 2008).

The servo chosen for the satellite is the Animatics SM2330. This servomotor can provide relatively high torque and thereby suppress high restoring momentums. The problem with a motor that can provide high torque is that it has limited maximum speed. Therefore speed and torque are competing features and a trade off between the two factors has to be made. In this case the high torque was chosen more important since the inability to suppress the restoring moments would make the vehicle uncontrollable.

In Figure 8.1, it is possible to see all three reaction-wheel assemblies. The x and y-wheels can easily be seen in the foreground and background of the satellite, while the third RWA is placed horizontal in the lower right side of the picture.

8.4.2 Ballast system

The ballast system is implemented as an actuator for vertical positioning. The principal of the system is that a piston is placed inside a cylinder and an assembly with a servo motor, gear wheels and electrical units makes the piston move inside the tank. The movement will pump water inn or out of the tank and thereby regulate the gravitational force acting on the underwater satellite. If this is performed the right way one can make the buoyancy force equal the gravitational force and make the vessel naturally buoyant.

The ballast system chosen for the satellite is the model XP250-12 Piston Tank, made by Engel, equipped with a 250 mL water tank and capable of adjusting the mass of the vessel by 250 g.

8.5 Communication

Communication between the satellite and the main stationary PC is done using Ethernet LAN. This is not an ideal solution at all (see Section 5.1), and a feature extension should be to replace the Ethernet cable with an acoustic or radio frequency wireless communication scheme. One might think that a solution like this would have problem with the high bandwidth, but since the satellite runs its own controller, most of the information will only

be sent in one direction from the satellite to the stationary PC, reducing the bandwidth requirements.

8.6 CPU board

The main calculating unit in the underwater satellite uses a PC/104 embedded computer board. This computer board can be seen in the middle of the picture in Figure 8.1. Important components of the PC/104 embedded computer board are: CPU, serial communication card, power supply and solid state storage. The PC/104 is a modular and stackable electrical circuit developed for embedded applications requiring the desktop PC bus. The CPU board has a 500 MHz low power Pentium processor with 1 GB of RAM. The system has also 4 GB of solid storage, which is sufficient to store the operating system (OS), programs and data.

8.7 Software

The software needed for the sphere satellite should also be available for other similar projects, and therefore, the software was designed to be easy maintainable, straightforward and intuitive. This implies that the specific code is placed in low level drivers.

Testing of new and different control schemes is perhaps the main motivation for this platform, and therefore, it is important to be able to switch between control algorithms in an intuitive, fast, and easy way. In the following section a short description of software used to satisfy these requirements is presented. The overall structure of the software is shown in Figure 8.2.

8.7.1 Operating system

Since the most important part in control applications is to communicate with sensors and actuators to provide data to the control algorithm, a real-time operating system (RTOS) is needed. The QNX Neutrino real-time operating system was chosen for this matter. This RTOS is designed specifically for embedded applications, and it includes features like task prioritizing, scheduling and resource sharing. The OS is also very scalable and one can thus exclude non-relevant functions, saving computation time and data storage.

8.7.2 Matlab Real-time workshop and Simulink

To satisfy the requirement for easy implementation of new control schemes, the Matlab Real-time workshop (RTW) in combination with Simulink is used. Simulink has a graphical user interface, and it is easy and intuitive to develop control algorithms. When the control algorithm is produced the Matlab Real-time workshop can be used to transform the graphical interface in Simulink to C source code. The source code can then be moved to the satellite, compiled and run on the target QNX system.

Another feature of the combined solution with Matlab Real-time workshop and Simulink is that it provides a communication interface between the stationary host computer and the QNX target. The host is running the graphical Simulink program and it is possible to send and view the measurement and control signals sent from the satellite on the host computer. This is very practical and one can thereby see the live measurements and store them for later analysis.

8.7.3 Low-level interfaces

Low level drivers have be developed to take care of the communications between the actuators, sensors and the general system. These interfaces includes the servo motors, IMU, ADC/DAC and the Ethernet interface. The low-level drivers are implemented as shared libraries on the QNX target, and are loaded by the code generated by the RTW toolbox. It is therefore not necessary to compile these low-level drives for each time a new, higher level software is tested.

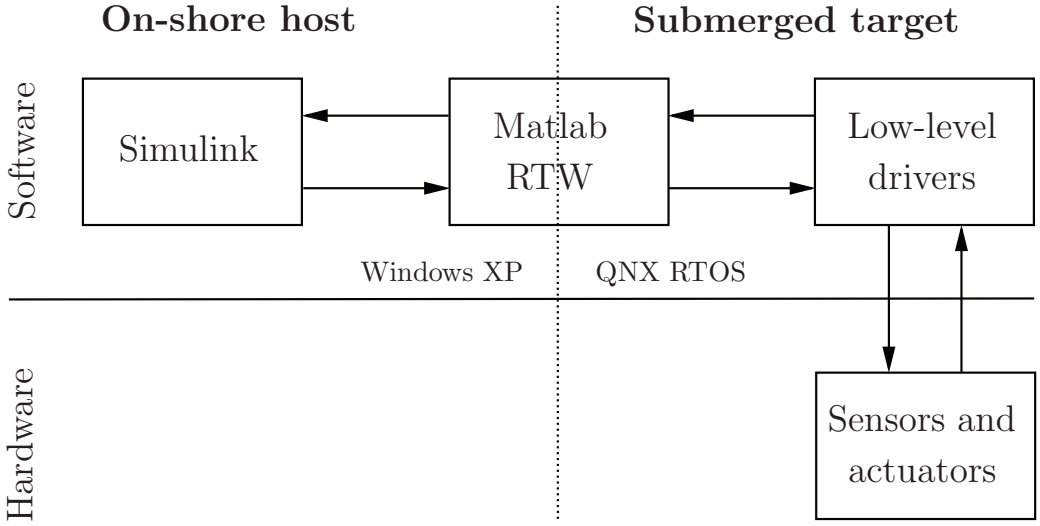

Figure 8.2: Overall structure of the soft- and hardware.

Chapter 9

Experiments and results

This chapter contains the most important experiments and results from the tests of the AUVSAT. The chapter is divided into three parts where the first part presents the results when sliding mode and backstepping control were implemented. In this section, angular velocity measurements were available for both controllers. The second part implements the nonlinear observer for the angular velocity and the output from this observer is feed to the sliding mode controller. The third and final part of this chapter shows the results from the experiments of attitude synchronization without angular velocity measurements.

9.1 Pre-testing of controller and observer

All systems have been simulated prior to the real experiments with Matlab and Simulink. The simulations do not use the AUVSAT at all, and thus serve as a fine tool to test if the controller and observer functions properly. In addition, the simulations gave a good indication of suitable values for different gains used by the controllers and observers. However, these results are left out of the paper, since the main focus of the thesis is to control the underwater satellite. The "off-line" simulations was just a step on the way to reach the main goal. It may however be mentioned that simulations showed that the controllers, observers and the synchronization scheme behaved really well, even with realistic noise ratios and modulation errors.

9.2 Angular velocity tracking

The setup of the lab is described in Chapter 8 and after the satellite was assembled the Ethernet cable was connected between the on-shore host and the submerged target. The cable was attached to a rotating device above the water tank, to minimized the unwanted effect from the cable (see Section 5.1).

The control objective is to track an commanded angular velocity reference signal $\boldsymbol{\omega}_c^n$ given in the NED-coordinate frame. The reference signal is stated in Equation (9.1) and is a sequence of a square signal with a period of 60 s and a time varying sinusoidal reference

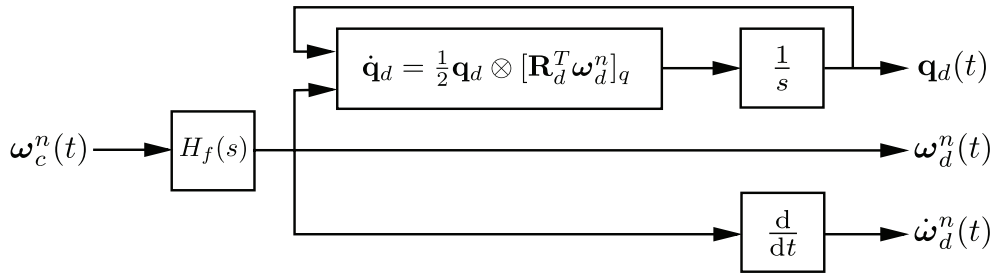

Figure 9.1: The reference-block diagram.

signal. In this way one can truly validate the performance of the controller. The experiment was sampled at 50 Hz for about 550 s.

$$\boldsymbol{\omega}_c^n(t) = \begin{cases} 0.3 \sin\left(\frac{2\pi}{110}(t-30)\right) & \text{if} \quad 30 \leq t \leq 360 \\ 0.2 \text{ square}\left(\frac{1}{60}, t\right) & \text{if} \quad 400 \leq t \leq 550 \\ 0 & \text{Else} \end{cases} \tag{9.1}$$

An overview of the Simulink diagram can be seen in Figure 9.2 where the filter box is the first order filter described in Section 5.2, and the controller is placed in the "Attitude controller"-box.

The "Reference"-box can be seen in Figure 9.1 and calculates the desired attitude in addition to the desired angular velocity and its derivative. The generalized velocities are all given in the NED-frame. To avoid having infinite $\dot{\boldsymbol{\omega}}_d^n(t)$ a simple second order filter with time constants $T_1 = 1$ s and $T_2 = 2$ s has been implemented. The filter can be seen in Equation (9.2) where s is the Laplace-transform variable.

$$H_f(s) = \frac{\omega_{d,i}}{\omega_{c,i}}(s) = \frac{1}{(T_1 s + 1)(T_2 s + 1)} \quad \forall i \in \{x, y, z\} \tag{9.2}$$

Remark 9.1. In the given setup only commanded angular velocity about the z-axis is performed. This was not the intention from the beginning, but testing showed that commanding angular velocity about all three axes made the satellite crash with the walls constantly. One crash was even so powerful that the Ethernet-cable was torn off, resulting in a big leakage. This was quite serious since the electronic inside the sphere does not endure humidity, but luckily only three small cables had to be fixed and replaced.

Remark 9.2. Note that the satellite is equipped with a "depth controller". The depth controller makes sure that the vehicle stays in the right vertical position such that the satellite always is submerged and at the same time makes sure that it does not touch the bottom of the tank. The depth controller is not shown in the overall diagrams, since it is not in the scope of this thesis, and it does not influence the attitude behavior. It should however be mentioned that the depth controller is implemented as a PID-controller, taking pressure

measurements as input and returning relative vertical position. This vertical position is then sent to the ballast system which is presented in Section 8.4.2. The controller is developed by Thomas Krogstad.

Remark 9.3. Notice that no torques are provided to the actuators before 10 seconds have gone in the logging sequence. In this way, one makes sure that the hardware and software are properly initialized and ready for the experiment.

Remark 9.4. It is assumed throughout the rest of this paper that when angular velocity is shown in a plot, it is actually the filtered angular velocity. This is done to facilitate the readability of the experiments and can be carried out since it is shown in Section 5.2 that the filter works satisfactorily, smoothening out the high frequent measurements and is still capable of responding quickly.

9.2.1 Sliding mode controller

This section presents the results from experiments with the sliding mode controller, seen in Equation (4.13). The different plots from the experiment can be seen in Figure 9.3. The sliding mode gains, used in the experiment, can be seen in Table 9.1 and have been found using a combination between the trying and failing method and the pre-testing explained in Section 9.1.

In addition to the series of plots presented in this section, it is also shown an experiment in Appendix D where the same system has been tested. However, this time, a different choice of tuning parameters has been chosen where the ratio between the tuning parameters $\mathbf{K}$ and $\mathbf{P}$ is different. In this section, $\mathbf{P} \gg \mathbf{K}$ resulting in a high weight on the angular velocity error. The controller will thereby penalize angular velocity errors hard and force the satellite to converge to the desired velocity. The experiment in Appendix D, on the other hand, tries to balance the attitude and angular velocity error. In this way, it tries to make both attitude and angular velocity converge to the desired values simultaneously. This is of coarse much harder than only controlling the angular velocity, since the satellite now has to have the desired angular velocity and be at the right attitude at the same time.

Since the controller is designed as an angular velocity controller, the main objective is to track the desired angular velocity. One will thereby choose $\mathbf{P} \gg \mathbf{K}$ which results in less weight on the attitude error. Having a more balanced weight between the attitude and the angular velocity will nevertheless be investigated in Section 9.4.

Gain-symbol	Value	Denomination
$\mathbf{K}$	$0.5 \cdot 10^{-3} \cdot \mathbf{I}$	1/s
$\mathbf{D}$	$1.3 \cdot 10^{-3} \cdot \mathbf{I}$	1/sm
$\mathbf{P}$	$1.1 \cdot \mathbf{I}$	1/sm

Table 9.1: Sliding mode controller gains where $\mathbf{I}$ is the identity matrix.

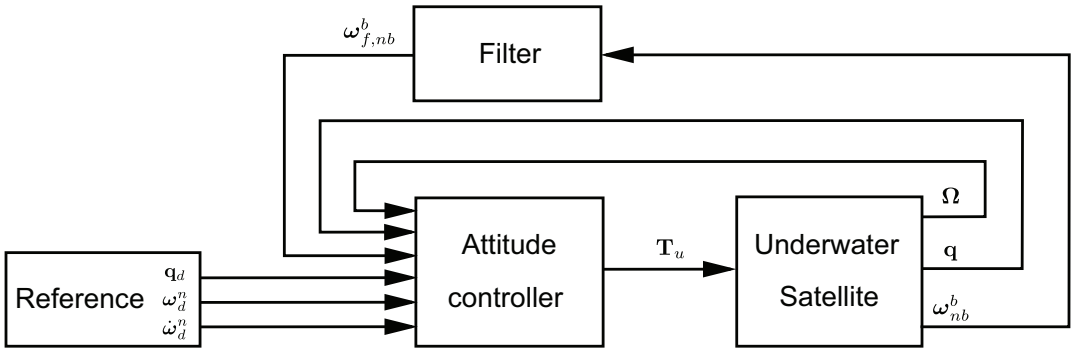

Figure 9.2: Block diagram of the controller and the system with filtering of the angular velocity measurement.

Plots and descriptions

- Figure 9.3(a) presents the angular velocity in all three degrees of freedom. The generalized velocity about the x and y-axis were supposed to be zero, but this is clearly not the case. However, the mean values for these parameters are close to zero, and no significant peaks are spotted.

- Figure 9.3(b) illustrates the overall performance of the controller and is thereby the most important plot of this experiment. The figure compares the desired angular velocity reference against the measured angular velocity about the z-body axis.

- Figure 9.3(c) shows the angular velocity errors for all three degrees of freedom. Not surprisingly, it can be seen that the biggest peaks arises when the reference signal changes from one constant set point to the next in the square sequence of the signal. In addition, it can be seen that the errors are well below 0.05 rad/s most of the time.

- Figure 9.3(d) shows the output from the sliding mode controller. Note that the commanded torque $\mathbf{T}_u$ is far from the maximum allowed torque $\boldsymbol{\tau}_{\max} = 0.358$ Nm. However, experience showed that commanded torques above 30 % of max torque made the system uncontrollable.

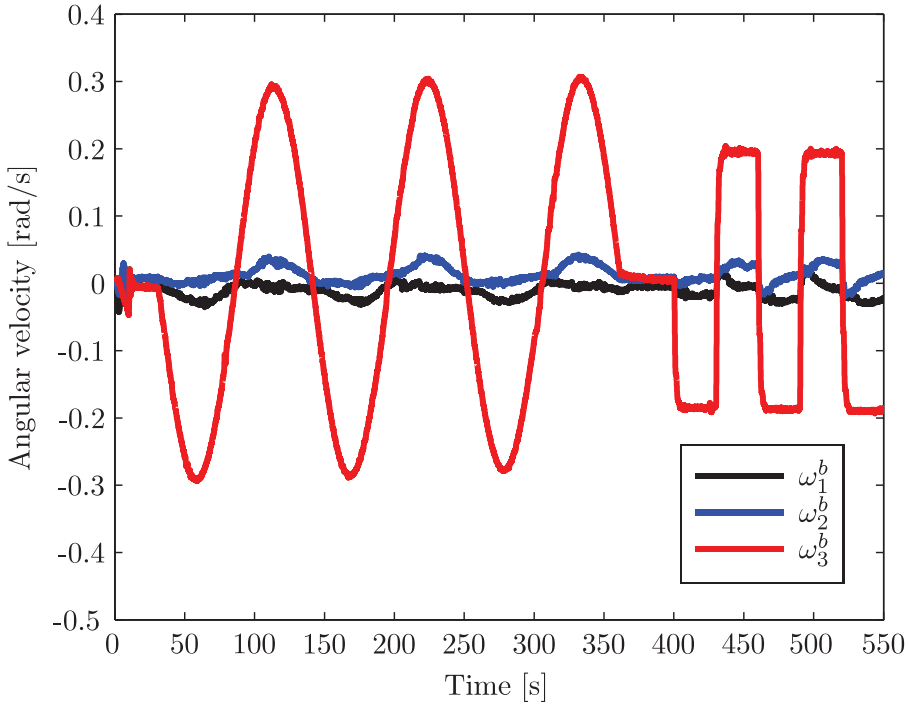

(a) Angular velocity of the satellite.

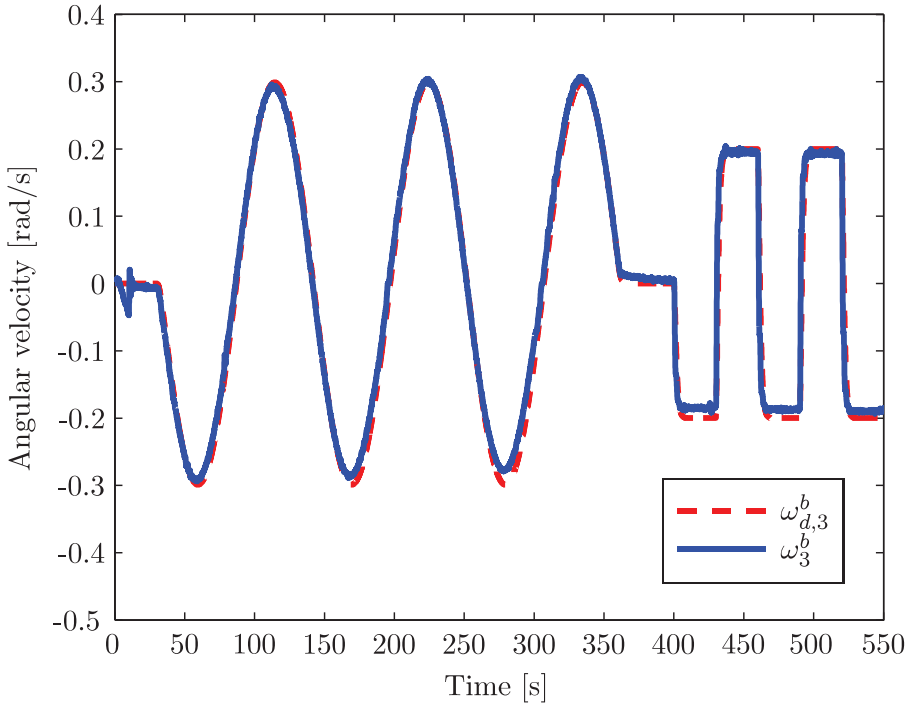

(b) Reference and angular velocity about the z-axis.

Figure 9.3: Plots from the experiments with sliding mode controller and observer.

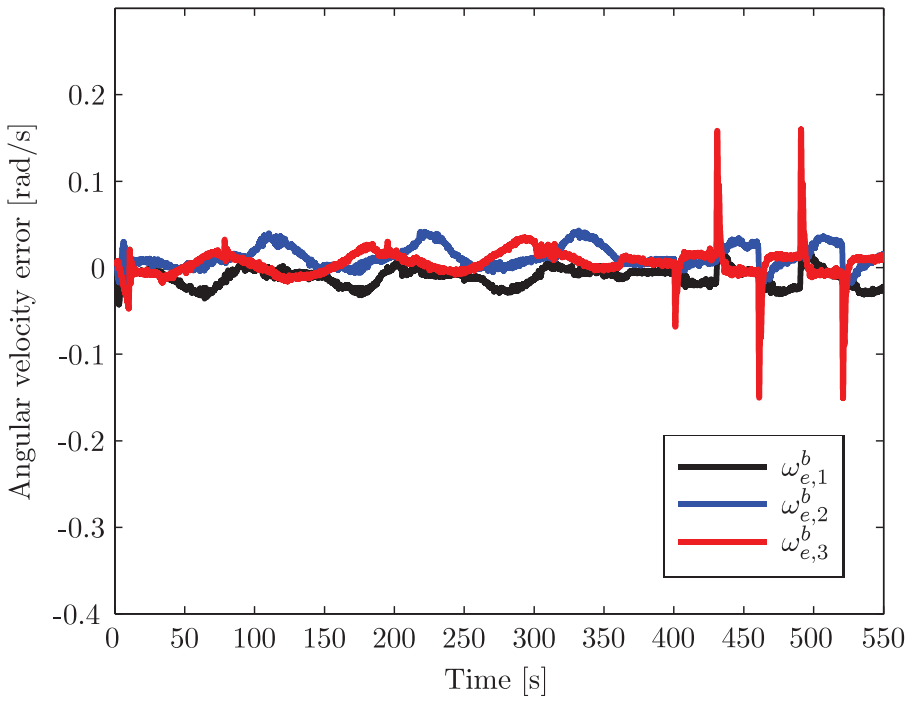

(c) Angular velocity error.

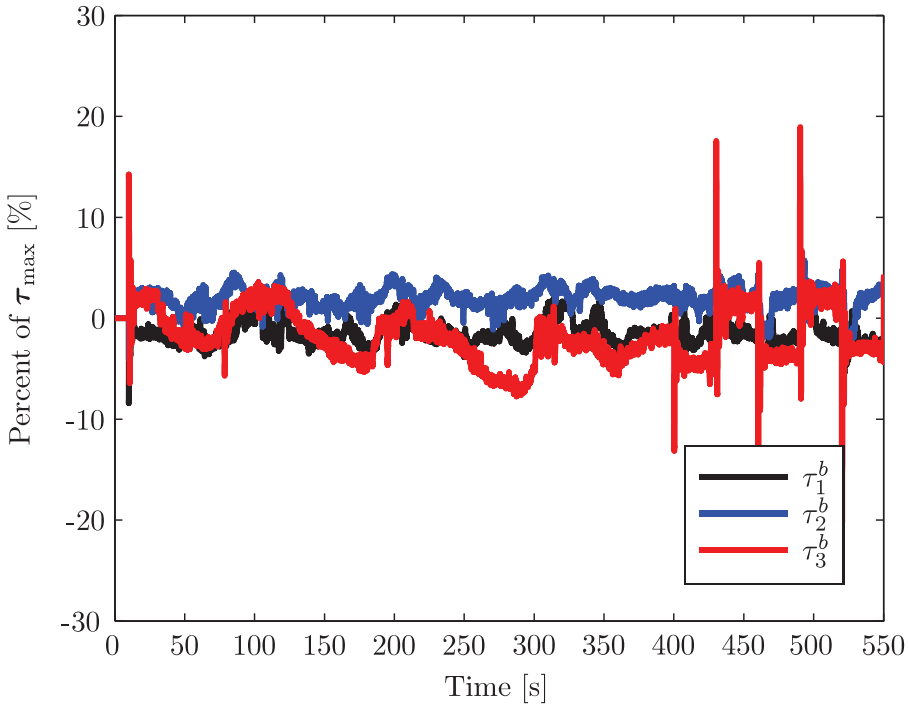

(d) Torque applied to the satellite.

Figure 9.3: Plots from the experiments with sliding mode controller and observer.

9.2.2 Backstepping controller

This section presents the results from experiments with the backstepping controller, seen in Equation (4.30). The different plots from the experiment can be seen in Figure 9.4. The chosen backstepping gains, used in the experiment, can be seen in Table 9.2 and have been found using a combination between the trying and failing method. In addition, knowledge learned from the SM controller has also been used to find suitable gain values since each term of the controllers can more or less be compared directly. An overview of the system is shown in Figure 9.2 and is in general equal the system stated in the previous section. However, the "attitude control"-box is changed with the backstepping controller.

Gain-symbol	**Value**	**Denomination**
k	$0.5 \cdot 10^{-3}$	1/s
$\mathbf{K}_1$	$0.5 \cdot 10^{-3} \cdot \mathbf{I}$	1/sm
$\mathbf{K}_2$	$1.2 \cdot \mathbf{I}$	1/sm

Table 9.2: Backstepping controller gains where $\mathbf{I}$ is the identity matrix.

Plots and descriptions

The experiments was again sampled at 50 Hz for about 550 s with the commanded angular velocity $\boldsymbol{\omega}_c^n$, seen in Equation (9.1). The different plots from the experiments with backstepping controller can be seen in Figure 9.4.

- Figure 9.4(a) compares the desired angular velocity reference against the measured angular velocity about the z-body axis.
- Figure 9.4(b) shows the angular velocity errors for all three degrees of freedom. It can be seen that the errors are well below 0.05 rad/s except in the transactions between two different setpoint in the square sequence of the signal.
- Figure 9.4(c) shows the output from the backstepping controller. The commanded torque $\mathbf{T}_u$ is far from the maximum allowed torque.

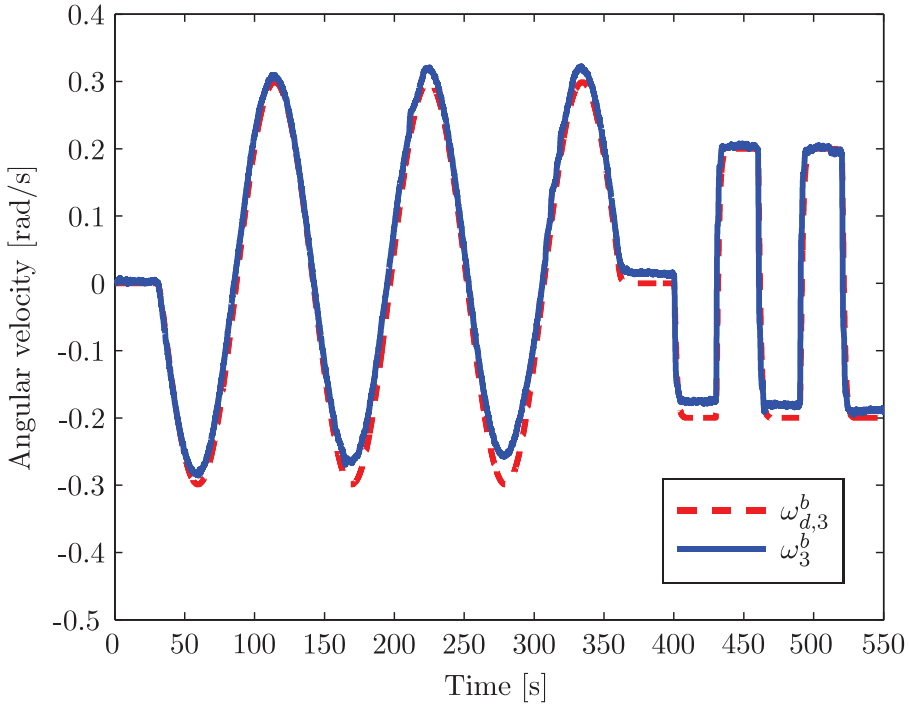

(a) Reference and angular velocity about the z-axis.

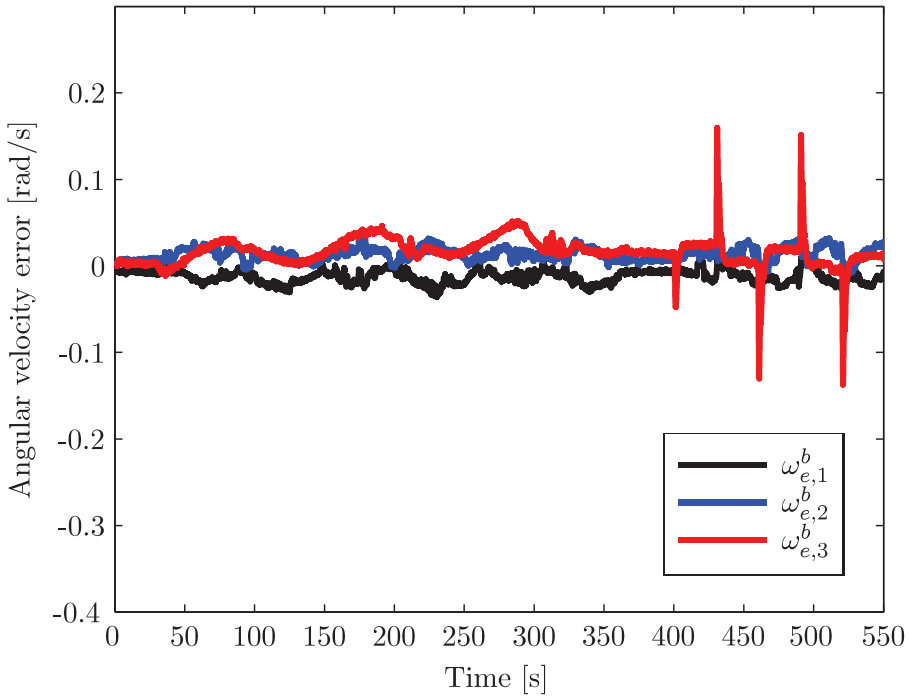

(b) Angular velocity error.

Figure 9.4: Plots from the experiments with backstepping controller.

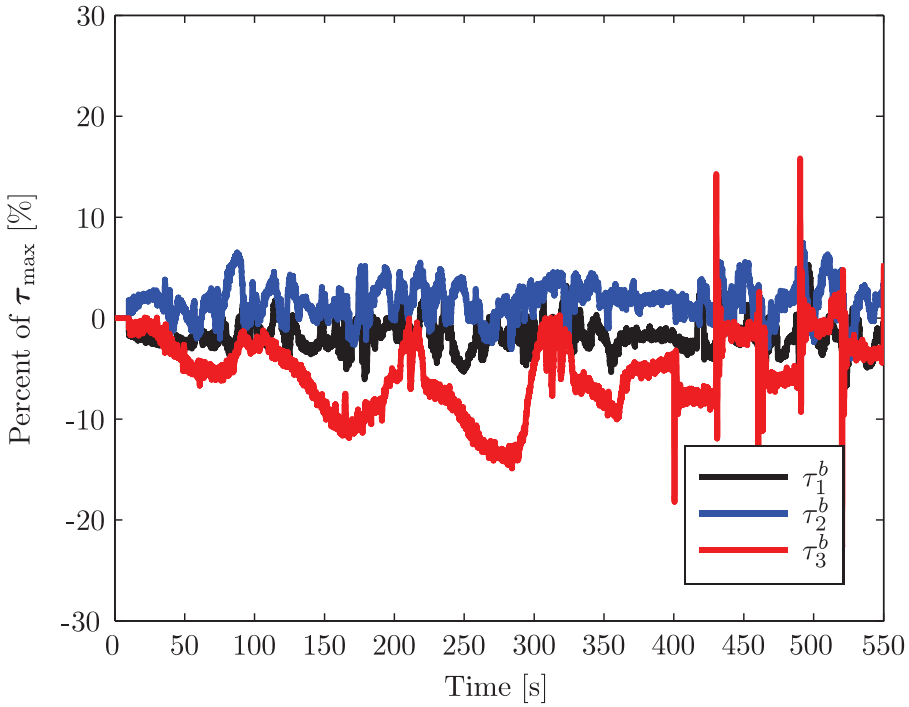

(c) Torque applied to the satellite.

Figure 9.4: Plots from the experiments with backstepping controller.

9.3 Angular velocity tracking with observer

The setup for this part of the assignment is identical with the setup from the last section except the topic regarding the angular velocity feedback which is estimated instead of filtered. The resulting block diagram is shown in Figure 9.5. The observer and controller gains shown in Table 9.3, have been found with the trying and failing method in addition to the "off-line" simulation testing described in Section 9.1. It can also be noted that the controller gain $\mathbf{P}$ had to be lowered to reach a satisfactorily behavior.

Remark 9.5. The observer system is expressed in the BODY reference frame with the angular velocity dynamics instead of the angular momentum dynamics described in Section 5.3. This allows us to utilize knowledge of the known commanded torque $\mathbf{T}_u$ into the satellite system and copy this signal into the observer.

Remark 9.6. Because of the derivative term of the reference signal, $\boldsymbol{\omega}_d^n(t)$, marked oscillations occurred when the system were to follow the squared reference signal. This happened even though the reference signal was run through a second-order filter with the intention of avoiding the problem with high derivative values. Therefore it was decided that the time derivative of the reference should be switched to zero in this part of the experiment. In example, $\dot{\boldsymbol{\omega}}_d^n(t) = \mathbf{0}$ when the system is tracking the squared signal. However, this is no significant loss of generality since the derivative of a squared signal is always zero except where jumps occur.

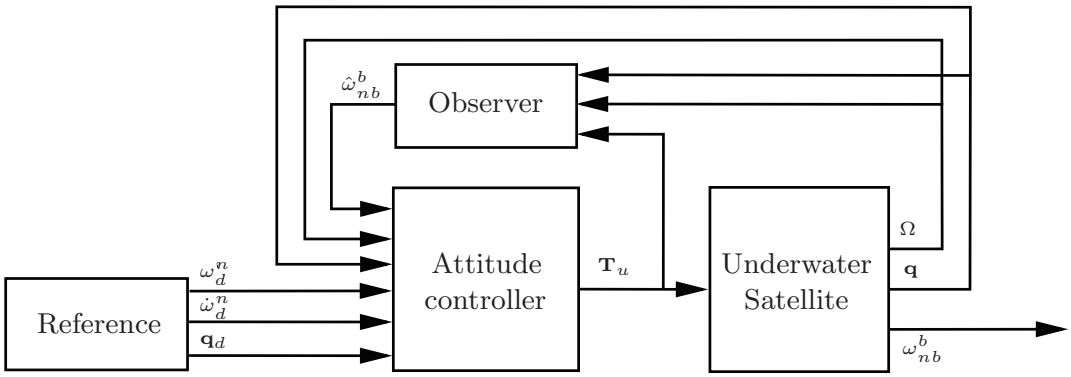

Figure 9.5: Block diagram of the system with a nonlinear observer for angular velocity.

Plots and descriptions

Once again the experiment was sampled for about 550 s where the commanded angular velocity $\boldsymbol{\omega}_c^n$ changed between different constant set points and a time varying sinusoidal reference signal. The different plots from the experiment with sliding mode controller and observer for angular velocity can be seen in Figure 9.6.

Gain-symbol	Value	Denomination
$\mathbf{K}$	$0.9 \cdot 10^{-3} \cdot \mathbf{I}$	1/s
$\mathbf{D}$	$1.3 \cdot 10^{-3} \cdot \mathbf{I}$	1/sm
$\mathbf{P}$	$0.9 \cdot \mathbf{I}$	1/sm
k_p	17.0	$\mathrm{kg^2m^4/s^2}$
k_v	12.0	1/s

Table 9.3: Sliding mode controller and observer gains where $\mathbf{I}$ is the identity matrix.

- Figure 9.6(a) compares the estimated angular velocity $\hat{\boldsymbol{\omega}}$ with the measured angular velocity. The plot thereby shows whether the observer works or not. Note that the angular velocity about the x-axis is left out since it is almost identical with the angular velocity about the y-axis. It should also be noted that the plot about the y-axis is investigated in a shorter time period to emphasize the filtering and time delay caused by the observer.

- Figure 9.6(b) shows the desired angular velocity plotted against the measured angular velocity. The measured velocity is of coarse not used in the closed-loop system, but works as comparison for the estimated angular velocity. In this way one can easily see and validate the performance of the observer.

- Figure 9.6(c) illustrates the difference between the desired and the measured angular velocity.

- Figure 9.6(d) shows the commanded torque applied to the system. This time, it can be noted that the values are getting close to the critical value $\boldsymbol{\tau}_c = 0.3\,\boldsymbol{\tau}_{\max}$.

- Figure 9.6(e) shows that during the startup period the observer uses some time to converge to the real angular velocity. In this phase, called the *detumbling phase*, there is no regulation of the satellite and the controller is disabled. For satellites in general, this is a popular strategy. Right after the satellite has left the mother ship and is sent into space it has a lot of initial generalized velocities. However it is not a good idea to turn on the regulator right a way, but instead let the external forces suppress the movement for a while. When most of the initial generalized speed has become stable and as small as possible, one can turn on the regulator and go into the next phase of ordinary satellite control.

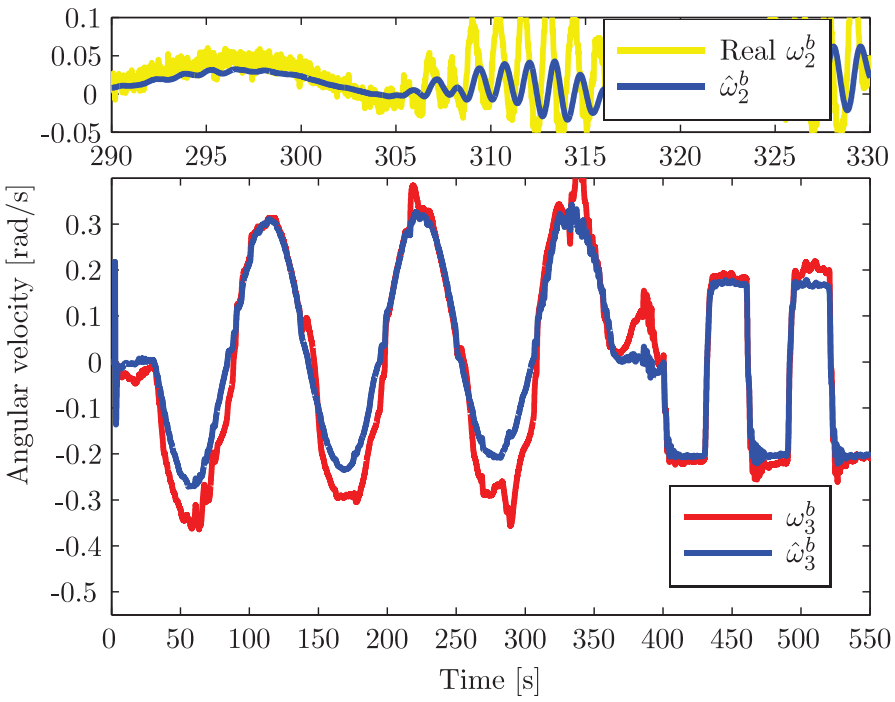

(a) Estimated and measured angular velocity about the y and z axis.

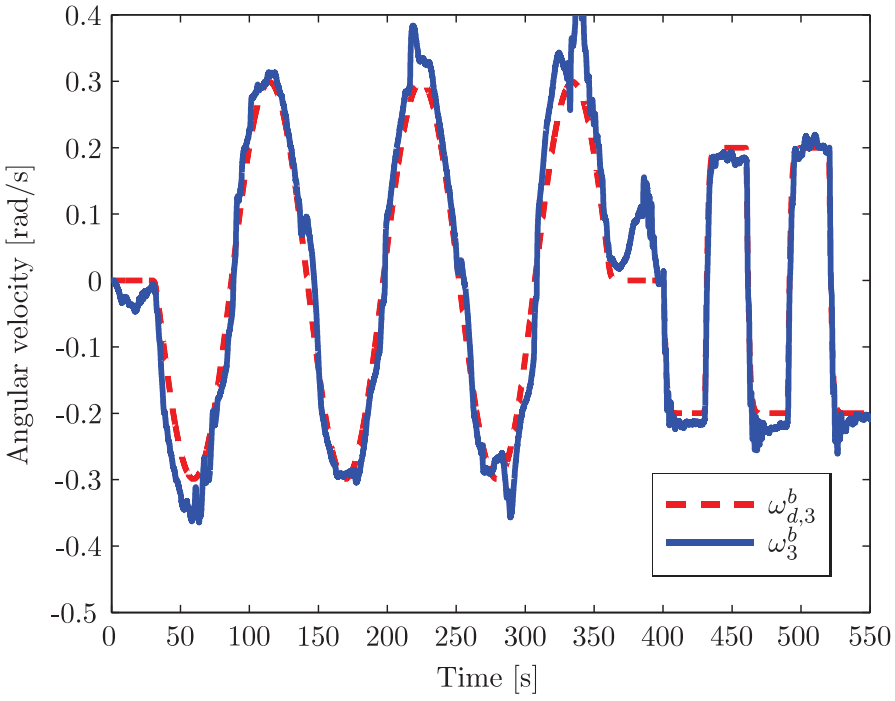

(b) Reference and angular velocity about the z-axis.

Figure 9.6: Plots from the experiments with sliding mode controller and observer.

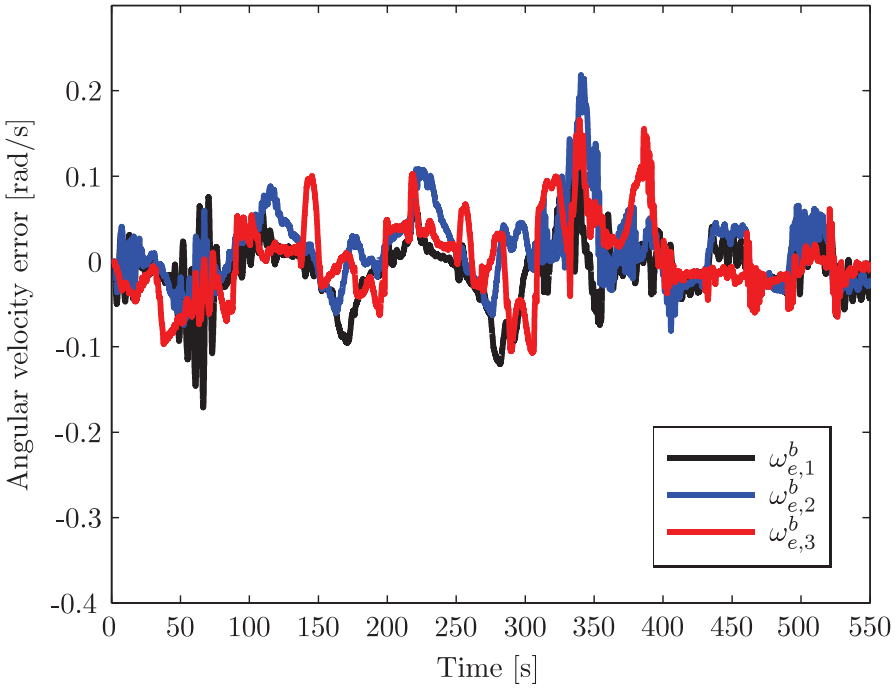

(c) Angular velocity error.

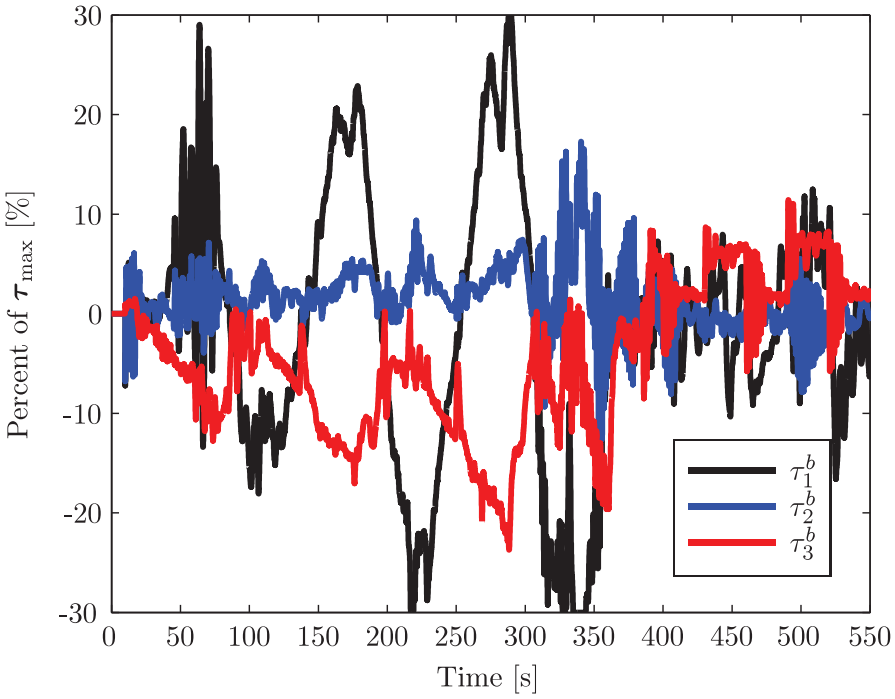

(d) Torque applied to the satellite.

Figure 9.6: Plots from the experiments with sliding mode controller and observer.

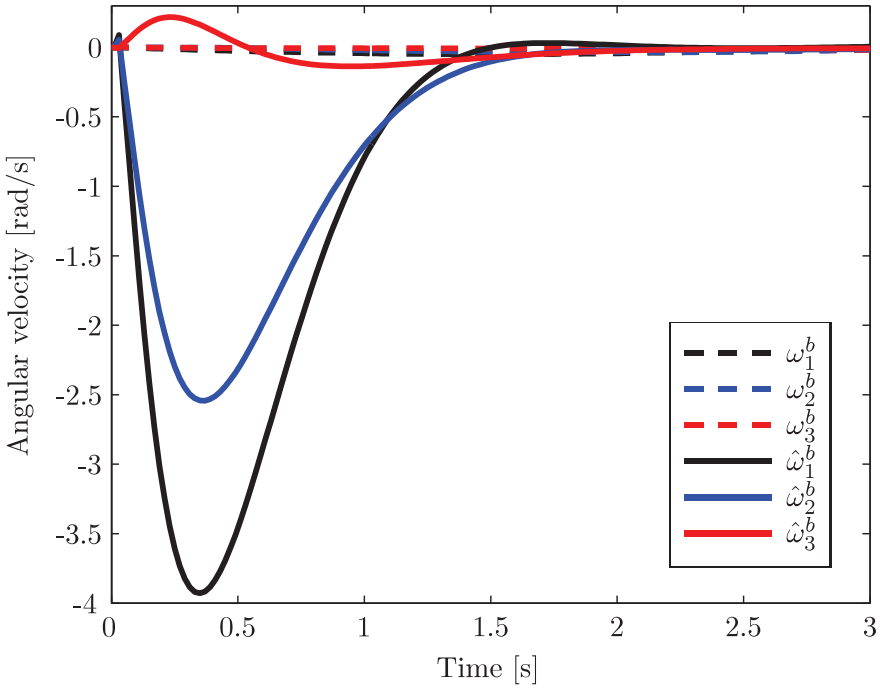

(e) The initialization period for the angular velocity observer.

Figure 9.6: Plots from the experiments with sliding mode controller and observer.

9.4 Synchronization control with angular velocity observers

This section presents the results form the synchronization experiment with controller seen in Equation (7.35) and the observers seen in Equation (7.10).

Due to the limited test facility, explained in Section 5.1, it was impossible to run an experiment with both the leader and the follower satellite at the same time. Since the leader satellite is completely independent of the follower, it is possible to divide the experiments into two different simulations. The first part includes the leader satellite while the follower satellite is going to be used in the second part of the experiment. The overall structure of the leader can be seen in Figure 9.7(a) whereas the follower system can be seen in Figure 9.7(b). The measured and estimated parameters $\mathbf{q}_l(t)$, $\hat{\mathbf{q}}_l(t)$, $\hat{\boldsymbol{\omega}}^n_{nl}(t)$, $\mathbf{a}_D(t)$ and the corresponding time-vector for each parameter were stored in the memory of the computer after the experiment with the leader. These sets were then going to be used as inputs for the next part of the experiment with the follower satellite.

Despite the above mentioned case, the synchronization scheme setup is similar to the setup used for the angular velocity tracking with observer, explained in Section 9.3. However, one significant difference in this setup, is that the observer and controller are both expressed in the NED coordinate frame, even though measurements and torque input are still given in the BODY frame. However, this is not a significant problem since it is assumed that the attitude of both the leader and the follower are known exactly at any time, and one can thus easily express the vectors in the NED or the BODY frame according to own choices.

The results from the synchronization scheme experiment can be seen in Figure 9.8 whereas the gains used by the controller and observer can be seen in Table 9.4. Remember that the derivative of the desired angular velocity were set to zero during the squared part of the tracking when the leader satellite was examined (see Remark 9.6).

Remark 9.7. In this part of the experiment, it is attempted to control both the attitude of the satellite and the angular velocity at the same time. It is therefore important to choose the tuning gains $\mathbf{A}_u$ and $\boldsymbol{\Lambda}$ to have approximately same values. This is a different strategy as compared to the cases in Section 9.2–9.3 where the main focus were to control the angular velocity. It is therefore assumed that the angular velocity tracking for these experiments will be harder to control.

Plots and descriptions

The plots from the synchronization scheme can be seen in Figure 9.8 and were sampled at 50 Hz for about 550 s. The commanded angular velocity $\boldsymbol{\omega}^n_c$, seen in Equation (9.1), were again sent through the second order reference-filter to remove unwanted jumps in the reference signal.

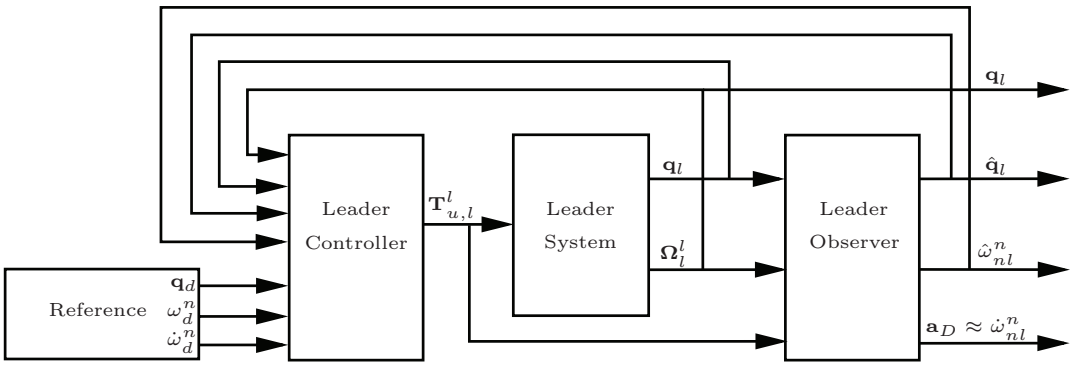

(a) Diagram of the leader satellite.

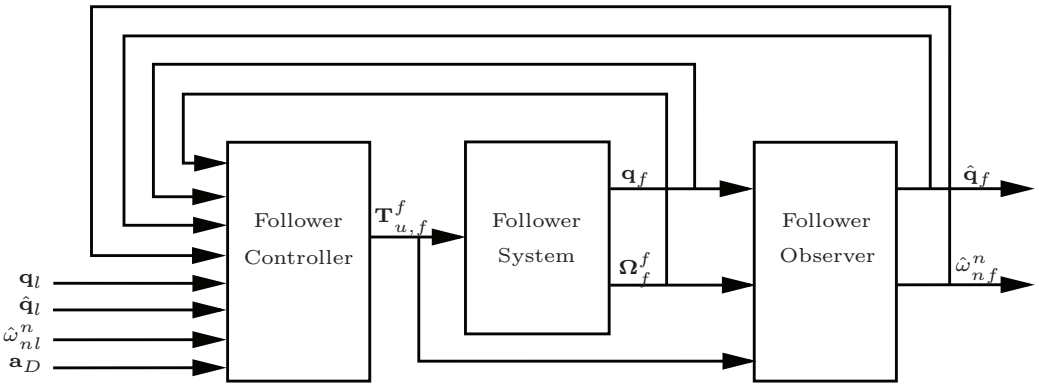

(b) Diagram of the follower satellite.

Figure 9.7: Structure of the tracking and synchronization scheme. In reality, the right side of (a) is connected with the left side of (b).

Gain-symbol	**Value**	**Denomination**
$\mathbf{A}_u$	$0.3 \cdot \mathbf{I}$	1/s
$\boldsymbol{\Lambda}$	$1.1 \cdot \mathbf{I}$	1/s
$k_{p,l}$	17.0	$\mathrm{kg^2m^4/s^2}$
$k_{p,f}$	17.0	$\mathrm{kg^2m^4/s^2}$
$k_{v,l}$	12.0	1/s
$k_{v,f}$	12.0	1/s

Table 9.4: Synchronization control and observer gains where $\mathbf{I}$ is the identity matrix.

- Figure 9.8(a) compares the desired attitude with the leader and the follower. All though the figure might look disorderly, it gives an insight in the development of the different attitudes. It can be seen that the leader satellite converges faster than the follower, which is not surprising.
- Figure 9.8(b) illustrates the attitude error for the tracking problem. It can be seen that the attitude error stays below 0.3 which corresponds to approximately 32° about the z-axis. In the squared part of the experiments the attitude error is somewhat smaller and is always less than 28°.
- Figure 9.8(c) shows the attitude error for the synchronization problem. The errors are clearly more significant in this plot than in Figure 9.8(b) and it can be seen that the error remains below the threshold $0.4 \approx 56°$. When the system is tracking the sinusoidal reference, this is somewhat better and the error stays below 24° about the z-axis.
- Figure 9.8(d) compares the desired angular velocity trajectory with the measured generalized velocity for the leader and the follower. Not surprisingly, the leader follows the desired trajectory much better than the follower.
- Figure 9.8(e) shows the angular velocity error for the tracking problem.
- Figure 9.8(f) illustrates the angular velocity error between the leader and the follower. It can be seen that the errors are clearly worse than for the tracking problem. In addition, if the error between the desired trajectory and the follower were plotted, the errors would have been even more visible.
- Figure 9.8(g) is an illustration of the commanded torque to the leader satellite. Notice that the commanded torque stays below 10 % most of the time, which implies effective use of commanded torque.
- Figure 9.8(h) shows the calculated output from the controller in the follower satellite. The torque sequence is rapid and highly oscillating with amplitudes reaching the maximum allowed torque. This is clearly not a desirable input for the actuators and may cause wear and tear of the equipment.

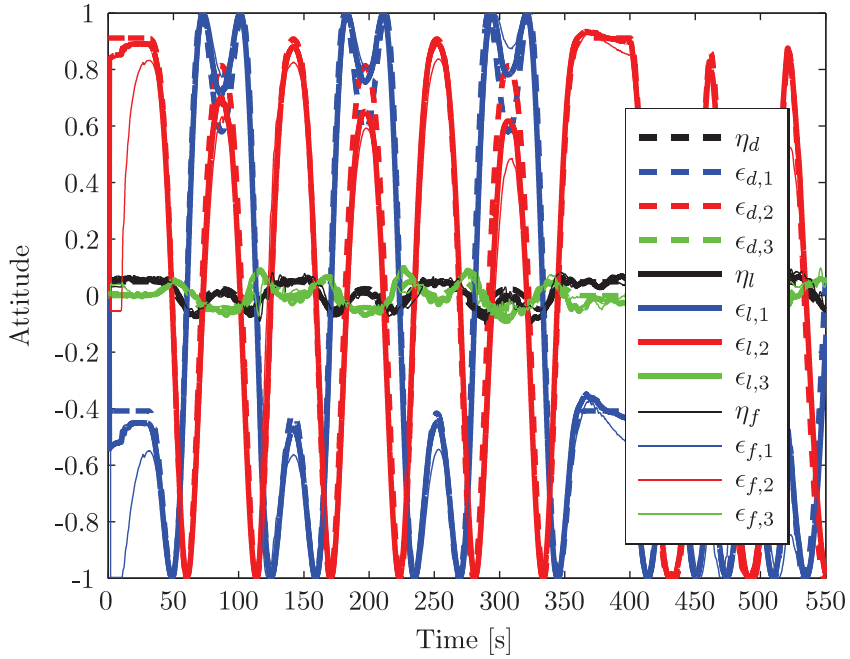

(a) Attitude of leader and follower compared with desired attitude. Note that $\mathbf{q}_f$ is multiplied with -1 since $\mathbf{e}_f^T$ is converging towards $\mathbf{q}_{id}^T = \begin{bmatrix} -1 & \mathbf{0}^T \end{bmatrix}$. See Figure 9.8(c).

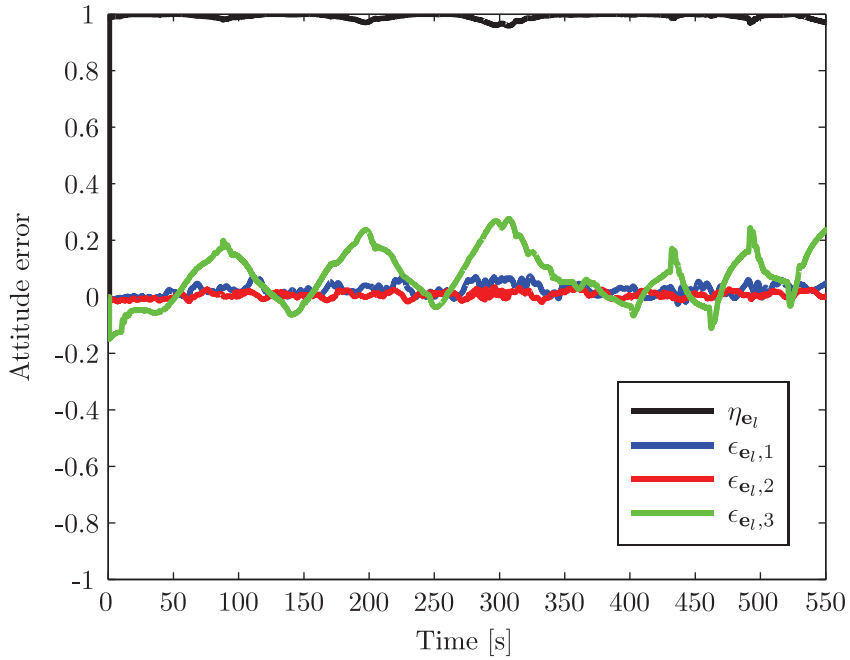

(b) Attitude error between the desired and leader attitude, $\mathbf{e}_l$.

Figure 9.8: Plots from synchronization experiment.

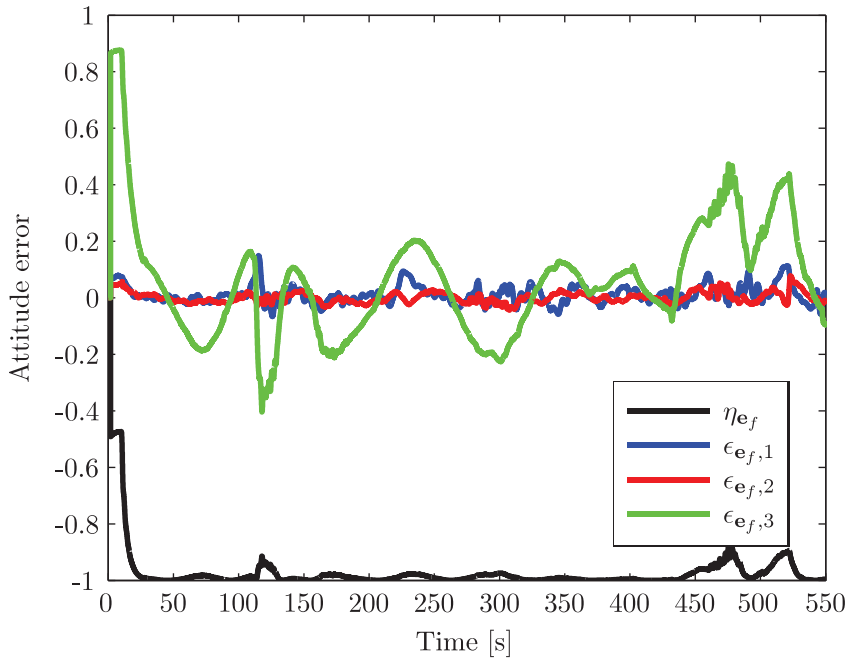

(c) Attitude error between the leader and follower attitude, $\mathbf{e}_f$.

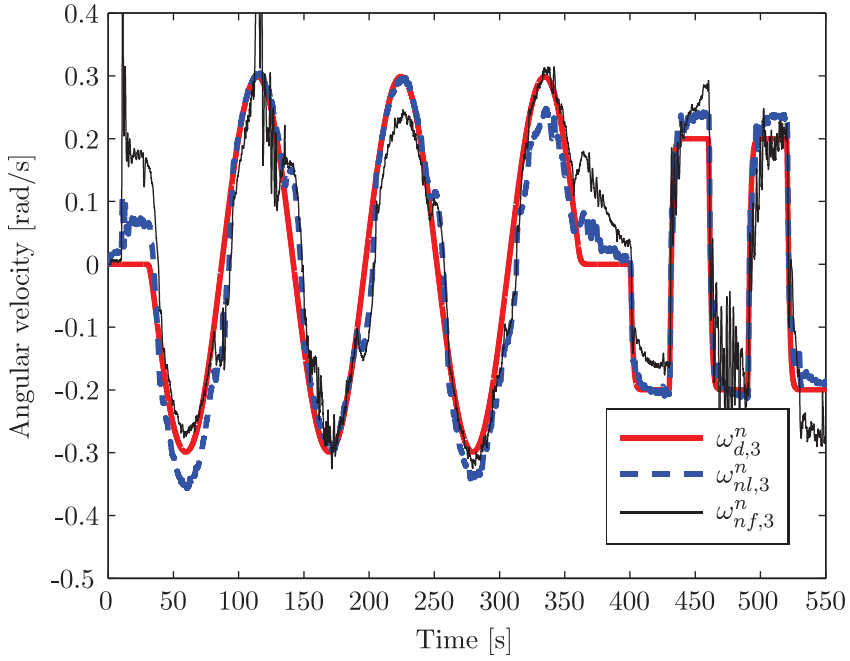

(d) Angular velocity of the leader and follower compared to the desired angular velocity about the z-axis.

Figure 9.8: Plots from synchronization experiment.

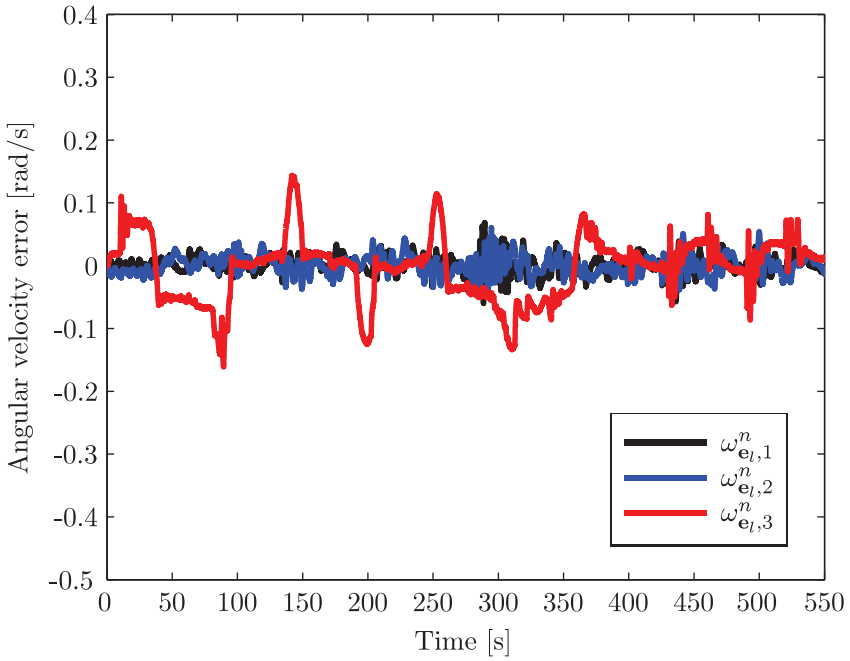

(e) Angular velocity error between the desired trajectory and leader satellite, i.e. $\boldsymbol{\omega}^n_{id} - \boldsymbol{\omega}^n_{il}$.

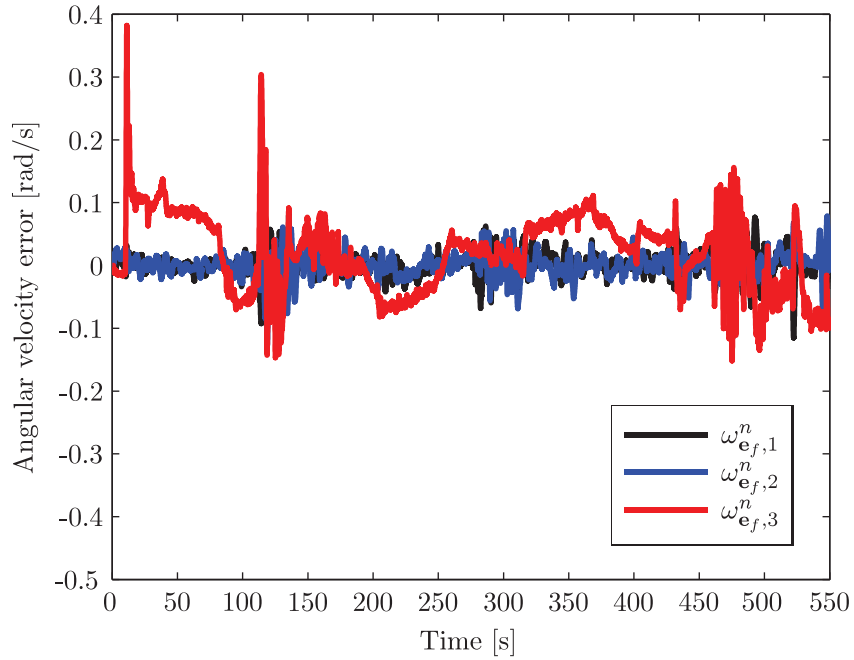

(f) Angular velocity error between the leader and follower satellite, i.e. $\boldsymbol{\omega}^n_{il} - \boldsymbol{\omega}^n_{if}$.

Figure 9.8: Plots from synchronization experiment.

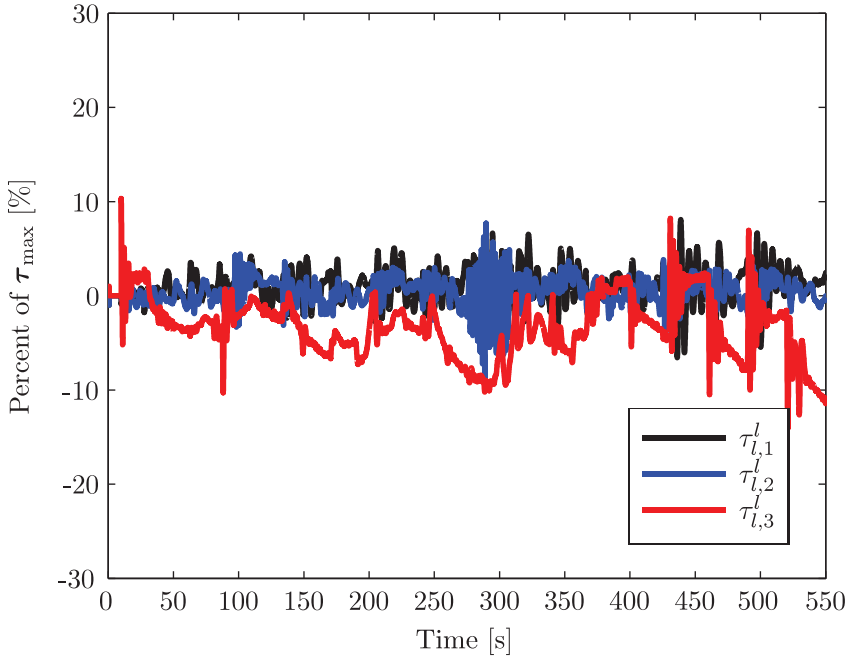

(g) Torque applied to the leader satellite.

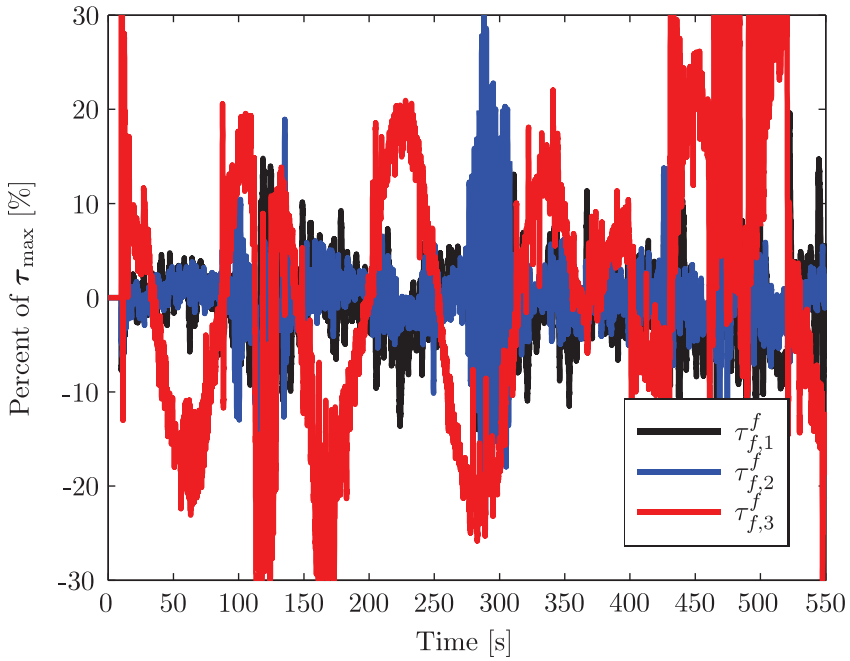

(h) Torque applied to the follower satellite.

Figure 9.8: Plots from synchronization experiment.

Chapter 10

Discussion

This chapter presents a discussion around the results from the experiments presented in Chapter 9. The various experiments are compared for similarities and differences and important elements are taken into considerations.

10.1 Experiment with angular velocity tracking without observer

The sliding mode and the backstepping controller, seen in Equation (4.13) and (4.30), respectively, were tested in a setup where angular velocity were available for feedback. This is the best way to test the performance of the controllers and similarities and differences can therefore be compared accurately.

10.1.1 Sliding mode controller

Figure 9.3(b) illustrates the behavior of the system with the sliding mode controller. It can be seen that the system tracks the desired angular velocity in an excellent manner and thereby works satisfactorily. There are none uncontrolled oscillations, which is the case when an observer for angular velocity is implemented. However, Figure 9.3(b) shows that there in some cases may occur small standard deviations when the system tracks different constant set points. To fix this problem, it might be helpful to implement an integral action in the controller, but this would make the controller more complex and not necessary improve the performance noticeable. After all, these standard deviations are acceptable and small deviations will always occur in physical systems.

From Figure 9.3(a) it can clearly be seen that the angular velocity about the x and y-axis do not follow the zero reference. This effect arises since the satellite is not perfectly balanced. However, the effect can be minimized by lowering the controller gains, but then again, the performance about the z-axis will be poorer. This problem has no easy fix, and will in most cases always be present.

10.1.2 Backstepping controller

Figure 9.4(a) demonstrates the performance of the system with the backstepping controller. The controller controls the system in a good manner and the system behaves in the same way as with the sliding mode controller. This is however of no big surprise, since it can be seen that they are very much alike. For example, choosing $\mathbf{K}_1 = \mathbf{K}$, $\mathbf{K}_2 = \mathbf{J}_s\mathbf{P}$ and setting $\mathbf{D} = k = 0$ makes the two different controllers identical. With the chosen backstepping gain values, it can be seen that the system has standard deviations when tracking the squared reference signal and misalignments in the sinusoidal sequence. The standard deviations and misalignments are clearly more marked than is the case for the SM controller. When comparing the commanded torque between the two controllers it may be noticed that the SM controller uses the torque in a more efficient way (see Figure 9.3(d) and Figure 9.4(c)). On the other hand it is possible that tuning the backstepping controller gains more closely will make the behavior better. Nevertheless, since the sliding mode controller has less standard deviation, is more accurate, and uses less torque, it may be concluded that the SM controller is noticeable better than the backstepping controller. Thus, the sliding mode controller was chosen as controller when the angular velocity observer was implemented.

10.2 Experiment with observer for angular velocity estimation

Figure 9.6(a) shows the comparison between the estimated and the measured angular velocity signal about the y and z-axis. Notice that ω_2^b in the first plot of this figure is the unfiltered angular velocity measurement. This is done to illustrate that the observer works as a low-pass filter smoothening and dampening the high-frequent measurement signal. By close inspection it can also be seen that the observer adds an unwanted phase shift of about 0.5 s for this specific case. This is and inescapable drawback for all observers, but it turns out that the phase shift is acceptable for this system.

Plot number two of Figure 9.6(a) shows the estimate of the angular velocity about the z-axis. This is where most of the dynamics take place and it can be seen that the observer works quite good when the squared-shaped signal is tracked. However, the observer has some small standard deviations in addition to small parts with an oscillating behavior. Remember that the derivative of the reference signal, $\dot{\boldsymbol{\omega}}_d^n = \mathbf{0}$ in this section due to the problem mentioned in Remark 9.6. This has dramatically improved the behavior compared to (Jørgensen, 2009) and the article submitted to the "49th IEEE Conference on Decision and Control", seen in Appendix E by Jørgensen and Gravdahl.

When the system is tracking the sinusoidal reference, it can be noticed that the observer performs less satisfying. Some mismatches are due to crashes with the surrounding walls, but most of them are caused by of the shortcomings of the observer. This can especially be seen when the observer is estimating the maximum and minimum of the sinusoidal angular velocity signal. Some improvements can however be achieved by finding better tuning gains, but another observer strategy might also be an option, e.g. an extended Kalman

filter.

Figure 9.6(b)–9.6(c) presents the overall performance of the system. The reference angular velocity is compared with the angular velocity measurement in Figure 9.6(b) whereas the difference between the two generalized velocities is seen in Figure 9.6(c). The behavior of the system is in general acceptable, but it may be seen that the system struggles when the system is tracking the sinusoidal signal. This is of no big surprise, since the observer errors are noticeable in this time interval and therefore, the problems experienced with the observer will be reflected and magnified for the total system. This can clearly be seen from the responses in the two figures. Nevertheless, the overall performance is acceptable compared to the system without angular velocity estimation, since it is expected that removing one set of measurements will make the system harder to control.

The commanded torque, calculated by the controller and seen in Figure 9.6(d), should also be commented. The torque sequence is clearly not as effective as it can be. The commanded torque is rapid, oscillating and is in general at a higher level than without angular velocity estimation. It should also be noted that the torque level reached the experienced critical level of 30 % of $\boldsymbol{\tau}_{\max}$ at some occasions. This indicates that the system is tuned to the maximum limit, and should possibly have been lowered to a more suitable level. This assumption can be strengthened by considering the experiments of the leader in the synchronization scheme, seen in Figure 9.8(b), (d), (e) and (g). The tracking problem of the leader is essentially the same as this system, and it can be seen that the leader satellite tracks the desired trajectory in a similar manner, but with a torque sequence which is much more effective. Therefore, it may be concluded that it is possible to find a better sett of gains which will improve the overall performance.

10.3 Synchronization control with angular velocity observers

First of all, in this part of the experiments, it is attempted to control both the attitude and the angular velocity at the same time. The controller must therefore make sure that the satellite has the right angular velocity in addition to being at the right attitude.

The attitude and attitude errors for the leader and follower can be seen in Figure 9.8(a)–9.8(c). Figure 9.8(a) compares the desired attitude trajectory with the measured attitude of the leader and the follower. The first 50 seconds of this plot shows that the attitude of the leader converges towards the desired trajectory, while the follower's attitude converges towards the leader's attitude. The attitude error between the follower and the desired trajectory will be a function of both the leader and the follower attitude errors, whereas the attitude error between the leader and the desired trajectory will only be dependent on the leader. Therefore, the follower will always have a phase shift compared with the desired attitude as long as there is excitation in the system.

By closer inspection of Figure 9.8(b) it can be seen that the attitude error between the desired attitude trajectory and the leader stays below 32° about the z-axis. This is quite

much and will in some cases be insufficient for operational requirement. For instance, if the satellite is going to be used in a communication scheme between the satellite and a ground station, it is most likely that a message sent or received with a 32° error will be lost. On the other hand, if a message is going to be sent between two closely cooperating vehicles, it is possible that the error-values are acceptable.

From Figure 9.8(c) it may be concluded that the attitude error between the leader and the follower is noticeable larger than the error between the leader and the desired attitude trajectory. As can be calculated from the figure, the maximum attitude error after the convergence period is approximately 56°. This is dramatically higher than the 32° threshold as calculated from Figure 9.8(b), but to be expected since the input for the leader is a mathematically given smooth trajectory, while the input to the follower consist of raw measurements. In addition, these measurements can be exposed to sources of errors and can thus further aggravate the circumstances.

All though there is no figure illustrating the attitude error between the desired attitude trajectory and the measured follower's attitude, it is assumed that this error will be even higher than the error between the leader and the follower. This claim can also be confirmed by utilizing the quaternion-multiplication $\mathbf{e}_{df} = \mathbf{e}_l \otimes \mathbf{e}_f$, but is left out of the thesis, since it is a quite obvious fact. Nevertheless, it should be mentioned that the average error between the follower and the desired attitude is in fact significantly higher, all though the maximum threshold is approximately the same as in Figure 9.8(c).

The graph in Figure 9.8(d) compares the desired angular velocity with the leader and the follower. It can be seen from this figure in addition to Figure 9.8(e) that the leader system tracks the desired angular velocity trajectory in a good manner. The behavior is in fact comparable with the experiments presented in Section 9.3, and similar angular velocity responses can be seen. This is according to theory since the two systems have the same observer-structure, and the only significant distinction is the implemented controllers. Even so, one important difference can be observed: the use of torque for the leader in the synchronization scheme is dramatically better than the use of torque in Section 9.3 (See Figure 9.6(d) and Figure 9.8(g)). The reason for this is probably due to none optimal tuning of the gains for the system in Section 9.3, but it is also possible that the controller used in the current experiment is better. One important difference between the two controllers is that the leader synchronization controller is dependent on the observer errors. This is not the case for the system with the sliding mode controller, since the SM controller was developed assuming that angular velocity measurements were available for feedback. The synchronizing controller, on the other hand, was constructed with the knowledge that angular velocity measurements were not available, and could thereby utilize knowledge of the current observer errors in stead. It is therefore possible for the synchronizing controller to exploit the state of the observer to perform the correct action.

The performance of the angular velocity synchronization problem can be seen in Figure 9.8(d) and Figure 9.8(f). It is quite clear that the behavior is not as good as for the tracking problem. The angular velocity performance is occasionally highly oscillating, is rapid and has tendencies to a drifting behavior. It was also experienced that small unforeseen events made the satellite lose track and become unstable. This is obviously an

undesirable action, but is in some extent anticipated. One reason for this behavior is that the input to the follower satellite is taken directly from the leader satellite measurements and its estimations. The errors from the leader will therefore be reflected and magnified for the follower satellite, and can occasionally even destabilize the satellite.

The oscillating action seen in Figure 9.8(d) can be explained by looking closely at the commanded torque to the actuators, seen in Figure 9.8(h). It can be seen that the torque level reaches the critical threshold of 30 % of the maximum allowed torque at several occasions. It has in addition a high frequency behavior with high amplitudes. This is undoubtedly not good for the actuators and probably caused wear and tear for the torque-providing equipment. The satellite was in fact making strange noises and the experiment should most likely have been stopped right away. Nevertheless, due to the excitement of a functioning control system, the experiment was carried out without questioning the consequences. However, in the next experiment, a first order filter was implemented between the output from the controller and the input to the actuators to smooth out the torque signal. This clearly made a difference and eliminated the unusual noise. The performance of the system with the new filter implemented, behaved similar as without the filter, but with a slightly noticeable drop in performance. It is therefore indisputable that the filter should be implemented in future experiments.

Another aspect, which can not be seen directly from the figures, is that the follower satellite's CPU is running close to its maximum capacity. This is documented by the communication application used between the on-shore host and the QNX target. Whether or not this is actually restraining the performance is hard to say, but it is possible that the system can be affected by the problem.

All these troubles implies that the follower system is on the edge of its capabilities and it is therefore quite remarkable that the follower is in fact able to follow the leader, to a certain extent.

Remark 10.1. Note that the experiments with observer often became unstable when a noticeable unforeseen disturbance affected the system. This disturbance could be a person pushing the satellite with enough force in the right direction or in some cases, a powerful crash with one of the walls. This can however not be seen directly from the plots, but is worth mention since it gives a characterization of the robustness of the system.

The systems without observer could also be manipulated so that they became unstable, but experience showed that the force needed to do so had to be much higher than compared to the cases with observer implemented.

11 Concluding remarks

11.1 Conclusions

In this thesis the topic of controlling and synchronizing the attitude of spherical-shaped spacecrafts have been studied. Each vehicle is actuated by means of three orthogonally mounted reaction wheels and the vessel can thereby be controlled in three degrees of freedom. Using methods from nonlinear system theory a robust sliding mode controller in addition to a backstepping controller have been proposed and implemented on the AUVSAT for single vehicle control. With the given controllers, two Lyapunov function candidates have been constructed and asymptotic stability is proven for the overall system.

When angular velocity measurements are not present in the spacecraft, a nonlinear observer is derived to estimate the generalized velocity. Asymptotic stability is proven for the observer using LaSalle's and Matrosov's theorems.

A leader-follower synchronization scheme has been developed for the cases where more than one spacecraft is required. It is assumed that angular velocity measurements are not present, and the nonlinear observer is therefore used in both the leader and the follower satellite to estimate the angular velocity. Two backstepping controllers are also derived making sure that the leader follows a mathematically given trajectory, while the follower satellite follows the leader's attitude.

The various systems were tested in a lab setup where the AUVSAT was submerged in water and thereby emulating a gravity free environment. Experiments were carried out to evaluate the performance of the controllers, observers and the leader-follower synchronization scheme. In each experiment the system is set to track a sinusoidal time-varying trajectory in addition to a square-shaped angular velocity reference signal.

The results show that the sliding mode and the backstepping controller works quite similar with a satisfactorily behavior throughout the experiment. However, there is some lack of performance for the overall system with observer, and especially tracking of the sinusoidal reference signal is inadequate.

In the leader-follower synchronization experiment, it is seen that the leader follows the desired trajectory, while the follower converges towards the leader's attitude. However, misalignment, drifting, and oscillation have been noticed. These undesirable behaviors are especially seen for the follower satellite and the system is clearly on the edge of its capabilities. Nevertheless, all aspect considered, the performance of the complete system is satisfactorily and good results have been shown.

11.2 Recommendations

The most obvious next step in the evaluation of the different proposed controllers, observers and synchronization scheme, is to perform experiments in all three degrees of freedom. This might be done at the "Marine Cybernetics Laboratory" at Tyholt in Trondheim, an excellent facility for testing of ocean structures.

Another interesting aspect is to investigate if simple linear controllers, based on linearization, can work satisfactorily. After all, the linear controller is by far the most used active controller worldwide and is often very robust because of its many tuning theories. In addition a linear controller is less computational demanding than nonlinear controllers, which is important in satellite architectures where computational power is limited. A different interesting feature is to see if an extended Kalman filter would make the estimation of the angular velocity better than the implemented observer. The extended Kalman filter is a well tested observer and might give a better result.

In Section 5.1 it is mentioned that the experiments tuned out to be greatly affected by the Ethernet cable connecting the QNX target with the on-shore host. It is therefore of great interest to remove this cable and use wireless transmission instead. The benefit would be a system almost fully emulating a true satellite traveling in space. However, this would require additional equipment and further investigation has to be carried out.

The job of implementing wireless transmission could also be seen as a part of making the experiment platform more attractive for other students, and it may be possible to develop a test bench that can be used as a lab exercise in e.g. nonlinear control subjects. However this would require an examination of the complete lab setup, where the equipment has to be more robust for ignorance errors and it must be easier to set up the experiments. Today it takes almost an hour to prepare the experiment and half an hour to restore the equipment to its startup state. This is of course far too much if many students are going to use the underwater satellite test bench.

A suggestion for future work on the theoretical part of the assignment, is to investigate the possibility for a local version of the extended Matrosov's theorem, presented in (Loria et al., 2002). The proposed theorem has among others, the advantage of applying an arbitrary number of auxiliary functions to prove uniform global asymptotic stability (UGAS). This was also carried out as a part of the stability analysis for the observer in Chapter 6. Here it turned out that one was actually capable of satisfying all assumptions for the theorem and one could thereby apparently conclude with UGAS for the observer. However, since unit quaternion has been chosen as attitude parameterization, one actually has two equilibriums, and it is therefore impossible to conclude with global asymptotic stability. It is therefore motivating to develop a local version of the extended Matrosov's theorem, and utilize all its benefits to conclude with uniform local asymptotic stability.

References

A. Abdessameud and A. Tayebi, "Attitude synchronization of a group of spacecraft without velocity measurements," *IEEE Transactions on Automatic Control*, vol. 54, no. 11, pp. 2642–2648, 2009.

J. Ahmed and D. S. Bernstein, "Globally convergent adaptive control of spacecraft angular velocity without inertia modeling," in *Proceedings of the American Control Conference*, vol. 3, 1999, pp. 1540–1544.

E. Alfaro-Cid, E. W. McGookin, D. J. Murray-Smith, and T. I. Fossen, "Genetic algorithms optimization of decoupled sliding mode controllers: simulated and real results," *Control Engineering Practice*, vol. 13, no. 6, pp. 739 – 748, 2005.

O. A. Bauchau and L. Trainelli, "The vectorial parameterization of rotation," *Nonlinear dynamics*, vol. 32, no. 1, pp. 71–92, 2009.

A. K. Bondhus, K. Y. Pettersen, and J. T. Gravdahl, "Leader/follower synchronization of satellite attitude without angular velocity measurements," in *European Control Conference and the 44th IEEE Conference on Decision and Control*, 2005, pp. 7270–7277.

A. K. Bondhus, "Leader-follower synchronization of mechanical systems," Ph.D. dissertation, Norwegian University of Science and Technology, 2010.

Y. Bouteraa and J. Ghommam, "Synchronization control of multiple robots manipulators," in *Proceedings of the 6th International Multi-Conference on Systems, Signals and Devices*, 2009, pp. 1–6.

A. E. Bryson, Jr., *Control of Spacecraft and Aircraft*. Princeton University Press, 1994.

D. W. Casbeer, R. W. Beard, T. W. McLain, S.-M. Li, and R. K. Mehra, "Forest fire monitoring with multiple small UAVs," in *Proceedings of the American Control Conference*, vol. 5, 2005, pp. 3530–3535.

C.-T. Chen, *Linear System Theory and Design*, 3rd ed. Oxford University Press, 1999.

Y. P. Chen and S. C. Lo, "Sliding-mode controller design for spacecraft attitude tracking maneuvers," *IEEE Transactions on Aerospace and Electronic Systems*, vol. 29, no. 4, pp. 1328–1333, 1993.

B. T. Costic, D. M. Dawson, M. S. De Queiroz, and V. Kapila, "A quaternion-based adaptive attitude tracking controller without velocity measurements," in *Proceedings of the 39th IEEE Conference on Decision and Control*, vol. 3, 2000, pp. 2424–2429.

J. Diebel, "Representing attitude: Euler angles, unit quaternions, and rotation vectors," Stanford University, Tech. Rep., 2006.

O. Egeland and J. M. Godhavn, "Passivity-based adaptive attitude control of a rigid spacecraft," *IEEE Transactions on Automatic Control*, vol. 39, no. 4, pp. 842–846, 1994.

O. Egeland and J. T. Gravdahl, *Modeling and Simulation for Automatic Control*. Marine Cybernetics, 2002.

O. E. Fjellstad, "Control of unmanned underwater vehicles in six degrees of freedom: A quaternion feedback approach," Ph.D. dissertation, Norwegian University of Science and Technology, 1994.

O. E. Fjellstad and T. I. Fossen, "Quaternion feedback regulation of underwater vehicles," in *Proceedings of the Third IEEE Conference on Control Applications*, vol. 2, 1994, pp. 857–862.

T. I. Fossen, *Marine Control Systems, Guidance, Navigation, and Control of Ships, Rigs and Underwater Vehicles*. Marine Cybernetics, 2002.

——, *Modelling and Control of Marine Vessels*. Norwegian University of Science and Technology, 2009, draft Copy.

W. Gawronski and E. M. Craparo, "Antenna scanning techniques for estimation of spacecraft position," in *Proceedings of the IEEE Aerospace Conference*, vol. 2, 2002, pp. 2–939–2–948.

K. Groves and A. Serrani, "Modeling and nonlinear control of a single-link flexible joint manipulator," Department of Electrical and Computer Engineering, The Ohio State University, USA, Tech. Rep., 2004.

W. Hahn, *Stability of Motion*. Springer-Verlag, 1967.

C. D. Hall, "Attitude dynamics of orbiting gyrostats," in *Dynamics of Natural and Artificial Celestial Bodies*, H. Pretka-Ziomek, E. Wnuk, P. K. Seidelmann, and D. Richardson, Eds., 2002, pp. 177–186.

C. D. Hall, "Spinup dynamics of gyrostats," *Journal of Guidance, Control, and Dynamics*, no. 18, pp. 1177–1183, 1995.

C. D. Hall, P. Tsiotras, and H. Shen, "Tracking Rigid body motion using thrusters and momentum wheels," *Journal of the Astronautical Sciences*, vol. 50, no. 3, pp. 311–323, 2002.

Q. Hu, M. I. Friswell, D. J. Wagg, and S. Neild, "Adaptive backstepping fault-tolerant control for flexible spacecraft with bounded unknown disturbances," in *Proceedings of the 48th IEEE Conference on Decision and Control*, 2009, pp. 788–793.

P. C. Hughes, *Spacecraft Attitude Dynamics*. John Wiley & Sons Inc, 1986.

Z. Ismail and R. Varatharajoo, "A study of reaction wheel configurations for a 3-axis satellite attitude control," *Advances in Space Research*, vol. In Press, Accepted Manuscript, 2009.

Y. Jiang, Q. Hu, and G. Ma, "Adaptive backstepping fault-tolerant control for flexible spacecraft with unknown bounded disturbances and actuator failures," *ISA Transactions*, vol. 49, no. 1, pp. 57–69, 2010.

J. Jin, S. Ko, and C.-K. Ryoo, "Fault tolerant control for satellites with four reaction wheels," *Control Engineering Practice*, vol. 16, no. 10, pp. 1250 – 1258, 2008.

T. A. Johansen and K. J. Hunt, "A computational approach to approximate input/state feedback linearization," in *Proceedings of the 39th IEEE Conference on Decision and Control*, vol. 5, 2000, pp. 4467–4472.

U. Jørgensen, *Attitude Control for Satellites: AUVSAT*, Norwegian University of Science and Technology, December 2009, specialization project.

H. K. Khalil, *Nonlinear System*, 3rd ed. Prentice Hall, 2002.

K. Köprübasi and M. W. L. Thein, "Spacecraft attitude and rate estimation using sliding mode observers," in *International Conference on Recent Advances in Space Technologies*, 2003, pp. 165–170.

R. Kristiansen, A. Loría, A. Chaillet, and P. J. Nicklasson, "Spacecraft relative rotation tracking without angular velocity measurements," *Automatica*, vol. 45, no. 3, pp. 750–756, 2009.

T. R. Krogstad, J. T. Gravdahl, and R. Kristiansen, "Coordinated control of satellites: The attitude case," *Proceedings of the 56th International Astronautical Congress (IAC), Fukuoka, Japan*, 2005.

T. R. Krogstad, J. T. Gravdahl, E. Børhaug, and K. Y. Pettersen, "AUVSAT: An experimental platform for spacecraft formation flying," *Proceedings of the 59th International Astronautical Congress, Glasgow, Scotland*, 2008.

T. R. Krogstad, "Attitude control of satellites in clusters," Master's thesis, Norwegian University of Science and Technology, 2005.

——, "Attitude synchronization in spacecraft formations. Theoretical and experimental results," Ph.D. dissertation, Norwegian University of Science and Technology, 2010.

M. Krstić, I. Kanellakopoulos, and P. V. Kokotović, *Nonlinear and Adaptive Control Design*. John Wiley & Sons, Inc, 1995.

E. Kyrkjebø, K. Y. Pettersen, M. Wondergem, and H. Nijmeijer, "Output synchronization control of ship replenishment operations: Theory and experiments," *Control Engineering Practice*, vol. 15, no. 6, pp. 741–755, 2007, special Section on Control Applications in Marine Systems - CAMS2004, Control Applications in Marine Systems.

C. Li and G. Ma, "Adaptive backstepping control for attitude tracking of a spacecraft," in *IEEE International Symposium on Industrial Electronics*, 2007, pp. 83–88.

A. Loria, E. Panteley, D. Popovic, and A. R. Teel, "An extension of matrosov's theorem with application to stabilization of nonholonomic control systems," in *Proceedings of the 41st IEEE Conference on Decision and Control*, vol. 2, 2002, pp. 1528–1533.

S. Ma and E.-K. Boukas, "A singular system approach to robust sliding mode control for uncertain markov jump systems," *Automatica*, vol. In Press, Corrected Proof, 2009.

V. M. Matrosov, "On the stability of motion," *Journal of Applied Mathematics and Mechanics*, vol. 26, no. 5, pp. 1337 – 1353, 1962.

D. C. B. Owen, "Fundamentals of 3D game development," Michigan State University, Tech. Rep., 2009, read-date: 11.10.2009, http://www.cse.msu.edu/~cse473/lecture6.ppt.

W. Perruquetti and J. P. Barbot, *Sliding Mode Control in Engineering*. Marcel Dekker, Inc., 2002.

W. Ren, "Distributed attitude synchronization for multiple rigid bodies with euler-lagrange equations of motion," in *Proceedings of the 46th IEEE Conference on Decision and Control*, 2007, pp. 2363–2368.

S. Salcudean, "A globally convergent angular velocity observer for rigid body motion," *IEEE Transactions on Automatic Control*, vol. 36, no. 12, pp. 1493–1497, 1991.

D. P. Scharf, F. Y. Hadaegh, and S. R. Ploen, "A survey of spacecraft formation flying guidance and control (part 1): guidance," in *Proceedings of the American Control Conference*, vol. 2, 2003, pp. 1733 – 1739.

——, "A survey of spacecraft formation flying guidance and control. part ii: control," in *Proceedings of the American Control Conference*, vol. 4, 2004, pp. 2976 – 2985.

D. Shevitz and B. Paden, "Lyapunov stability theory of nonsmooth systems," *IEEE Transactions on Automatic Control*, vol. 39, no. 9, pp. 1910–1914, 1994.

T. Society of Naval Architects and Marine Engineers, "Nomenclature for treating the motion of a submerged body through a fluid," *Technical and Research Bulletin No*, 1950.

M. W. Spong, S. Hutchinson, and M. Vidyasagar, *Robot Modeling and Control*. John Wiley & Sons, Inc., 2006.

A. Tayebi, "Unit quaternion observer based attitude stabilization of a rigid spacecraft without velocity measurement," in *45th IEEE Conference on Decision and Control*, 2006, pp. 1557–1561.

P. Tsiotras, H. Shen, and C. Hall, "Satellite attitude control and power tracking with energy/momentum wheels," *Journal of Guidance, Control, and Dynamics*, vol. 24, pp. 23–34, 2001.

B. Wang, K. Gong, D. Yang, and J. Li, "Fine attitude control by reaction wheels using variable-structure controller," *Acta Astronautica*, vol. 52, no. 8, pp. 613–618, 2003.

J. T. Y. Wen and K. Kreutz-Delgado, "The attitude control problem," *IEEE Transactions on Automatic Control*, vol. 36, no. 10, pp. 1148–1162, 1991.

B. Wie, *Space Vehicle Dynamics and Control*. American Institute of Aeronautics and Astronautics, 1998.

C.-H. Won, "Comparative study of various control methods for attitude control of a leo satellite," *Aerospace Science and Technology*, vol. 3, no. 5, pp. 323 – 333, 1999.

B. Xiao, Q.-L. Hu, and G. Ma, "Adaptive sliding mode backstepping control for attitude tracking of flexible spacecraft under input saturation and singularity," *Proceedings of the Institution of Mechanical Engineers. Journal of Aerospace Engineering*, vol. 224, no. 2, 2010.

J. Yongqiang, L. Xiangdong, Q. Wei, and H. Chaozhen, "Time-varying sliding mode controls in rigid spacecraft attitude tracking," *Chinese Journal of Aeronautics*, vol. 21, no. 4, pp. 352 – 360, 2008.

K. D. Young, V. I. Utkin, and U. Ozguner, "A control engineer's guide to sliding mode control," *IEEE Transactions on Control Systems Technology*, vol. 7, no. 3, pp. 328–342, 1999.

Appendices

Appendix A

Calculations

A.1 Dynamic error calculation

By starting with the expression of the orientation error $\mathbf{e}$ stated in Equation (4.3), one can derive it with respect to time and get the following:

$$\dot{\mathbf{e}} = \underbrace{\mathbf{q}_d^{-1} \otimes \dot{\mathbf{q}}}_{\mathbf{Q}_1} + \underbrace{\dot{\mathbf{q}}_d^{-1} \otimes \mathbf{q}}_{\mathbf{Q}_2}. \tag{A.1}$$

If we look at the expression for $\mathbf{Q}_1$ only, we get:

$$\mathbf{Q}_1 = \begin{bmatrix} \eta_d\dot{\eta} + \boldsymbol{\epsilon}_d^T\dot{\boldsymbol{\epsilon}} \\ \eta_d\dot{\boldsymbol{\epsilon}} - \dot{\eta}\boldsymbol{\epsilon}_d - \mathbf{S}(\boldsymbol{\epsilon}_d)\dot{\boldsymbol{\epsilon}} \end{bmatrix} = \begin{bmatrix} \eta_d & \boldsymbol{\epsilon}_d^T \\ -\boldsymbol{\epsilon}_d & \eta_d\mathbf{I} - \mathbf{S}(\boldsymbol{\epsilon}_d) \end{bmatrix} \begin{bmatrix} \dot{\eta} \\ \dot{\boldsymbol{\epsilon}} \end{bmatrix}. \tag{A.2}$$

In Fossen (Fossen, 2009) it is shown that,

$$\begin{bmatrix} \dot{\eta} \\ \dot{\boldsymbol{\epsilon}} \end{bmatrix} = \frac{1}{2} \begin{bmatrix} -\boldsymbol{\epsilon}^T \\ \eta\mathbf{I} + \mathbf{S}(\boldsymbol{\epsilon}) \end{bmatrix} \boldsymbol{\omega}_{nb}^b. \tag{A.3}$$

This can be substituted into Equation (A.2), which results in the expression shown in Equation (A.4)

$$\mathbf{Q}_1 = \frac{1}{2} \begin{bmatrix} -\eta_d\boldsymbol{\epsilon}^T + \eta\boldsymbol{\epsilon}_d^T + \boldsymbol{\epsilon}_d^T\mathbf{S}(\boldsymbol{\epsilon}) \\ \boldsymbol{\epsilon}_d\boldsymbol{\epsilon}^T + \eta_d\eta\mathbf{I} + \eta_d\mathbf{S}(\boldsymbol{\epsilon}) - \eta\mathbf{S}(\boldsymbol{\epsilon}_d) - \mathbf{S}(\boldsymbol{\epsilon}_d)\mathbf{S}(\boldsymbol{\epsilon}) \end{bmatrix} \boldsymbol{\omega}. \tag{A.4}$$

Now considering expressions for $-\boldsymbol{\epsilon}_e^T$ and $\eta_e\mathbf{I} + \mathbf{S}(\boldsymbol{\epsilon}_e)$, seen in Equation (4.4), a simpler expression for $\mathbf{Q}_1$ is obtained.

$$\begin{aligned} -\boldsymbol{\epsilon}_e^T &= -\left(\eta_d\boldsymbol{\epsilon} - \eta\boldsymbol{\epsilon}_d - \mathbf{S}(\boldsymbol{\epsilon}_d)\boldsymbol{\epsilon}\right)^T, \\ &= -\left(\eta_d\boldsymbol{\epsilon}^T - \eta\boldsymbol{\epsilon}_d^T - \boldsymbol{\epsilon}^T[\mathbf{S}(\boldsymbol{\epsilon}_d)]^T\right), \\ &= -\eta_d\boldsymbol{\epsilon}^T + \eta\boldsymbol{\epsilon}_d^T - \boldsymbol{\epsilon}^T\mathbf{S}(\boldsymbol{\epsilon}_d). \end{aligned} \tag{A.5}$$

And by using the relation $-\boldsymbol{\epsilon}^T\mathbf{S}(\boldsymbol{\epsilon}_d) = \boldsymbol{\epsilon}_d^T\mathbf{S}(\boldsymbol{\epsilon})$, the final expression for $-\boldsymbol{\epsilon}_e^T$ is found:

$$-\boldsymbol{\epsilon}_e^T = -\eta_d\boldsymbol{\epsilon}^T + \eta\boldsymbol{\epsilon}_d^T + \boldsymbol{\epsilon}_d^T\mathbf{S}(\boldsymbol{\epsilon}). \tag{A.6}$$

Now, the next step in the computation of $\mathbf{Q}_1$ is to compute $\eta_e\mathbf{I} + \mathbf{S}(\boldsymbol{\epsilon}_e)$.

$$\begin{aligned}\eta_e\mathbf{I} + \mathbf{S}(\boldsymbol{\epsilon}_e) &= (\eta_d\eta + \boldsymbol{\epsilon}_d^T\boldsymbol{\epsilon})\mathbf{I} + \mathbf{S}(\eta_d\boldsymbol{\epsilon} - \eta\boldsymbol{\epsilon}_d - \mathbf{S}(\boldsymbol{\epsilon}_d)\boldsymbol{\epsilon}),\\ &= \eta_d\eta\mathbf{I} + \boldsymbol{\epsilon}_d^T\boldsymbol{\epsilon}\mathbf{I} + \eta_d\mathbf{S}(\boldsymbol{\epsilon}) - \eta\mathbf{S}(\boldsymbol{\epsilon}_d) - \mathbf{S}(\mathbf{S}(\boldsymbol{\epsilon}_d)\boldsymbol{\epsilon}).\end{aligned} \tag{A.7}$$

It may be shown by the properties of the triple product (Egeland and Gravdahl, 2002) that, $\mathbf{S}(\mathbf{S}(\boldsymbol{\epsilon}_d)\boldsymbol{\epsilon}) = \boldsymbol{\epsilon}\boldsymbol{\epsilon}_d^T - \boldsymbol{\epsilon}_d\boldsymbol{\epsilon}^T$ and that $\boldsymbol{\epsilon}_d^T\boldsymbol{\epsilon}\mathbf{I} = \boldsymbol{\epsilon}\boldsymbol{\epsilon}_d^T - \mathbf{S}(\boldsymbol{\epsilon}_d)\mathbf{S}(\boldsymbol{\epsilon})$. Substituting these relations into Equation (A.7) results in:

$$\begin{aligned}\eta_e\mathbf{I} + \mathbf{S}(\boldsymbol{\epsilon}_e) &= \eta_d\eta\mathbf{I} + \boldsymbol{\epsilon}\boldsymbol{\epsilon}_d^T - \mathbf{S}(\boldsymbol{\epsilon}_d)\mathbf{S}(\boldsymbol{\epsilon}) + \eta_d\mathbf{S}(\boldsymbol{\epsilon}) - \eta\mathbf{S}(\boldsymbol{\epsilon}_d) - \boldsymbol{\epsilon}\boldsymbol{\epsilon}_d^T + \boldsymbol{\epsilon}_d\boldsymbol{\epsilon}^T,\\ &= \boldsymbol{\epsilon}_d\boldsymbol{\epsilon}^T + \eta_d\eta\mathbf{I} + \eta_d\mathbf{S}(\boldsymbol{\epsilon}) - \eta\mathbf{S}(\boldsymbol{\epsilon}_d) - \mathbf{S}(\boldsymbol{\epsilon}_d)\mathbf{S}(\boldsymbol{\epsilon}).\end{aligned} \tag{A.8}$$

By comparing Equation (A.8) and (A.6) with Equation (A.4), it is easily seen that $\mathbf{Q}_1$ may be written as:

$$\mathbf{Q}_1 = \frac{1}{2}\begin{bmatrix} -\boldsymbol{\epsilon}_e^T \\ \eta_e\mathbf{I} + \mathbf{S}(\boldsymbol{\epsilon}_e)\end{bmatrix}\boldsymbol{\omega} = \frac{1}{2}\begin{bmatrix} -\boldsymbol{\epsilon}_e^T \\ \mathbf{T}(\mathbf{q}_e)\end{bmatrix}\boldsymbol{\omega}. \tag{A.9}$$

A similar calculation can be performed for $\mathbf{Q}_2$, knowing that (Fjellstad, 1994)

$$\begin{bmatrix}\dot{\eta}_d \\ \dot{\boldsymbol{\epsilon}}_d\end{bmatrix} = \frac{1}{2}\begin{bmatrix} -\boldsymbol{\epsilon}_e^T \\ \eta_e\mathbf{I} + \mathbf{S}(\boldsymbol{\epsilon}_e)\end{bmatrix}\boldsymbol{\omega}_{nd}^d, \tag{A.10}$$

where $\boldsymbol{\omega}_{nd}^d$ is the desired angular velocity given in the "desired" frame d, and can be expressed in either the BODY or the NED frame by using the relation $\boldsymbol{\omega}_{nd}^d = \mathbf{R}_b^d(\mathbf{q}_e)\boldsymbol{\omega}_{nd}^b$ or $\boldsymbol{\omega}_{nd}^d = \mathbf{R}_n^d(\mathbf{q}_d)\boldsymbol{\omega}_{nd}^n = \mathbf{R}^T(\mathbf{q}_d)\boldsymbol{\omega}_{nd}^n$. The expression for $\mathbf{Q}_2$ then becomes:

$$\mathbf{Q}_2 = \begin{bmatrix}\eta & \boldsymbol{\epsilon}^T \\ \boldsymbol{\epsilon} & -\eta\mathbf{I} + \mathbf{S}(\boldsymbol{\epsilon})\end{bmatrix}\frac{1}{2}\begin{bmatrix} -\boldsymbol{\epsilon}_d^T \\ \eta_d\mathbf{I} + \mathbf{S}(\boldsymbol{\epsilon}_d)\end{bmatrix}\mathbf{R}(\mathbf{q}_e)\boldsymbol{\omega}_{nd}^b. \tag{A.11}$$

With a lot of calculations, similar to the ones for $\mathbf{Q}_1$, but left out of this paper due to no extra insight in the system, you end up with the expression

$$\mathbf{Q}_2 = -\frac{1}{2}\begin{bmatrix} -\boldsymbol{\epsilon}_e^T \\ \eta_e\mathbf{I} + \mathbf{S}(\boldsymbol{\epsilon}_e)\end{bmatrix}\boldsymbol{\omega}_{nd}^b. \tag{A.12}$$

Finally, the complete expression for $\dot{\mathbf{e}}$ used in this paper can easily be expressed as:

$$\dot{\mathbf{e}} = \frac{1}{2}\begin{bmatrix} -\boldsymbol{\epsilon}_e^T \\ \eta_e\mathbf{I} + \mathbf{S}(\boldsymbol{\epsilon}_e)\end{bmatrix}\boldsymbol{\omega}_e, \tag{A.13}$$

since the definition of the angular velocity error $\boldsymbol{\omega}_e = \boldsymbol{\omega}_{nb}^b - \boldsymbol{\omega}_{nd}^b$.

A.2 Time derivative of the angular velocity error

To calculate the time derivative of the rotation matrix in the expression for the angular velocity error we start by listing some of the used properties in the calculation:

- $\dot{\mathbf{R}}_b^a = \mathbf{R}_b^a \mathbf{S}(\boldsymbol{\omega}_{ab}^b)$ (Krogstad, 2005).
- $\boldsymbol{\omega}_{ab}^a = -\boldsymbol{\omega}_{ba}^a$ (Spong et al., 2006).
- $\mathbf{R}_b^a = \left(\mathbf{R}_a^b\right)^T$.
- $\mathbf{S}(\mathbf{x})\mathbf{x} = \mathbf{0}$.
- $\mathbf{S}(\alpha\mathbf{x} + \beta\mathbf{y}) = \alpha\mathbf{S}(\mathbf{x}) + \beta\mathbf{S}(\mathbf{y})$.

We start by stating the angular velocity error shown in Equation (4.2b) written in a more convenient manner:

$$\boldsymbol{\omega}_e^b = \boldsymbol{\omega}_{nb}^b - \mathbf{R}_n^b \boldsymbol{\omega}_d^n = \boldsymbol{\omega}_{nb}^b - \boldsymbol{\omega}_d^b. \tag{A.14}$$

Then we can start the calculation of $\dot{\mathbf{R}}_n^b = \dot{\mathbf{R}}^T$:

$$\begin{aligned}
\dot{\mathbf{R}}_n^b \boldsymbol{\omega}_d^n &= \mathbf{S}(\boldsymbol{\omega}_{bn}^b)\mathbf{R}_n^b \boldsymbol{\omega}_d^n, \\
&= -\mathbf{S}(\boldsymbol{\omega}_{nb}^b)\boldsymbol{\omega}_d^b \\
&= -\mathbf{S}\left(\boldsymbol{\omega}_e^b + \boldsymbol{\omega}_d^b\right)\boldsymbol{\omega}_d^b, \\
&= -\mathbf{S}(\boldsymbol{\omega}_e^b)\boldsymbol{\omega}_d^b - \mathbf{S}(\boldsymbol{\omega}_d^b)\boldsymbol{\omega}_d^b, \\
&= -\mathbf{S}(\boldsymbol{\omega}_e^b)\mathbf{R}_n^b \boldsymbol{\omega}_d^n, \\
&= -\mathbf{S}(\boldsymbol{\omega}_e)\mathbf{R}^T \boldsymbol{\omega}_d^n,
\end{aligned}$$

which gives the final expression used in this project:

$$\dot{\mathbf{R}}_n^b = -\mathbf{S}(\boldsymbol{\omega}_e)\mathbf{R}^T. \tag{A.15}$$

A.3 The "regular function" class

According to (Shevitz and Paden, 1994), the class of functions, called "regular functions" can be defined as shown in Definition A.1.

Definition A.1. *The function $f(x,t) : \mathbb{R}^m \times \mathbb{R} \to \mathbb{R}$ is called a regular if*

1. *for all ν, the usual one-sided directional derivative $f'(x;\nu)$ exists,*
2. *for all ν, $f'(x;\nu) = f^\circ(x;\nu)$ where*

$$f^\circ(x;\nu) = \limsup_{y \to x,\, t \downarrow 0} \frac{f(y + t\nu) - f(y)}{t}. \tag{A.16}$$

Appendix B

Matrosov's Theorem

This theorem is useful for analyzing nonlinear time-varying systems where the Lyapunov function candidate derivative is only negative semi-definite. This theorem adds an auxiliary function, which does not need to be positive definite. However, the time derivative of this auxiliary function must be "definitely non-zero" (Hahn, 1967, Def. 55.1) on the set where the Lyapunov function derivative is identically zero.

Theorem B.1 (Matrosov's Theorem (Hahn, 1967))**.** *Consider the system*

$$\dot{\mathbf{x}} = \mathbf{f}(\mathbf{x}, t), \quad \mathbf{f} : \mathbb{R}^n \times \mathbb{R} \to \mathbb{R}^n, \quad \mathbf{f} \text{ is bounded.} \tag{B.1}$$

Let two functions $V(\mathbf{x}, t)$ and $W(\mathbf{x}, t)$ be given which are continuous on the domain $\mathbb{D}$ and satisfy the following assumptions:

Assumption B.1. *$V(\mathbf{x}, t)$ is positive definite and decrescent.*

Assumption B.2. *The derivative $\dot{V}$ can be bounded from above by a non-positive continuous t-independent function $U(\mathbf{x})$ such that*

$$\dot{V}(\mathbf{x}, t) \leq U(\mathbf{x}) \leq 0. \tag{B.2}$$

Assumption B.3. *The function $W(\mathbf{x}, t)$ is bounded.*

Assumption B.4. *The derivative $\dot{W}$ is "definitely non-zero" on the set*

$$\mathbb{N} = \{\mathbf{x} \mid U(\mathbf{x}) = 0\}. \tag{B.3}$$

Then the equilibrium of Equation (B.1) *is uniformly asymptotically stable (UAS) on $\mathbb{D}$.*

Appendix C

Lab setup and pictures

In this appendix a sketch of water tank with the submerged AUVSAT is shown. In addition two pictures taken from the experiments are also presented, together with explanations.

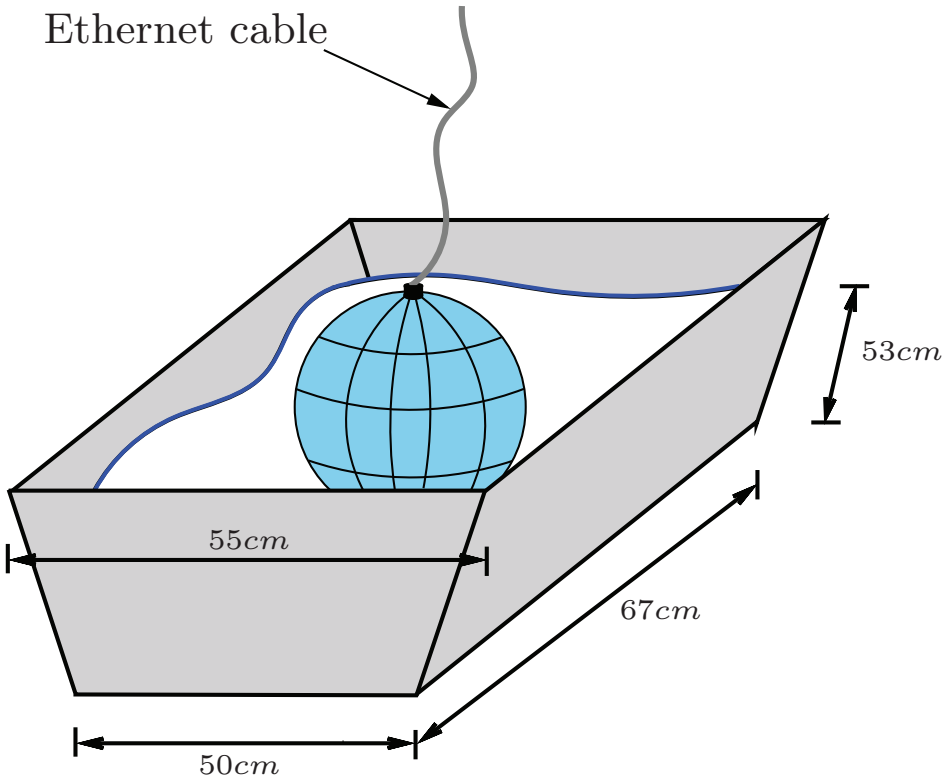

Figure C.1: Sketch of the water tank where the experiments and testing are taking place. The Ethernet cable connecting the QNX target with the host, is fasten in a rotating device above the satellite.

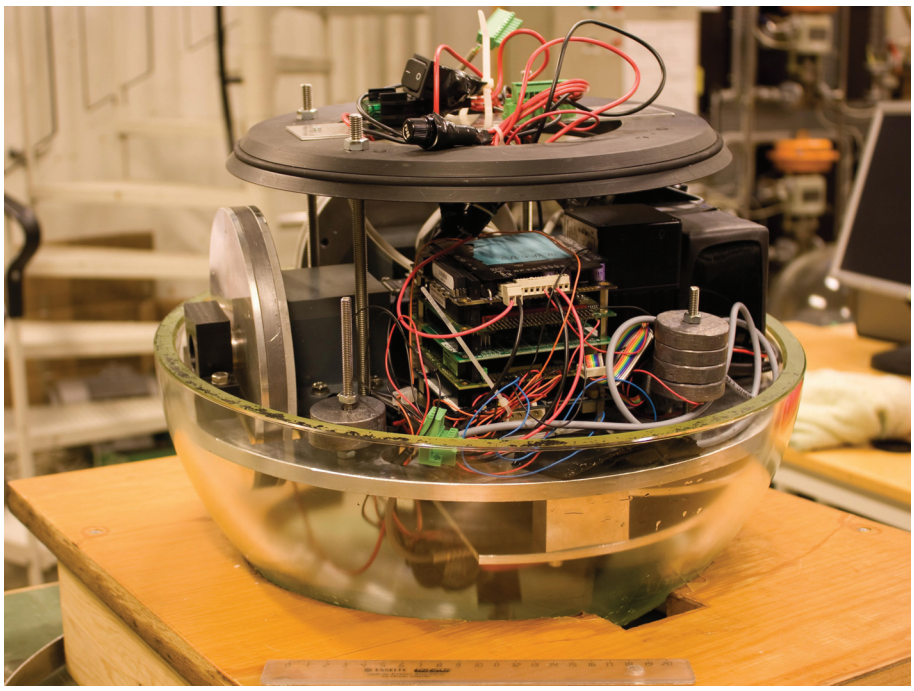

(a) The wheel at the left is one of the reaction wheels, whereas the PC/104 CPU card can be seen in the middle. At the bottom of the figure, a 20 cm ruler is placed to see the ratios.

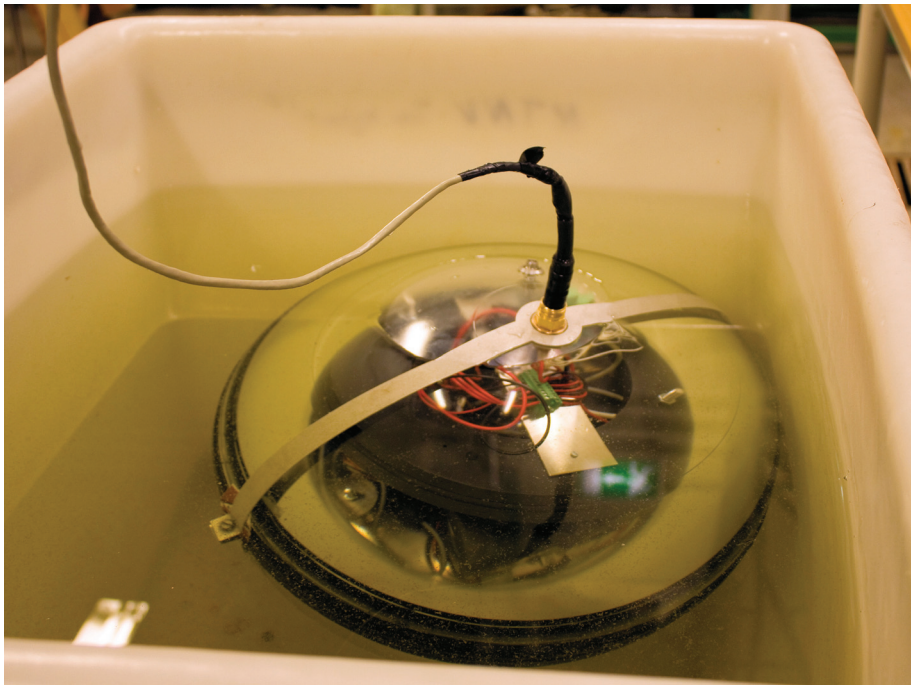

(b) The picture shows the submerged AUVSAT in the water tank. The seen cable is the Ethernet cable connecting the QNX target with the laptop host.

Figure C.2: Pictures of AUVSAT.

Appendix D

Another sliding mode controller experiment

Another sliding mode experiment has been tested in this appendix. The setup is identical with the setup in Section 9.2.1, but with another choice of tuning parameters. The reason for this is to illustrate the consequences of choosing the values of $\mathbf{K}$ and $\mathbf{P}$ almost the same, and in this way attempt to control both the attitude and the angular velocity together, at the same time. This is clearly harder than only controlling the angular velocity and it can be seen that the angular velocity tracking is undoubtedly poorer.

The choice of tuning parameters can be seen in Table D.1 and the results of the experiment can be seen in Figure D.1.

Gain-symbol	**Value**	**Denomination**
$\mathbf{K}$	$0.9 \cdot \mathbf{I}$	1/s
$\mathbf{D}$	$1.3 \cdot 10^{-3} \cdot \mathbf{I}$	1/sm
$\mathbf{P}$	$1.1 \cdot \mathbf{I}$	1/sm

Table D.1: Sliding mode controller gains where $\mathbf{I}$ is the identity matrix.

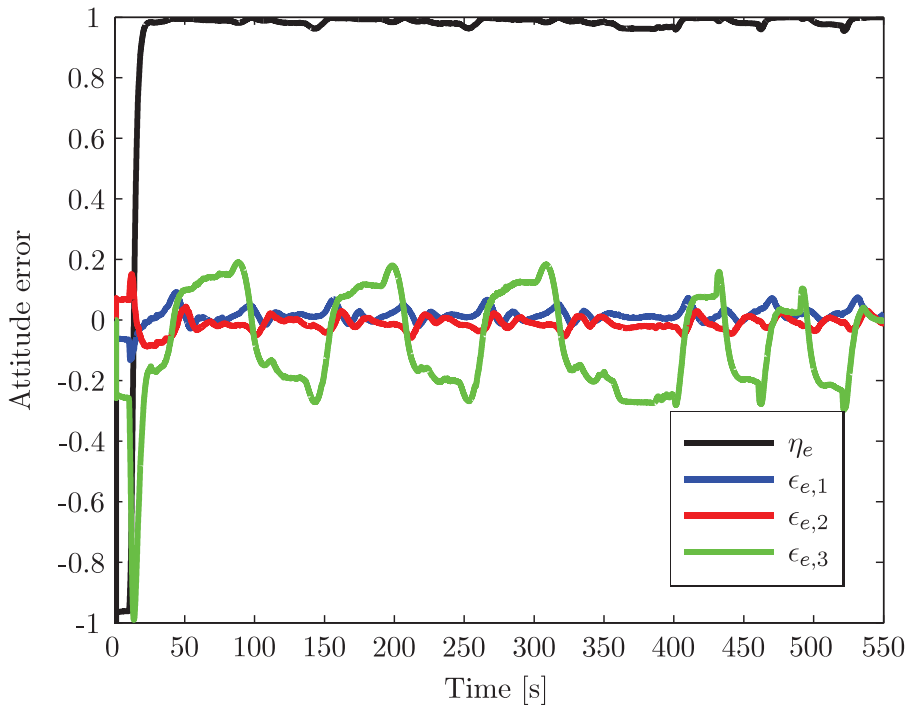

(a) Attitude error between the desired and the measured attitude.

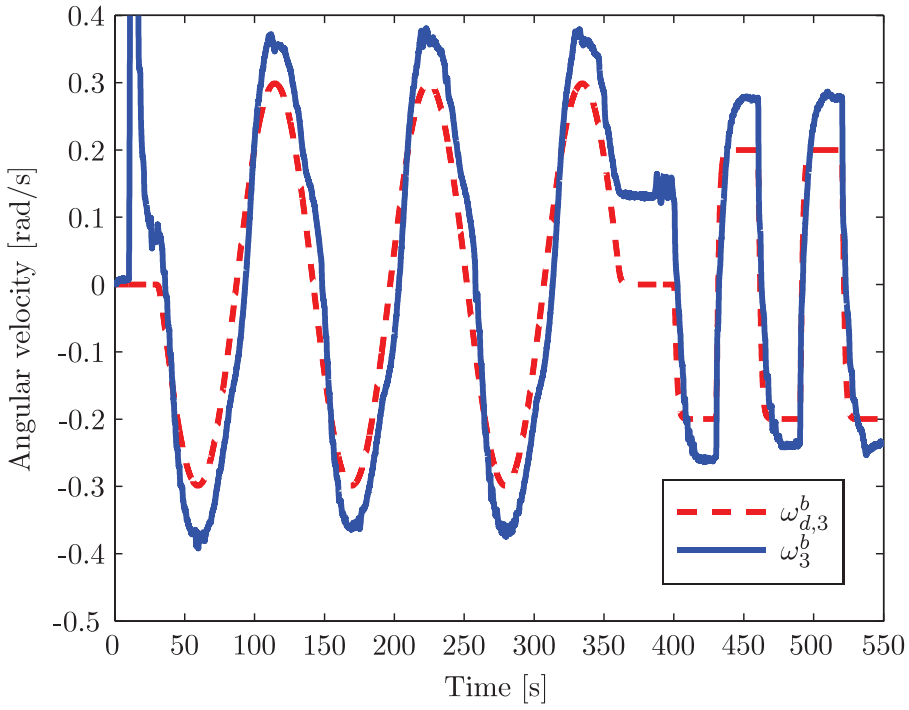

(b) Desired angular velocity compared with measured angular velocity.

Figure D.1: Plots from a second experiments with sliding mode controller.

Appendix E

Paper sent to the 49th IEEE Conference on Decision and Control

Based on the work performed in (Jørgensen, 2009) and this thesis, a scientific article has been submitted to the 49th IEEE Conference on Decision and Control. The conference will be held Wednesday through Friday, December 15-17, 2010 at the Hilton Atlanta Hotel in Atlanta, Georgia USA.

The submitted article can be seen in the next pages of this appendix and has been constructed in cooperation with Professor Jan Tommy Gravdahl.

Observer Based Sliding Mode Attitude Control: Theoretical and Experimental Results

Ulrik Jørgensen
Department of Engineering Cybernetics,
Norwegian University of Science and Technology
7491 Trondheim, Norway

Jan Tommy Gravdahl
Department of Engineering Cybernetics,
Norwegian University of Science and Technology
7491 Trondheim, Norway

***Abstract*—In this paper we present the design of a sliding mode controller for attitude control of spacecrafts actuated by three orthogonal reaction wheels. The system with controller is proved to be asymptotically stable in the sense of Lyapunov. Due to cases where spacecrafts do not have angular velocity measurements, an estimator for the generalized velocity is derived and convergence is proven. The approach is tested on an experimental platform with a sphere shaped Autonomous Underwater Vehicle SATellite: AUVSAT, developed at the Norwegian University of Science and Technology.**

I. Introduction

The contribution of this paper is the design of a output feedback nonlinear attitude control scheme and its verification on the sphere shaped underwater satellite, AUVSAT [1], [2]. Several control schemes have been proposed for attitude control of satellites, ranging from linear control in [3], $\mathbf{H}_2$ and $\mathbf{H}_\infty$ in [4], to the nonlinear control based on vectorial backstepping in [5].

The attitude of AUVSAT is actuated by means of reaction wheels. This is a popular and well proven attitude control method and it has been implemented for both small [6] and large satellites [7]. A solution with three orthogonally mounted reaction wheels can be seen in [8], whereas a redundant solution with four reaction wheels can be seen in [9]. In addition, [10] presents a comparison of several configurations based on three or four reaction wheel actuators.

The method proposed for controlling the angular velocity of the AUVSAT is a sliding mode (SM) controller. The SM controller is a well known nonlinear controller that have been applied to many practically systems [11]. It is considered to be very robust and thereby practical for systems affected by disturbances [12].

The problem of controlling motion of rigid body systems has been studied in great detail in the literature of aerospace, marine systems and robotics. However, most of these control techniques require knowledge of the actual angular velocity [13]. Unfortunately, angular velocity measurement is often omitted due to cost or space restrictions and it is therefore important to estimate the angular velocity. [14] and [15] presents similar results for attitude stabilization control when angular velocity is not present using a velocity filter. Another solution is to estimate the angular velocity using an extended Kalman filter [16] or a nonlinear observer [5], [17]. The latter solution is used in this paper.

The paper is completed with implementing the sliding mode controller and the observer in the submerged underwater satellite. The AUVSAT is equipped with a ballast system, making it naturally buoyant. The naturally buoyant system will make it possible to emulate a weightless state, similar to the conditions for a satellite in space. The AUVSAT is therefore an ideal vehicle for testing and demonstrating the proposed control method.

II. Modeling

In this section, the model of a satellite actuated by means reaction wheels will be derived.

A. Kinematics

The attitude kinematics will be described using Euler parameters, due to the properties as a nonsingular and computational effective representation. The Euler parameters may be defined from the angle-axis parameters θ and $\mathbf{k}$ as

$$\eta \triangleq \cos(\frac{1}{2}\theta), \quad \boldsymbol{\epsilon} \triangleq \mathbf{k}\sin(\frac{1}{2}\theta), \tag{1}$$

and gathered in one attitude vector

$$\mathbf{q} \triangleq \begin{bmatrix}\eta & \boldsymbol{\epsilon}^T\end{bmatrix}^T, \tag{2}$$

which has unit length and is called a unit quaternion.

According to [18], the rotation matrix corresponding to the quaternion (2) is given by

$$\mathbf{R}(\eta, \boldsymbol{\epsilon}) = \mathbf{I} + 2\eta\mathbf{S}(\boldsymbol{\epsilon}) + 2\mathbf{S}(\boldsymbol{\epsilon})^2, \tag{3}$$

where $\mathbf{I} \in \mathbb{R}^{3\times3}$ is the identity matrix and $\mathbf{S}(\,\cdot\,) \in \mathbb{R}^{3\times3}$ is the skew-symmetric vector cross product operator defined such that $\mathbf{x}_1 \times \mathbf{x}_2 = \mathbf{S}(\mathbf{x_1})\mathbf{x}_2,\ \forall\ \mathbf{x} \in \mathbb{R}^{3\times1}$. Note that the quaternion representation has an inherent redundancy and the quaternions $\mathbf{q}$ and $-\mathbf{q}$ represent the same physical orientation, but $\mathbf{q}$ is rotated 2π relative to $-\mathbf{q}$ about an arbitrary axis [19].

Let $\{\mathrm{b}\}$ be a coordinate frame attached to a rigid spacecraft and $\{\mathrm{i}\}$ an inertial reference frame. Then it can be seen that the kinematic differential equations can be expressed [20] as

$$\dot{\mathbf{R}}_b^i = -\mathbf{S}(\boldsymbol{\omega}_{ib}^b)\mathbf{R}_b^i, \tag{4}$$

where $\boldsymbol{\omega}_{ib}^b$ is the angular velocity of the body frame $\{\mathrm{b}\}$ relative the inertial frame $\{\mathrm{i}\}$ decomposed in the body frame, and

Preprint submitted to 49th IEEE Conference on Decision and Control.
Received March 24, 2010.

$\mathbf{R}_b^i$ is the rotation matrix between the frames. For simplicity, $\mathbf{R}_b^i$ is denoted $\mathbf{R}$ throughout the paper.

Using (2)–(4) the kinematic differential equations can then be expressed as

$$\dot{\mathbf{q}} = \frac{1}{2}\mathbf{E}(\mathbf{q})\boldsymbol{\omega}_{ib}^b, \tag{5}$$

where $\mathbf{E}(\mathbf{q}) = \begin{bmatrix} -\boldsymbol{\epsilon}^T \\ \mathbf{T}(\mathbf{q}) \end{bmatrix}$ and $\mathbf{T}(\mathbf{q}) = \eta\mathbf{I} + \mathbf{S}(\boldsymbol{\epsilon})$.

B. Kinetics

Assuming that the satellite is a rigid body with the origin of the body frame placed coinciding with the center of gravity (CG), we may use Euler's second axiom to express the momentum for the wheels and the complete system [21]. The momentum of the wheels can be written as

$$\mathbf{H}_w = \mathbf{J}_w\boldsymbol{\omega}_{ib}^b + \mathbf{J}_w\boldsymbol{\Omega}, \tag{6}$$

where $\mathbf{J}_w$ is the inertia matrix of the wheels and $\boldsymbol{\Omega} = \begin{bmatrix}\Omega_1 & \Omega_2 & \Omega_3\end{bmatrix}^T$ is the angular velocity rate of each reaction wheel. The complete angular momentum of the vehicle is expressed as

$$\mathbf{H} = \mathbf{J}\boldsymbol{\omega}_{ib}^b + \mathbf{J}_w\boldsymbol{\Omega}, \tag{7}$$

where $\mathbf{J}$ is the total moment of inertia including the reaction wheels. Differentiating (6)–(7) with respect to time and using Euler's second axiom, one may write the dynamic equation for the satellite actuated by means of three orthogonal reaction wheels as [9], [22]

$$\mathbf{J}_s\dot{\boldsymbol{\omega}}_{ib}^b = -\mathbf{S}(\boldsymbol{\omega}_{ib}^b)\mathbf{H} - \boldsymbol{\tau}_u^b + \boldsymbol{\tau}_{ex}^b, \tag{8a}$$

$$\mathbf{J}_w\dot{\boldsymbol{\Omega}} = -\mathbf{J}_w\dot{\boldsymbol{\omega}}_{ib}^b + \boldsymbol{\tau}_u^b, \tag{8b}$$

where $\mathbf{J}_s = \mathbf{J} - \mathbf{J}_w$ is the inertia matrix for the system without wheels, $\boldsymbol{\tau}_{ex}^b$ is the external torque applied to the system and $\boldsymbol{\tau}_u^b$ is the commanded torque to the motors and thereby the manipulative variable.

III. Control design

The control objective is to control the angular velocity of the satellite to a desired time varying angular velocity reference $\boldsymbol{\omega}_d^i(t)$. From (5) it can be seen that the corresponding time varying desired attitude $\mathbf{q}_d(t)$ can be expressed as

$$\dot{\mathbf{q}}_d = \frac{1}{2}\mathbf{E}(\mathbf{q}_d(t))\mathbf{R}^T(\mathbf{q}_d(t))\boldsymbol{\omega}_d^i(t), \tag{9}$$

where $\mathbf{R}(\mathbf{q}_d)$ is the rotation matrix from the desired to the inertial frame.

A. Error dynamics

We may define the angular velocity error as

$$\boldsymbol{\omega}_e = \boldsymbol{\omega} - \mathbf{R}^T(\eta, \boldsymbol{\epsilon})\boldsymbol{\omega}_d^i(t), \tag{10}$$

where the desired angular velocity is given in the inertial frame and $\boldsymbol{\omega} = \boldsymbol{\omega}_{ib}^b$. It is also assumed throughout the paper that angular velocities without superscript is decomposed in the body frame.

The relative attitude error is defined using the quaternion product [19] as

$$\mathbf{q}_e \triangleq \mathbf{q}_d^{-1} \otimes \mathbf{q} = \begin{bmatrix}\eta_e & \boldsymbol{\epsilon}_e^T\end{bmatrix}^T, \tag{11}$$

where $\mathbf{q}_d$ and $\mathbf{q}$ are the desired and actual attitude, respectively. $\mathbf{q}_d^{-1}$ is called the complex conjugate of $\mathbf{q}_d$ and it can be seen that $\mathbf{q}_d^{-1} = \begin{bmatrix}\eta_d & -\boldsymbol{\epsilon}_d^T\end{bmatrix}^T$. $\otimes$ denotes the quaternion product, which is defined between the two quaternions $\mathbf{q}_1 = \begin{bmatrix}\eta_1 & \boldsymbol{\epsilon}_1^T\end{bmatrix}^T$ and $\mathbf{q}_2 = \begin{bmatrix}\eta_2 & \boldsymbol{\epsilon}_2^T\end{bmatrix}^T$ as

$$\mathbf{q}_1 \otimes \mathbf{q}_2 = \begin{bmatrix}\eta_1 & -\boldsymbol{\epsilon}_1^T \\ \boldsymbol{\epsilon}_1 & \eta_1\mathbf{I} + \mathbf{S}(\boldsymbol{\epsilon}_1)\end{bmatrix}\begin{bmatrix}\eta_2 \\ \boldsymbol{\epsilon}_2\end{bmatrix}. \tag{12}$$

It can be seen from (11)–(12) and the inherent redundancy of the quaternion parameterization that $\mathbf{q}_e = \begin{bmatrix}\pm 1 & \mathbf{0}^T\end{bmatrix}^T$ when the attitude of the satellite is aligned with the desired attitude. $\mathbf{0}$ denotes the 3×1 zero-vector.

Using (8)–(11) it can be seen that the error dynamics may be written as

$$\dot{\mathbf{q}}_e = \frac{1}{2}\mathbf{E}(\mathbf{q}_e)\boldsymbol{\omega}_e, \tag{13a}$$

$$\begin{aligned}\mathbf{J}_s\dot{\boldsymbol{\omega}}_e = {} & \mathbf{J}_s\mathbf{S}(\boldsymbol{\omega}_e)\mathbf{R}^T\boldsymbol{\omega}_d^i - \mathbf{J}_s\mathbf{R}^T\dot{\boldsymbol{\omega}}_d^i \\ & - \mathbf{S}(\boldsymbol{\omega})\mathbf{H} - \boldsymbol{\tau}_u + \boldsymbol{\tau}_{ex},\end{aligned} \tag{13b}$$

where $\dot{\mathbf{R}}^T = -\mathbf{S}(\boldsymbol{\omega}_e)\mathbf{R}^T$ has been used. A detailed derivation of (13a) can be seen in [23].

B. Sliding mode controller

In this section a sliding mode controller will be proposed to control the angular velocity of the satellite. The SM controller is inspired by [20] and [22], while some modifications are carried out in order to adapt it to the sphere shaped satellite. The derivation of the SM controller consists of two parts: making every trajectory converge to the sliding manifold ($\mathbf{s} = \mathbf{0}$) and then making sure that the trajectories reach the desired equilibrium.

Let the sliding variable $\mathbf{s} \in \mathbb{R}^{3\times 1}$ be defined as

$$\mathbf{s} \triangleq \boldsymbol{\omega}_e + \mathbf{K}\boldsymbol{\epsilon}_e, \tag{14}$$

where $\mathbf{K} \in \mathbb{R}^{3\times 3}$, $\mathbf{K} = \mathbf{K}^T > 0$ is a tuning parameter.

If (14) is differentiated with respect to time and pre-multiplied with $\mathbf{J}_s$ we get

$$\begin{aligned}\mathbf{J}_s\dot{\mathbf{s}} = {} & \mathbf{J}_s\mathbf{S}(\boldsymbol{\omega}_e)\mathbf{R}^T\boldsymbol{\omega}_d^i - \mathbf{J}_s\mathbf{R}^T\dot{\boldsymbol{\omega}}_d^i - \mathbf{S}(\boldsymbol{\omega})\mathbf{H} \\ & - \boldsymbol{\tau}_u + \boldsymbol{\tau}_{ex} + \mathbf{J}_s\mathbf{K}\dot{\boldsymbol{\epsilon}},\end{aligned} \tag{15}$$

where (8a) and (10) have been used in addition to the fact that $\dot{\mathbf{R}}^T = -\mathbf{S}(\boldsymbol{\omega}_e)\mathbf{R}^T$.

Choose the control variable $\boldsymbol{\tau}_u$ to cancel all the nonlinear terms in (15) and include proportional and derivative action by adding the terms $\mathbf{D}sgn(\mathbf{s})$ and $\mathbf{P}\mathbf{s}$, where $\mathbf{D}$, $\mathbf{P} \in \mathbb{R}^{3\times 3}$ are positive definite. Note that $\dot{\boldsymbol{\epsilon}}$ can be calculated from the relationship in (13a), avoiding time differentiation of $\boldsymbol{\epsilon}$, and $sgn(\mathbf{s})$ is the sign function defined in (16) performed on each element in $\mathbf{s}$.

$$sgn(x) = \begin{cases} +1 & \text{if} \quad x \geq 0, \\ -1 & \text{if} \quad x < 0. \end{cases} \tag{16}$$

Preprint submitted to 49th IEEE Conference on Decision and Control.
Received March 24, 2010.

Proposition 1. *The error dynamics* (13)*, with the sliding mode controller given by*

$$\begin{aligned}\boldsymbol{\tau}_u = \mathbf{J}_s\mathbf{S}(\boldsymbol{\omega}_e)\mathbf{R}^T\boldsymbol{\omega}_d^i - \mathbf{J}_s\mathbf{R}^T\dot{\boldsymbol{\omega}}_d^i - \mathbf{S}(\boldsymbol{\omega})\mathbf{H} + \boldsymbol{\tau}_{ex} \\ + \mathbf{J}_s\mathbf{K}\dot{\boldsymbol{\epsilon}} + \mathbf{J}_s\mathbf{D}sgn(\mathbf{s}) + \mathbf{J}_s\mathbf{P}\mathbf{s}\end{aligned} \tag{17}$$

have an asymptotically stable equilibrium in $(\boldsymbol{\omega}_e, \mathbf{q}_e) = (\mathbf{0}, \mathbf{1}_q)$ *where* $\mathbf{1}_q = \begin{bmatrix}\pm 1 & \mathbf{0}^T\end{bmatrix}^T$.

Proof: Consider the radially unbounded Lyapunov function candidate:

$$V_1 = \frac{1}{2}\mathbf{s}^T\mathbf{s} > 0, \quad \forall \quad \mathbf{s} \neq \mathbf{0}, \tag{18}$$

and differentiating it with respect to time along the trajectory we get

$$\dot{V}_1 = -\mathbf{s}^T\mathbf{P}\mathbf{s} - \mathbf{s}^T\mathbf{D}sgn(\mathbf{s}) < 0, \ \forall\, \mathbf{s} \neq \mathbf{0}. \tag{19}$$

According to [24], this proves that the non-smooth $\mathbf{s}$-system is AS, thus every trajectory will converge to the sliding manifold. In fact, one can guaranty finite time convergence [25], since

$$\frac{\partial V_1}{\partial t} \leq -\vartheta\sqrt{V_1}, \tag{20}$$

where $\vartheta = \sqrt{2}\lambda_{\min}(\mathbf{D}) > 0$ and $\lambda_{\min}(\mathbf{D})$ is the smallest eigenvalue of $\mathbf{D}$. From (20), we get

$$2\sqrt{V_1} \leq V_1(\mathbf{s}(0)) - \vartheta t. \tag{21}$$

This shows that the system will converge to the sliding manifold with the finite convergence time T_c, upper bounded according to

$$T_c \leq \frac{V_1(\mathbf{s}(0))}{\vartheta}. \tag{22}$$

Given that we are in sliding mode, $\mathbf{s} = \mathbf{0}$, we may write

$$\boldsymbol{\omega}_e = -\mathbf{K}\boldsymbol{\epsilon}_e. \tag{23}$$

We then introduce the second Lyapunov function candidate:

$$V_2 = 1 - \eta_e, \tag{24}$$

which is a positive definite function since $-1 \leq \eta_e \leq 1$. The time derivative along the solution then becomes

$$\dot{V}_2 = -\dot{\eta}_e = \frac{1}{2}\boldsymbol{\epsilon}_e^T\boldsymbol{\omega}_e = -\frac{1}{2}\boldsymbol{\epsilon}_e^T\mathbf{K}\boldsymbol{\epsilon}_e \tag{25a}$$

$$\leq -\frac{1}{2}\lambda_{\min}(\mathbf{K})\boldsymbol{\epsilon}_e^T\boldsymbol{\epsilon}_e = -\frac{1}{2}\lambda_{\min}(\mathbf{K})\left(1 - \eta_e^2\right), \tag{25b}$$

where $\lambda_{\min}(\mathbf{K}) > 0$ is the smallest eigenvalue of $\mathbf{K}$ and (13a) and (23) have been used, in addition to the unit-length property of $\mathbf{q}_e$.

Since V_2 is positive definite, and $\dot{V}_2$ is negative definite, thus, $(1 - \eta_e^2) \to 0$, as times goes to infinity, and $\eta_e \to \pm 1$. Because $\eta_e^2 + \boldsymbol{\epsilon}_e^T\boldsymbol{\epsilon}_e = 1$, also $\boldsymbol{\epsilon}_e \to \mathbf{0}$ and the error attitude $\mathbf{q}_e \to \mathbf{1}_q$. It can also be noticed that $\boldsymbol{\omega}_e$ will converge to $\mathbf{0}$ since $\boldsymbol{\omega}_e = -\mathbf{K}\boldsymbol{\epsilon}_e$ in sliding mode, and when $\boldsymbol{\epsilon}_e \to \mathbf{0}$ so will $\boldsymbol{\omega}_e$. We can then conclude that the complete system, with the given controller, is asymptotically stable. ■

IV. Observer design

Assuming that only attitude of the vehicle and speed of the wheels are available for measurements, an observer is needed to estimate the angular velocity of the satellite. This can be done in different ways, including an extended Kalman filter and a nonlinear observer. In this paper the latter alternative is used and the observer scheme is inspired by [5] and [17].

A. Observer dynamic equations

As the calculations are less involved in the inertial frame, we express the momentum dynamics as

$$\Sigma : \begin{cases}\dot{\mathbf{H}}^i &= \mathbf{R}_b^i\boldsymbol{\tau}_{ex}^b, \\ \dot{\mathbf{q}} &= \frac{1}{2}\mathbf{E}(\mathbf{q})\underbrace{\left[\left(\mathbf{R}_b^i\mathbf{J}\right)^{-1}\mathbf{H}^i - \mathbf{J}^{-1}\mathbf{J}_w\boldsymbol{\Omega}\right]}_{\boldsymbol{\omega}}.\end{cases} \tag{26}$$

We then define the observer system $\hat{\Sigma}$ as the copy of the dynamics with correction terms $\mathbf{g}_1(\tilde{\mathbf{q}})$ and $\mathbf{g}_2(\tilde{\mathbf{q}})$ as:

$$\hat{\Sigma} : \begin{cases}\dot{\hat{\mathbf{H}}}^i &= \mathbf{R}_b^i\left[\boldsymbol{\tau}_{ex}^b + \mathbf{g}_1\right] \\ \dot{\hat{\mathbf{q}}} &= \frac{1}{2}\mathbf{E}(\hat{\mathbf{q}})\left[\left(\mathbf{R}_b^i\mathbf{J}\right)^{-1}\hat{\mathbf{H}}^i - \mathbf{J}^{-1}\mathbf{J}_w\boldsymbol{\Omega} + \mathbf{g}_2\right]\end{cases} \tag{27}$$

where $\hat{\mathbf{H}}^i$ and $\hat{\mathbf{q}}$ are the estimated momentum and attitude, respectively. The correction terms $\mathbf{g}_1(\tilde{\mathbf{q}})$ and $\mathbf{g}_2(\tilde{\mathbf{q}})$ are to be determined later.

B. Error definition

The error variables between the real and estimated values for attitude, momentum and angular velocity, respectively, are defined as:

$$\tilde{\mathbf{q}} \triangleq \mathbf{q}^{-1} \otimes \hat{\mathbf{q}}, \tag{28a}$$

$$\tilde{\mathbf{H}}^i \triangleq \hat{\mathbf{H}}^i - \mathbf{H}^i, \tag{28b}$$

$$\tilde{\boldsymbol{\omega}}_{ib}^b \triangleq \hat{\boldsymbol{\omega}}_{ib}^b - \boldsymbol{\omega}_{ib}^b. \tag{28c}$$

The error between the estimated system $\hat{\Sigma}$ and the real system Σ is denoted $\tilde{\Sigma}$ and can be derived by differentiating (28) with respect to time, resulting in

$$\tilde{\Sigma} : \begin{cases}\dot{\tilde{\mathbf{H}}}^i &= \mathbf{R}_b^i\mathbf{g}_1(\tilde{\mathbf{q}}), \\ \dot{\tilde{\mathbf{q}}} &= \frac{1}{2}\mathbf{E}(\tilde{\mathbf{q}})\left[\left(\mathbf{R}_b^i\mathbf{J}\right)^{-1}\tilde{\mathbf{H}}^i + \mathbf{g}_2(\tilde{\mathbf{q}})\right].\end{cases} \tag{29}$$

Notice that $\tilde{\boldsymbol{\omega}}_{ib}^b = \left(\mathbf{R}_b^i\mathbf{J}\right)^{-1}\tilde{\mathbf{H}}^i$, as can be seen using (26)–(28).

Proposition 2. *The observer* $\hat{\Sigma}$ *defined in* (27) *with*

$$\mathbf{g}_1(\tilde{\mathbf{q}}) = -k_p sgn(\tilde{\eta})\mathbf{J}^{-1}\tilde{\boldsymbol{\epsilon}}, \tag{30a}$$

$$\mathbf{g}_2(\tilde{\mathbf{q}}) = -k_v sgn(\tilde{\eta})\tilde{\boldsymbol{\epsilon}}, \tag{30b}$$

and k_p, $k_v > 0$*, will converge to the actual system* Σ*, shown in* (26)*.*

Proof: To prove Proposition 2, we utilize [24, Th. 3.1]. This theorem proves that the ordinary smooth Lyapunov stability theory can be used for a class of non-smooth Lipschitz continuous Lyapunov functions and absolutely continuous state trajectories.

Preprint submitted to 49th IEEE Conference on Decision and Control.
Received March 24, 2010.

Consider the non-smooth Lyapunov function

$$V_o = \frac{1}{2}\left(\tilde{\mathbf{H}}^i\right)^T \tilde{\mathbf{H}}^i + 2k_p(1-|\tilde{\eta}|), \tag{31}$$

The time derivative of V_o along trajectories then becomes:

$$\dot{V}_o = \left(\tilde{\mathbf{H}}^i\right)^T \mathbf{R}_b^i \mathbf{g}_1(\tilde{\mathbf{q}}) + k_p sgn(\tilde{\eta})\tilde{\boldsymbol{\epsilon}}^T\left[\tilde{\boldsymbol{\omega}}_{ib}^b + \mathbf{g}_2(\tilde{\mathbf{q}})\right] \tag{32a}$$

$$= -k_v k_p \left(sgn(\tilde{\eta})\right)^2 \tilde{\boldsymbol{\epsilon}}^T\tilde{\boldsymbol{\epsilon}} \tag{32b}$$

$$\leq 0 \;\forall\; \tilde{\boldsymbol{\epsilon}}_e \neq \mathbf{0}. \tag{32c}$$

where it is assumed that $\mathbf{J}$ is symmetric [26], meaning $\mathbf{J}^T = \mathbf{J}$. Clearly, $\dot{V}_o$ is negative semidefinite, and one can thereby conclude that the observer is stable. V_o will also continue to decrease as long as the actual attitude differ from the estimated attitude, but when $\tilde{\boldsymbol{\epsilon}}_e = \mathbf{0}$, V_o vanishes. It is therefore essential to evaluate if the system can get stuck in these points with $\tilde{\mathbf{H}}^i \neq \mathbf{0}$.

Assume that $\tilde{\boldsymbol{\epsilon}}_e = \mathbf{0}$ and $\tilde{\mathbf{H}}^i \neq \mathbf{0}$. Then:

$$\dot{\boldsymbol{\epsilon}}_e = \pm\frac{1}{2}(\mathbf{R}_b^i\mathbf{J})^{-1}\tilde{\mathbf{H}}^i \neq \mathbf{0} \quad \forall \quad \tilde{\mathbf{H}}^i \neq \mathbf{0}, \tag{33}$$

since $(\mathbf{R}_b^i\mathbf{J})^{-1}$ is never equal the zero-matrix. Therefore, the system will continue to evolve and converge towards $(\boldsymbol{\epsilon}_e, \tilde{\mathbf{H}}^i) = (\mathbf{0}, \mathbf{0})$. Thus, the observer $\hat{\Sigma}$ will converge towards the actual system Σ as time goes to infinity. ■

This proof is also presented in [27] for rigid body systems actuated with external torques.

V. Experiments

This section contains simulations and results from the experiments with AUVSAT. The sphere shaped satellite is equipped with small-size and low-cost IMU sensor for attitude and angular velocity measurements, and a PC/104 embedded computer board with 0.5 GHz Pentium processor, running QNX Neutrino OS. In addition to the satellite, a host computer is provided for a graphical communication interface, and Ethernet LAN is used between the host and the QNX target. The host is running Matlab Real-time workshop in combination with Simulink which enables a rapid implementation of control laws, in addition to graphically represent measurements and control signals in real-time. Pictures of AUVSAT are showed in Figure 4.

The first part of the chapter presents the results of the sliding mode controller. To avoid noisy signals to the controller, the measurements of the angular velocity is filtered with a standard first order filter. In the second part we implement the nonlinear observer. The estimated angular velocity from this observer is used by the same sliding mode controller.

The control objective is to track an angular velocity reference signal $\boldsymbol{\omega}_d^i(t)$ given in the inertial coordinate frame. The reference signal is stated in (34) and is a sequence of a square signal with a period of 50 s, and time varying sinusoidal reference signal. In this way one can truly validate the performance of the controller. The experiment was sampled at 50 Hz for about 400 s with the gains shown in Table I and the parameters used for the satellite in Table II. The plots from the case without observer can be seen in Figure 2, whereas the results with angular velocity estimation can be seen in Figure 3. Note that desired trajectory is filtered by a second-order filter inside the "Reference"-block in Figure 1 and $\mathbf{q}_d(t)$ is calculated using (9).

$$\boldsymbol{\omega}_d^i(t) = \begin{cases} -0.2\text{square}\left(\frac{1}{50}, t\right) & 20 \text{ s} \leq t \leq 145 \text{ s} \\ -0.3\sin\left(\frac{2\pi}{30}(t+5)\right) & 175 \text{ s} \leq t \leq 280 \text{ s} \\ -0.4\sin\left(\frac{2\pi}{30}(t+5)\right) & 280 \text{ s} \leq t \leq 370 \text{ s} \\ 0 & \text{Else} \end{cases} \tag{34}$$

Table I
SLIDING MODE CONTROLLER AND OBSERVER GAINS.

	Parameter	Value
Controller gains:	$\mathbf{K}$	$2.0\cdot 10^{-3}\mathbf{I}$ 1/s
	$\mathbf{D}$	$1.0\cdot 10^{-3}\mathbf{I}$ 1/sm
	$\mathbf{P}^*$	$1.2\mathbf{I}$ 1/sm
Observer gains:	k_p	17.0 $\text{kg}^2\text{m}^4/\text{s}^2$
	k_v	12.0 1/s

* When observer is implemented: $\mathbf{P} = 0.5\cdot\mathbf{I}$ 1/sm

Table II
AUVSAT PARAMETERS

Parameter	Value
Inertia matrix $\mathbf{J}$	$\begin{pmatrix} 0.776 & -0.004 & 0.009 \\ -0.004 & 0.848 & -0.000 \\ 0.009 & -0.000 & 0.945 \end{pmatrix}$ kgm^2
Wheel inertia matrix $\mathbf{J}_w$	$0.0142\cdot\mathbf{I}\,\text{kgm}^2$
Max wheel torque	0.358 Nm
Max wheel speed	419 rad/s
Satellite mass	42.1 kg
Satellite diameter	42.8 cm

VI. Discussion

A. Experiments without observer

Figure 2 shows the behavior of the system with the sliding mode controller. It can be seen that the system tracks the desired angular velocity quite good. There are almost no uncontrolled oscillations, as we have $\boldsymbol{\omega}$ available for feedback. However, small adjustments can be made to make the performance even better.

B. Experiments with observer

Figure 3(a) shows the comparison between the estimated and the real measurements. Plot number three shows the estimation of the angular velocity about the z-axis. It can be seen that the observer works satisfactorily when the sinusoidal signal is tracked. However, the observer seems to have difficulties with estimation of the maximum and minimum angular velocity of the sinusoidal signal. When the system is tracking the constant reference signal, stationary deviation, oscillations and drift can be seen. It thereby looks like the observer perform satisfactorily when there is enough excitation in the system. Some improvement may be achieved by finding better gains,

Preprint submitted to 49th IEEE Conference on Decision and Control.
Received March 24, 2010.

but other observer strategies might also an alternative, e.g. extended Kalman filter.

In Figure 3(b) the overall performance of the system is shown. The reference angular velocity is compared with a filtered angular velocity measurement. (The filtered signal is selected as the comparison to facilitate the readability.) The behavior of the system is acceptable when the system is tracking the sinusoidal reference signal. However, the performance is clearly not as good as without the observer.

We can also see that the low performance of the observer in connection with the square signal still is present.

VII. Conclusion

In this paper the topic of controlling the attitude of a spherical spacecraft actuated by three orthogonally reaction wheels has been studied. Using methods from nonlinear system theory a robust nonlinear sliding mode controller has been designed and implemented on the AUVSAT to control the attitude. When angular velocity measurements are not present in the spacecraft, a nonlinear observer is derived to estimate the velocity.

The various systems were tested in a lab setup where the AUVSAT is submerged in water and thereby emulating a gravity free environment. Experiments were carried out to evaluate the performance of the controller, observer and the overall system. In each experiment the system is set to track a sequence of a square-shaped signal, in addition to a sinusoidal time varying angular velocity reference signal. The results show that the sliding mode controller works satisfactorily throughout the experiment, whereas the performance of the overall system with observer and controller is lower when tracking the squared reference signal. Nevertheless, all aspect considered; the performance of the complete system is satisfactorily.

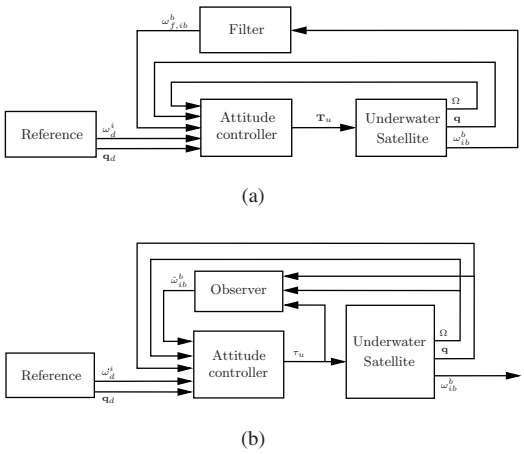

Figure 1. Block diagram of system where (a) filters the angular velocity measurement, whereas (b) estimates the angular velocity.

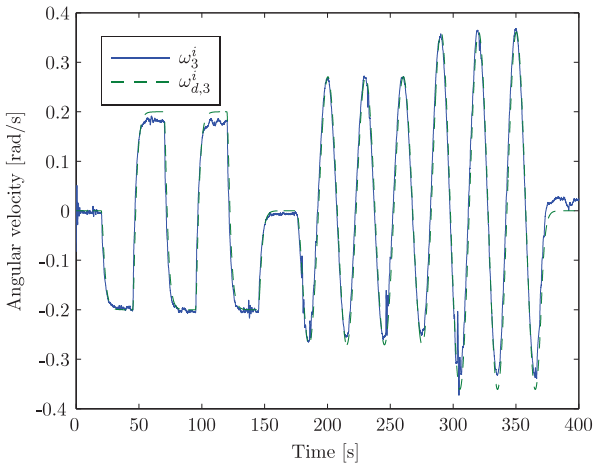

Figure 2. Experiments without observer. Comparing the angular velocity against the desired generalized velocity. All signals in the inertial frame.

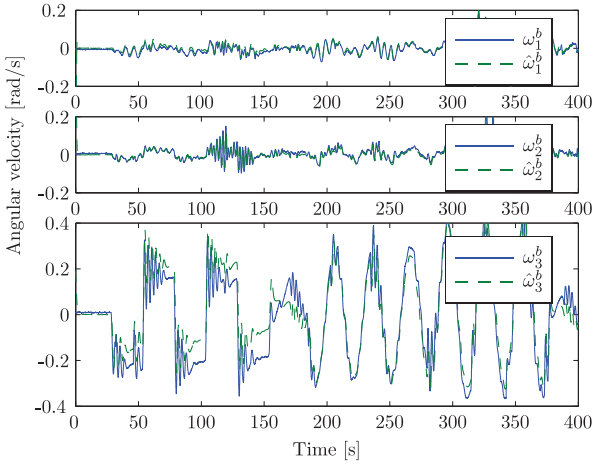

(a)

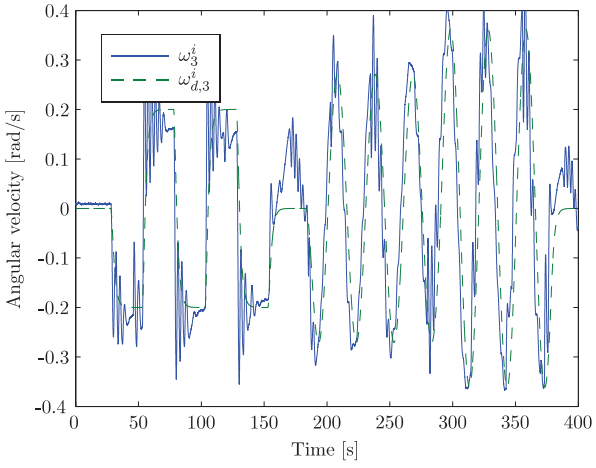

(b)

Figure 3. Plots from experiments with observer. (a) compares measured and estimated velocity about x, y and z axis, whereas (b) compares the reference against the filtered angular velocity about the z-axis.

Preprint submitted to 49th IEEE Conference on Decision and Control.
Received March 24, 2010.

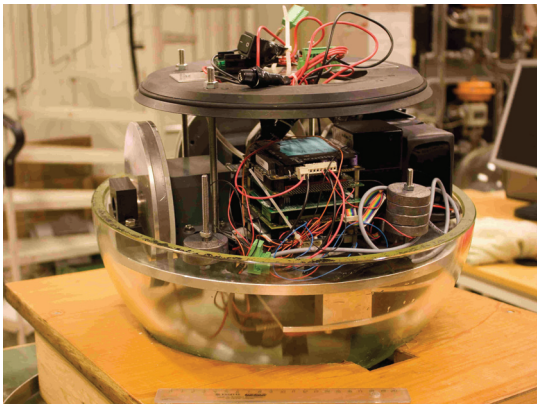

(a)

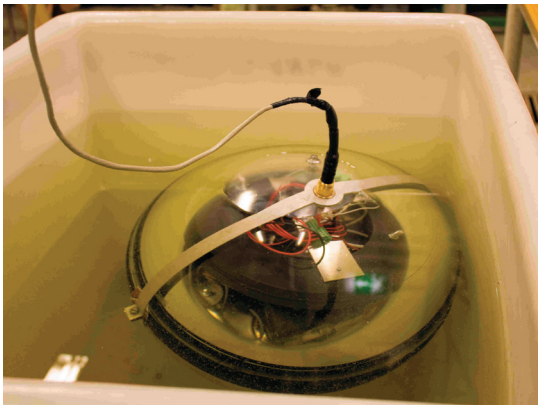

(b)

Figure 4. AUVSAT. (a) shows when the top sphere is detached to expose the inner construction and (b) shows the submerged satellite during experiments.

REFERENCES

[1] T. R. Krogstad, J. T. Gravdahl, E. Børhaug, and K. Y. Pettersen, "AUVSAT: An experimental platform for spacecraft formation flying," *Proceedings of the 59th International Astronautical Congress, Glasgow, Scottland*, 2008.

[2] T. R. Krogstad, "Attitude synchronization in spacecraft formations. theoretical and experimental results," Ph.D. dissertation, Norwegian University of Science and Technology, 2010.

[3] A. G. Parlos and J. W. Sunkel, "Adaptive attitude control and momentum management for large-angle spacecraft maneuvers," *Journal of Guidance, Control, and Dynamics*, vol. 15, pp. 1018–1028, July-Aug 1992.

[4] C.-H. Won, "Comparative study of various control methods for attitude control of a leo satellite," *Aerospace Science and Technology*, vol. 3, no. 5, pp. 323 – 333, 1999.

[5] A. K. Bondhus, K. Y. Pettersen, and J. T. Gravdahl, "Leader/follower synchronization of satellite attitude without angular velocity measurements," in *Decision and Control, 2005 and 2005 European Control Conference. CDC-ECC '05. 44th IEEE Conference on*, Dec. 2005, pp. 7270–7277.

[6] R. E. Zee, J. Matthews, and S. C. O. Grocott, "The MOST microsatellite mission: All systems go for launch," in: proceedings of 12th CASI Conferences on Aeronautics, November 2002.

[7] T. Kia, D. S. Bayard, and F. Tolivar, "A precision pointing control system for the space infrared telescope facility (SIRTF)," American Astronautical Society, Tech. Rep. AAS 97-067, 1997.

[8] S. S. Nudehi, U. Farooq, A. Alasty, and J. Issa, "Satellite attitude control using three reaction wheels," in *American Control Conference, 2008*, June 2008, pp. 4850–4855.

[9] J. Jin, S. Ko, and C.-K. Ryoo, "Fault tolerant control for satellites with four reaction wheels," *Control Engineering Practice*, vol. 16, no. 10, pp. 1250 – 1258, 2008.

[10] Z. Ismail and R. Varatharajoo, "A study of reaction wheel configurations for a 3-axis satellite attitude control," *Advances in Space Research*, vol. In Press, Accepted Manuscript, 2009.

[11] S. Ma and E.-K. Boukas, "A singular system approach to robust sliding mode control for uncertain markov jump systems," *Automatica*, vol. In Press, Corrected Proof, 2009.

[12] E. Alfaro-Cid, E. W. McGookin, D. J. Murray-Smith, and T. I. Fossen, "Genetic algorithms optimization of decoupled sliding mode controllers: simulated and real results," *Control Engineering Practice*, vol. 13, no. 6, pp. 739 – 748, 2005.

[13] S. Salcudean, "A globally convergent angular velocity observer for rigid body motion," *Automatic Control, IEEE Transactions on*, vol. 36, no. 12, pp. 1493–1497, Dec 1991.

[14] F. Lizarralde and J. T. Wen, "Attitude control without angular velocity measurement: a passivity approach," *Automatic Control, IEEE Transactions on*, vol. 41, no. 3, pp. 468 –472, mar 1996.

[15] B. T. Costic, D. M. Dawson, M. S. De Queiroz, and V. Kapila, "A quaternion-based adaptive attitude tracking controller without velocity measurements," in *Decision and Control, 2000. Proceedings of the 39th IEEE Conference on*, vol. 3, 2000, pp. 2424–2429.

[16] B. O. Sunde, "Sensor modelling and attitude determination for microsatellite," Master's thesis, Norwegian University of Science and Technology, 2005.

[17] T. R. Krogstad, J. T. Gravdahl, and R. Kristiansen, "Coordinated control of satellites: The attitude case," *Proceedings of the 56th International Astronautical Congress (IAC), Fukuoka, Japan*, 2005.

[18] O. Egeland and J. T. Gravdahl, *Modeling and Simulation for Automatic Control*. Marine Cybernetics, 2002.

[19] R. Kristiansen, A. Loría, A. Chaillet, and P. J. Nicklasson, "Spacecraft relative rotation tracking without angular velocity measurements," *Automatica*, vol. 45, no. 3, pp. 750–756, 2009.

[20] T. I. Fossen, *Marine Control Systems, Guidance, Navigation, and Control of Ships, Rigs and Underwater Vehicles*. Marine Cybernetics, 2002.

[21] C. D. Hall, "Spinup dynamics of gyrostats," *Journal of Guidance, Cotrol, and Dynamics*, no. 18, pp. 1177–1183, 1995.

[22] B. Wang, K. Gong, D. Yang, and J. Li, "Fine attitude control by reaction wheels using variable-structure controller," *Acta Astronautica*, vol. 52, no. 8, pp. 613–618, 2003.

[23] B. Vik, *Integrated Satellite and Inertial Navigation Systems*. Department of Engineering Cybernetics, NTNU, 2009.

[24] D. Shevitz and B. Paden, "Lyapunov stability theory of nonsmooth systems," *Automatic Control, IEEE Transactions on*, vol. 39, no. 9, pp. 1910–1914, sep 1994.

[25] W. Perruquetti and J. P. Barbot, *Sliding Mode Control in Engineering*. Marcel Dekker, Inc., 2002.

[26] T. I. Fossen, *Modelling and Control of Marine Vessels*. Norwegian University of Scinece and Technology, 2009, draft Copy.

[27] O. E. Fjellstad, "Control of unmanned underwater vehicles in six degrees of freedom: A quaternion feedback approach," Ph.D. dissertation, Norwegian University of Science and Technology, 1994.

Preprint submitted to 49th IEEE Conference on Decision and Control.
Received March 24, 2010.